NTNU
Det skapende universitet

10W GaN effektforsterker med Envelope Tracking og optimalisert tilpasning

Andreas Bognøy

Master i elektronikk
Innlevert: januar 2015
Hovedveileder: Morten Olavsbråten, IET

Norges teknisk-naturvitenskapelige universitet
Institutt for elektronikk og telekommunikasjon

Summary

Modern communication standards are based on signals which exploit high peak-to-average power ratio, signals which force the power amplifiers (PA) to operate at power back off large amounts of the time, where efficiency is poor. As a result, power amplifiers become an important component and advanced methods are being developed and improved in order to enhance efficiency. Among these methods is Envelope Tracking, a method where a dynamic supply is used for reducing supplied power at backed off RF power levels.

This thesis presents the design and characterization of a class AB PA in order to investigate its behavior when used in an envelope tracking setup. Design was based around a 10 W Cree general purpose GaN HEMT, and matching was done based on impedances found from load pull techniques. In addition, a set of different criteria for the envelope tracking has been investigated, showing varying results in terms of improvement and requirements.

Under fixed 28 V supply the PA showed a peak output power of 41.7 dBm at 2.4 GHz, having a 1 dB compression point at 41.0 dBm output power. A small signal gain of 14.1 dB was measured, and at the onset of compression the PA showed 12.2 dB gain. At peak output power, the measured power-added efficiency was 68.2 %. The PA also featured an undesired high-gain band from 2.4 GHz and all the way down to 100 MHz.

To estimate the envelope tracking performance, the PA was measured at reduced supply voltages, which were analyzed in Matlab. For 5-6 dB back off, improvements ranging from 2 % to 17 % could be achieved by adding envelope tracking, however reducing the gain as low as below 8 dB. The resulting performance was also compared to cases where a square supply function was applied, showing slight efficiency deterioration, but reducing the bandwidth requirement of the dynamic supply this could possibly serve as a good alternative as the envelope amplifier will operating with higher efficiency.

Sammendrag

Moderne kommunikasjonstandarder er basert på signaler som drar nytte av høy peak-to-average effektforhold, signaler som tvinger effektforsterkere (PA) til å operere i back-off store deler av tiden, hvor effektiviteten er lav. Som resultat, blir effektforsterkere viktige komponenter og avanserte metoder utvikles og forbedres for å kunne øke effektiviteten. Blant disse metodene finner man envelope tracking, en metode hvor en dynamisk effektforsyning brukes til å redusere forsyningsspenning ved RF back-off.

Denne oppgaven presenterer konstruksjon og karakterisering av en klasse AB effektforsterker, for å undersøke ytelsen når den brukes i et envelope tracking oppsett. Konstruksjonen var basert rundt en 10 W Cree general purpose GaN HEMT og matchingen ble utført basert på impedans som ble funnet ved hjelp av load pull teknikk. I tillegg har et sett med ulike kriterier for Envelope Tracking blitt undersøkt med ulike resultater når det gjelder forbedring og krav.

Under fast 28 V-tilførsel fikk effektforsterkeren en maksimal utgangseffekt på 41,7 dBm ved 2,4 GHz, med et 1 dB kompresjonspunkt for 41,0 dBm utgangseffekt. Det ble må lt en små signalforsterkning på 14,1 dB og ved starten av kompresjon målte forsterkeren en effektforsterkning på 12,2 dB. Ved maksimal utgangseffekt, var den målte PAE virkningsgrad på 68,2 %. Effektforsterkeren ga også et uønsket bånd med høy forsterkning fra 2,4 GHz og helt ned til 100 MHz.

For å estimere ytelsen for envelope tracking, ble effektforsterkeren målt med reduserte forsyningsspenninger, som ble analysert i Matlab. For back-off på 5-6 dB, ble det oppnådd forbedringer mellom 2 % og 17 % når det ble lagt til envelope tracking, men forsterkningen ble imidlertid redusert til så lite som under 8 dB. Den resulterende ytelsen ble også sammenlignet med tilfeller der en kvadratisk supply funksjon ble brukt, med en svak reduksjon i effektivitet som resultat. Ved å redusere båndbreddekravet for den dynamiske tilførselen, kan dette imidlertid være et godt alternativ til konvensjonell envelope tracking med lineær tracker.

Preface

This thesis is submitted in fulfillment of the requirements for the degree of master of science (MSc) at the Department of Electronics and Telecommunications, Norwegian University of Science and Technology (NTNU) and the work was carried out between september 2014 and january 2015.

I would like to than my supervisor, associate professor Morten Olavsbråten, for giving me the chance to work in this promising and exciting field. His feedback and guidance along this project has been of great value to me and for that I am grateful. I would also like to thank the Elpro lab for fabrication of the microstrip design. Last but not least, I would like to thank my friends and family for their never-ending motivation and encouragement.

Trondheim, Norway, January 2015
Andreas Bognøy

Contents

List of Tables

List of Figures

Abbreviations

ADS	=	Advanced Design Systems
CAD	=	Computer Aided Design
CMOS	=	Complementary Metal Oxide Semiconductor
CW	=	Continuous Wave
DPD	=	Digital Predistortion
DSP	=	Digital Signal Processor
DUT	=	Device Under Test
EA	=	Envelope Amplifier
EER	=	Envelope Elimination and Restoration
ET	=	Envelope Tracking
FET	=	Field Effect Transistor
GaAs	=	Gallium Arsenide
GaN	=	Gallium Nitride
HB	=	Harmonic Balance
HBT	=	Heterojunction Bipolar Transistor
HEMT	=	High Electron Mobility Transistor
HFET	=	Heterojunction Field Effect Transistor
IMD	=	Intermodulation Distortion
IMN	=	Input Matching Network
LDMOS	=	Laterally Diffused Metal Oxide Semiconductor
MMIC	=	Monolithic Microwave Integrated Circuit
MOSFET	=	Metal Oxide Semiconductor Field Effect Transistor
OMN	=	Output Matching Network
PA	=	Power Amplifier
PAE	=	Power-Added Efficiency
PCB	=	Printed Circuit Board
PAPR	=	Peak-to-Average Power Ratio
RF	=	Radio Frequency
RFPA	=	Radio Frequency Power Amplifier
RL	=	Return Loss
Si	=	Silicon
SiGe	=	Silicon Germanium
SM	=	Supply Modulator
SMC	=	Surface Mounted Component
VNA	=	Vector Network Analyzer
VSA	=	Vector Signal Analyzer
VSG	=	Vector Signal Generator

Chapter 1

Introduction

Wireless technology is getting more widespread by the minute. The need to be available anytime and anywhere is a problem both introduced and solved by wireless electronic devices. Especially the greatly increased use of handheld devices has increased the focus on research and development of wireless technology. Data rates can not seem to get large enough and quality of service constantly seem to be an issue among users. As a result, more complex signal forms emerge to increase the data rate and allow a larger number of subscribers to communicate simultaneously, making it harder to develop adequate RF electronics.

A limiting component in the RF output stage of transmitters is the power amplifier (PA). Among the required characteristics for the PA is good linearity, high gain and efficient operation, all which trade off against each other [1]. In a mobile handset, the PA is also one of the components which use the most power, and with the modern communication standards, which exhibit high peak-to-average power ratio (PAPR), the PA efficiency is decreased. Improvement of the PA efficiency is thus focused on as a way of improving the battery lifetime of mobile handsets and provides an advantage for electronics manufacturers.

Improvement of the PA efficiency is also beneficial for static transmitters, such as direct radio links, satellite links and, perhaps most notably, mobile carriers who operate a large number of base stations. Improved efficiency can therefore result in greatly reduced power expenses. A lot of research has therefore been conducted, resulting in development of advanced methods for improving the efficiency of PAs, allowing PAPR increase, as seen in figure 1.1.
Modern high power transmitters are often based on GaN HEMT transistor technology. The HEMT fields high current densities and allows high voltages, resulting in high gain and high power for a small device. Along with high saturated electron velocity, making it able to operate at relatively high frequencies. This makes the HEMT ideal for high power PAs and promising for the current most promising efficiency improvement technique, envelope tracking, a technique that improves efficiency for modern high-PAPR signals.

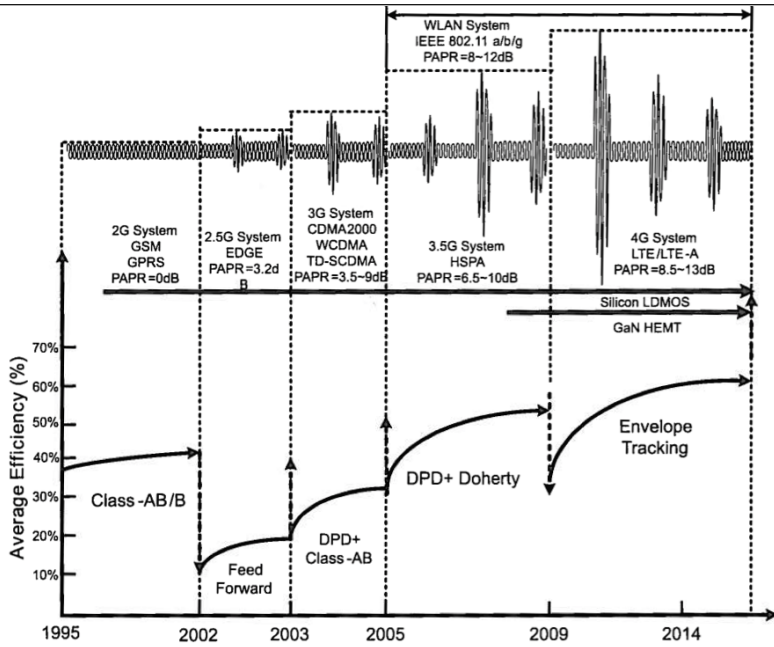

Figure 1.1: Technology development of RF PAs, figure from [1].

Envelope tracking is showing potential to become a method which can significantly improve efficiency while not necessarily deteriorating linearity of PAs too much. The basic concept of envelope tracking is to dynamically reduce the supplied power as output RF power is reduced by shaping the supply signal from the envelope of the RF signal. This results in the PA operating in, or closer to the highly efficient compression area for a wider dynamic range of output power.

This thesis presents the design and performance of a class AB GaN HEMT PA using Agilent ADS CAD software. The input and output matching networks have been optimized for high efficiency using source and load pull techniques. Fabrication was done in microstrip, and the PA characteristics were measured for fixed and reduced supply levels, which were then analyzed in Matlab for estimating the characteristics of the PA when utilizing envelope tracking. The specifications for the PA that were to be met are listed in table 1.1.

Table 1.1: Specifications for PA.

Parameter	**Specified value**
Frequency	2.4 GHz
Bandwidth (1 dB)	> 100 MHz
Gain	$> 12dB$
Output Power	> 40 dBm
$\|S_{11}\|$ [dB]	< -10 dB

Chapter 2

Basic Theory

2.1 Transmission Line Theory and Wave Propagation

When analyzing circuits using alternating currents and voltages, transmission line theory is not required provided that the wavelengths are substantially greater than the physical dimensions of a network. If the dimensions of the network equal a considerable fraction of a wavelength or more, transmission line theory needs to be considered [4].

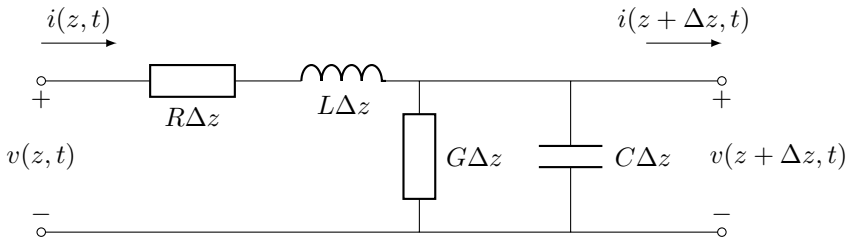

Figure 2.1: Lumped component equivalent of transmission line.

In this case, the transmission lines are considered distributed elements, where voltages and currents may vary in amplitude and phase over the length of the line. These waves are described by a pair of first-order partial differential equations called *telegrapher's equations* [5]. For sinusoidal steady-state conditions these can be solved, yielding the time-harmonic one-dimensional Helmholtz equations,

$$\frac{d^2V(z)}{dz^2} - \gamma^2 V(z) = 0 \tag{2.1}$$

$$\frac{d^2I(z)}{dz^2} - \gamma^2 I(z) = 0 \tag{2.2}$$

for the voltage and current phasors $V(z)$ and $I(z)$ of position z along the line, where

$$\gamma = \alpha + j\beta = \sqrt{(R + j\omega L)(G + j\omega C)}\ [m^{-1}] \tag{2.3}$$

is the propagation constant composed of an attenuation constant, α, and phase constant, β. The propagation constant is also dependent on the angular frequency, $\omega\,[rad/s]$ and the transmission line parameters explained in table 2.1. Solutions to (2.1) and (2.2) yield the

Table 2.1: Parameter descriptions.

Parameter	Description
R	Resistance per unit length in Ω/m
L	Inductance per unit length in H/m
G	Conductance per unit length in S/m
C	Capacitance per unit length in C/m

traveling wave solutions

$$V(z) = V_0^+ e^{-\gamma z} + V_0^- e^{\gamma z} \tag{2.4}$$

$$I(z) = I_0^+ e^{-\gamma z} + I_0^- e^{\gamma z} \tag{2.5}$$

where the plus and minus superscripts denote wave amplitudes traveling in the positive and negative z direction respectively. The exponential factors are representing the corresponding waves, such that $e^{-\gamma z}$ gives a forward traveling wave, and $e^{\gamma z}$ give a backward traveling wave along the length of the line, z.

The characteristic impedance of the transmission line is defined as

$$Z_0 = \frac{V_0^+}{I_0^+} = -\frac{V_0^-}{I_0^-} = \sqrt{\frac{R + j\omega L}{G + j\omega C}} \tag{2.6}$$

When terminating a transmission line with an arbitrary load impedance, Z_L, there may be a reflection of the incident wave, which is described by the voltage reflection coefficient,

$$\Gamma = \frac{V_0^-}{V_0^+} = \frac{Z_L - Z_0}{Z_L + Z_0} \tag{2.7}$$

For a fully passive network, Γ is a complex number with $|\Gamma| \in [0, 1]$, indicating the ratio of the incident wave, V_0^+, which is reflected as V_0^-. To obtain $\Gamma = 0$ the load impedance Z_L must be equal to the characteristic impedance, Z_0, otherwise a return loss is experienced, defined as

$$RL\ [\text{dB}] = -20 \log |\Gamma| \tag{2.8}$$

for $|\Gamma|$ given in (2.7) so that a matched load($\Gamma = 0$) has a return loss of $-\infty\,[\text{dB}]$ and a total reflection ($|\Gamma| = 1$) gives $RL = 0\,[\text{dB}]$.

The length of a transmission line is often expressed as an electric length, $\theta = \beta l$, which is the phase of a signal propagated along a line of length l. The input impedance of a transmission line of length l and terminated by Z_L, is given as

$$Z_{in} = Z_0 \frac{Z_L + Z_0 \tanh \gamma l}{Z_0 + Z_L \tanh \gamma l} \tag{2.9}$$

which yields two interesting special cases.

$$Z_{in} = \frac{Z_0^2}{Z_L} \tag{2.10}$$

for $l = \frac{\lambda}{4}$ and

$$Z_{in} = Z_0 \tag{2.11}$$

for $l = \frac{\lambda}{2}$.

2.1.1 Microstrip

Microstrip is a common planar transmission line technology that is relatively easy and cheap to design and fabricate for microwave systems and circuits. It is easily integratable with lumped components or MICs. The microstrip transmission line consists of a thin, narrow metal strip and a wide ground plane, separated by a dielectric substrate, as shown in figure 2.2. The topmost conductor has a width W, and the dielectric substrate has a

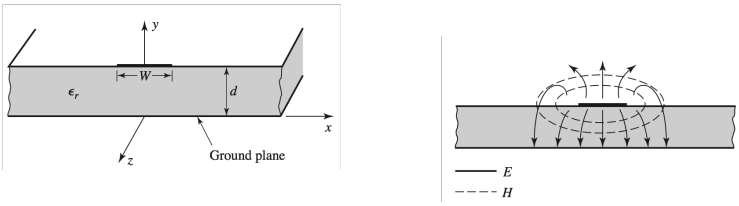

(a) **(b)**

Figure 2.2: Cross section of microstrip transmission line, showing geometry (a) and electromagnetic fields (b). Excerpt from [2].

thickness d and relative permittivity ε_r. The result is an electromagnetic field distribution as shown in figure 2.2, where the electric field exist between the conductors and the magnetic field exist around the narrow top conductor, both partly through the substrate and partly through air. The mode propagated by the microstrip lines is called quasi-TEM, that is Transverse Electro-Magnetic, which in fact has small transverse field components, unlike true TEM, but can be treated as such [6] as the transverse components are dominant. A resulting permittivity also exists as

$$\varepsilon_{\text{eff}} \approx \frac{\varepsilon_r + 1}{2} + \frac{\varepsilon_r - 1}{2} \left(1 + \frac{1}{\sqrt{1 + 12\frac{d}{W}}} \right) \tag{2.12}$$

which can be interpreted as the overall permittivity the propagating wave experiences being surrounded by both air and substrate [2]. The impedance of microstrip lines is calculated using the formulas

$$Z_0 = \frac{60}{\sqrt{\varepsilon_{eff}}} \ln \left(\frac{8d}{W} + \frac{W}{4d} \right) \tag{2.13}$$

for $\frac{W}{d} \leq 1$, and

$$Z_0 = \frac{120\pi}{\sqrt{\varepsilon_{eff}}\frac{W}{d} + 1.393 + 0.667\ln\left(\frac{W}{d} + 1.444\right)} \tag{2.14}$$

for $\frac{W}{d} \geq 1$, given the physical dimensions shown in figure 2.2. Solving for the ratio $\frac{W}{d}$ for a determined characteristic impedance Z_0 gives

$$\frac{W}{d} = \frac{8e^A}{e^{2A} - 2} \tag{2.15}$$

for $\frac{W}{d} < 2$, and

$$\frac{W}{d} = \frac{2}{\pi}\left[B - 1 - \ln(2B - 1) + \frac{\varepsilon_r - 1}{2\varepsilon_r}\left\{\ln(B - 1) + 0.39 - \frac{0.61}{\varepsilon_r}\right\}\right] \tag{2.16}$$

for $\frac{W}{d} > 2$ where

$$A = \frac{Z_0}{60}\sqrt{\frac{\varepsilon_r + 1}{2}} + \frac{\varepsilon_r - 1}{\varepsilon_r + 1}\left(0.23 + \frac{0.11}{\varepsilon_r}\right) \tag{2.17}$$

and

$$B = \frac{377\pi}{2Z_0\sqrt{\varepsilon_r}} \tag{2.18}$$

The wavelength of the waves propagated on the microstrip, λ_g can be found using the phase velocity of the respective wave,

$$v_p = \frac{c}{\sqrt{\varepsilon_{eff}}} \tag{2.19}$$

which gives the wavelength

$$\lambda_g = \frac{v_p}{f} = \frac{c}{f\sqrt{\varepsilon_{eff}}} \tag{2.20}$$

which can be combined with (2.9) to calculate microstrip impedances of given electric lengths.

2.2 S-Parameters

N-port networks can be described by a variety of different parameters, determined from different quotients of voltage and current on the ports. However at microwave frequencies short and open circuits are hard to implement, making it hard to measure current and voltages in order to determine some of these parameters [7]. As a result the most common way to describe an N-port device is by its S-matrix, or scattering matrix, containing S-parameters, defined in (2.21) and (2.22). These S-parameters are measured with matched termination of inputs and outputs, thus making them easier to determine at higher frequencies.

$$\mathbf{S} = \begin{bmatrix} S_{11} & S_{12} & \cdots & S_{1N} \\ S_{21} & S_{22} & \cdots & S_{2N} \\ \vdots & \vdots & \ddots & \vdots \\ S_{N1} & S_{N2} & \cdots & S_{NN} \end{bmatrix} \tag{2.21}$$

where S_{mn} is the ratio of a complex valued wave coming from port m and an incident wave on port n, when all other ports are terminated with matched loads.

$$S_{mn} = \left.\frac{V_m^-}{V_n^+}\right|_{V_k^+=0 \text{ for } k\neq n} \tag{2.22}$$

For a 2-port device 4 S-parameters exist, listed as a 2-by-2 S-matrix. Thus the relationship between the incident and reflected voltages shown in figure 2.6 is given as

$$\begin{bmatrix} V_1^- \\ V_2^- \end{bmatrix} = \begin{bmatrix} S_{11} & S_{12} \\ S_{21} & S_{22} \end{bmatrix} \begin{bmatrix} V_1^+ \\ V_2^+ \end{bmatrix} \tag{2.23}$$

As voltages and currents are hard to measure directly at higher frequencies and there not being any methods equally simple to measure, this is the most widely used method of describing circuits and devices. The S-parameters are also called small signal parameters, with S_{21} denoting the small signal gain. As a result, other parameters and properties are often determined from the S-parameters, and thus is maybe the parameter paid the most attention to during design.

It is worth noting that $|S_{11}|$ and $|S_{22}|$ for a two port is a definition equivalent compared to the return loss for a transmission line in (2.8), as

$$RL_{in}[\text{ dB}] = -20\log|S_{11}| = -|S_{11}|\text{ [dB]} \tag{2.24}$$

and

$$RL_{out}[\text{ dB}] = -20\log|S_{22}| = -|S_{22}|\text{ [dB]} \tag{2.25}$$

$|S_{11}|$ [dB] and $|S_{22}|$ [dB] are therefore also referred to as return losses.

2.3 Stability

Amplifiers are active devices and yield a certain amount of gain. As such, amplifiers are subject to uncontrolled oscillations, or generating chaotic output signals. Not only for the frequencies at which they are designed for operation, but also at higher and, perhaps most significantly, lower frequencies. Oscillations are initiated if the output or input impedances as seen by the transistor in figure 2.6 have a negative real part, forcing either reflection coefficients $|\Gamma_{in}| > 1$ or $|\Gamma_{out}| > 1$. These are defined as

$$\Gamma_{in} = \frac{V_1^-}{V_1^+} = S_{11} + \frac{S_{12}S_{21}\Gamma_L}{1 - S_{22}\Gamma_L} = \frac{Z_{in} - Z_0}{Z_{in} + Z_0} \tag{2.26}$$

and

$$\Gamma_{out} = \frac{V_2^-}{V_2^+} = S_{22} + \frac{S_{12}S_{21}\Gamma_S}{1 - S_{22}\Gamma_S} = \frac{Z_{out} - Z_0}{Z_{out} + Z_0} \tag{2.27}$$

Hence the stability is also dependent of Γ_S and Γ_L. Thus three different states of stability exist;

Unstable Transistor oscillates for any combination of input and output impedance. $|\Gamma_{in}| > 1$ and $|\Gamma_{out}| > 1$ for all Z.

Stable Transistor does not oscillate. Meaning $|\Gamma_{in}| < 1$ and $|\Gamma_{out}| < 1$ for all passive input and output impedances.

Conditionally Stable Transistor does not oscillate for a given range of termination impedances.

As the value of impedances and reflection coefficients are dependent on the frequency at RF, a PA can be unconditionally stable at some frequencies and unstable or conditionally stable on some frequencies. It can be shown that for a given frequency the set of stable Γ_S and Γ_L lie either on or outside the intersection of a circle and the smith diagram. These circles are known as stability circles [4], an example of which is shown in figure 2.3. Hence for a unconditionally stable PA the whole smith diagram will either be outside or inside the stability circles, if $|S_{11}| < 1$ or $|S_{22}| < 1$ respectively. For $|S_{11}| > 1$ or $|S_{22}| > 1$ unconditional stability is impossible.

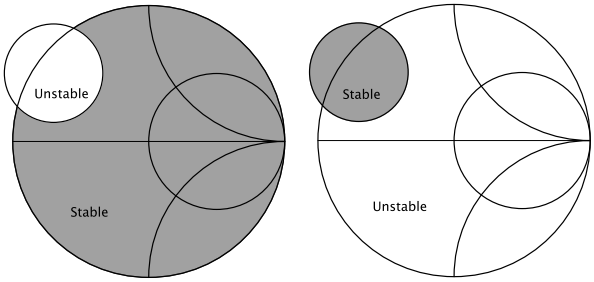

(a) $|S_{11}| < 1$ **(b)** $|S_{11}| > 1$

Figure 2.3: Output stability circles showing the stable area where $|\Gamma| < 1$ and unstable areas where $|\Gamma| > 1$ for S_{11} both larger and smaller than unity.

There are however methods which are easier for determining unconditional stability of a PA over a wide range of frequencies. These are known as the K-Δ [8] and μ-factor [9]. Unconditional stability is ensured if the K-Δ test is valid. This is defined as

$$K = \frac{1 - |S_{11}|^2 - |S_{22}|^2 + |\Delta|^2}{2|S_{12}S_{21}|} > 1 \tag{2.28}$$

An auxiliary condition is that

$$|\Delta| = |S_{11}S_{11} - S_{12}S_{21}| < 1 \tag{2.29}$$

Alternatively if the μ-factor test is regarded, unconditional stability is ensured only if

$$\mu = \frac{1 - |S_{11}|^2}{|S_{22} - \Delta S_{11}^*| + |S_{12}S_{21}|} > 1 \tag{2.30}$$

where Δ is still the determinant of the S-matrix, but unlike the K-Δ-test, there is no condition needed to be fulfilled. Another difference is that the μ-test does not only determine whether the device will be unconditionally stable or not, like the K-Δ-test, but also show how stable. I.e. a larger values of μ implies a greater margin to becoming unstable. In some cases, e.g. ADS, a μ' is also referred to, however this is used, which is essentially (2.30) with the port configuration switched around.

A common methodology for ensuring unconditional stability, or increasing the margin, is trading off gain by introducing loss at the input of the device. This also decreases

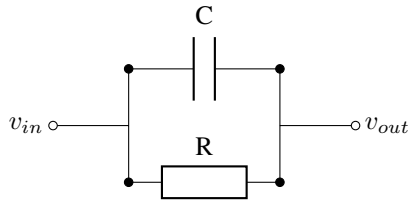

Figure 2.4: RC high pass configuration used for stabilization at low frequencies.

noise performance, but for a PA this is more desirable than lowering the output power by adding the loss at the output, which gives less noise exacerbation in comparison. A common configuration is shown in figure 2.4, and is used in series with the input of the PA. It consists of a resistor in parallel with a capacitor and ensures a low pass loss, with frequencies above

$$f_c \approx \frac{1}{2\pi RC} \tag{2.31}$$

shorted and hence gain at the fundamental frequency should not be harmed too much. This is a commonly used method as a lot of transistors suffer from instability at lower frequencies due to high gain at these frequencies.

Also crucial to ensure stability is by providing sufficient decoupling of the PA. This is commonly done using a capacitor for shorting unwanted frequencies at the supply side of the RF-choke in figure 2.7. The RF-choke is, ideally, open at the in-band frequencies, and thus decoupling on this side will not compromise the RF performance, only provide unwanted transients with a way to ground, removing the chance that they will resonate.

2.4 Power Amplifiers

A power amplifier (PA) is an electrical component for increasing the amplitude, and thus the power of an electronic signal by converting power from a DC source to RF. As opposed to other types of amplifiers, the most important property is being able to produce signals of sufficient power, and not necessarily have the highest gain or the best noise performance. In microwave electronics these amplifiers are typically used as an output stage in transmitters, amplifying signals to the level where they can be transmitted using an antenna. As the PA is designed to provide high output power, it requires attention to power efficiency, but without degrading performance such as linearity and bandwidth too much. A simple example of an output stage is shown in figure 2.5, where a digital signal processor (DSP)

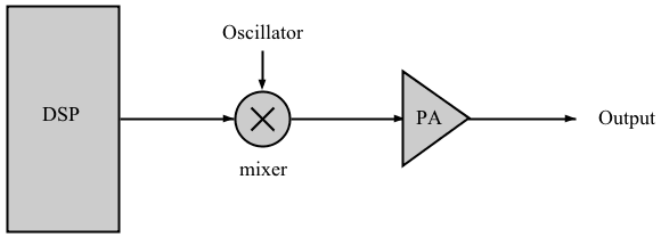

Figure 2.5: High abstraction level example of transmitter.

is used for producing and modulating a baseband signal with the information to be transmitted. The signal is then mixed up to the respective carrier frequency and then amplified by the PA before being transmitted by an antenna. The mixing can be done in several stages, by adding what is known as intermediate stage at a frequency lower than the RF frequency, but for simplicity this is left out of the illustration along with filtering. The PA can be disassembled to the form shown in figure 2.6, showing the most general parts of a solid state PA. A PA also needs impedance matching to obtain the desired input and output

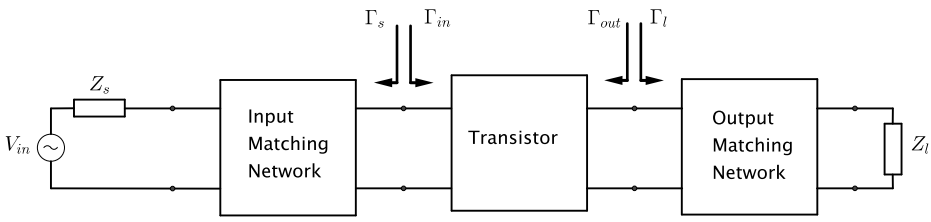

Figure 2.6: Example system overview of transistor PA.

impedances, or reflection coefficients, to achieve the wanted performance. This is done by properly designing the input and output matching networks, shown as input and output matching networks in figure 2.6 respectively. The mixer, or source, is represented by V_{in} and Z_S, and the antenna, or load, is represented by Z_l. A general example of the transistor

block is shown in figure 2.7. This figure shows the most basic, necessary parts of a transistor PA. RF chokes are included to force the RF power to be transmitted from v_{in} to v_{out} and not leak into the DC sources, V_g and V_d. Similarly DC-blocks are included to avoid DC leakage on the input and output. Common components for this task are inductors and capacitors, ideally having high impedance at RF and DC, respectively.

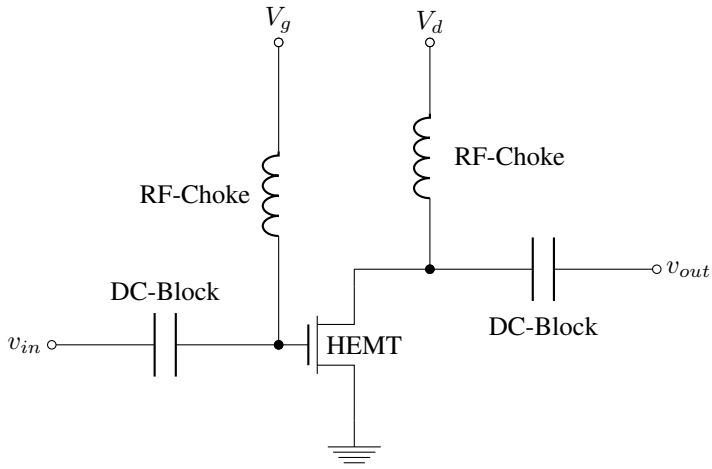

Figure 2.7: Example HEMT PA without matching networks, showing RF-ports, v_{in} and v_{out} and DC-ports, V_g and V_d.

2.4.1 Property Definitions

Efficiency

An important characteristic of a power amplifier is its efficiency, that is the ratio of the power drawn from a power source which is used to amplify the input signal. Several definitions exist, yielding slightly different numbers, but all in all try to quantify the same property. The most common definition used to compare efficiencies of PAs in literature is known as Power-Added Efficiency (PAE), defined as

$$\eta_{PAE} = \frac{P_{out} - P_{in}}{P_{DC}} \tag{2.32}$$

where P_{in}, P_{out} and P_{DC} denotes input, output and supply power respectively. This definition has become a common metric for the efficiency of RF PAs as it incorporates the input power. Especially single stage RF PAs tend to have relatively low gain and the simpler definition, known as drain efficiency, η, is therefore not a comprehensive metric of overall efficiency [1]. Drain efficiency is defined as

$$\eta = \frac{P_{out}}{P_{DC}} \tag{2.33}$$

hence the relationship to η_{PAE} is

$$\eta_{PAE} = \eta \left(1 - \frac{1}{G}\right) \tag{2.34}$$

where G denotes the gain of the PA. Thus for high gain amplifiers, the two definitions converge towards each other. The drain efficiency however is a fair metric to compare PAs for envelope tracking due to the straightforward definition of efficiency between the PA and the dynamic supply interface.

Gain

One fundamental figure of merit for an amplifier is the gain and several different definitions exist. For PAs the most common is to consider power gain, the amount the output signal has had its power increased. A common defintion for this is as defined in (2.35), the ratio of power dissipated in load to the power delivered to the input of the two port [4].

$$G_P = \frac{P_L}{P_{\text{in}}} = \frac{|S_{21}|^2(1 - |\Gamma_L|^2)}{(1 - |\Gamma_{in}|^2)|1 - S_{22}\Gamma_L|^2} \tag{2.35}$$

Other common definitions, available gain (G_A) and transducer power gain (G_T) are defined in (2.36) and (2.37) respectively. Available gain is the ratio of power available from the two port to the power available from the source while transducer power gain is the ratio of the power delivered to the load to the power available from the source.

$$G_A = \frac{P_{\text{avn}}}{P_{\text{avs}}} = \frac{|S_{21}|^2(1 - |\Gamma_S|^2)}{|1 - S_{11}\Gamma_S|^2(1 - |\Gamma_{\text{out}}|^2)} \tag{2.36}$$

$$G_T = \frac{P_L}{P_{\text{avs}}} = \frac{|S_{21}|^2(1 - |\Gamma_S|^2)(1 - |\Gamma_L|^2)}{|1 - \Gamma_S\Gamma_{\text{in}}|^2|1 - S_{22}\Gamma_L|^2} \tag{2.37}$$

In general G_P is independent of Z_S, while G_A assumes conjugate matching and depends on Z_S, and G_T depends on both Z_S and Z_L. The gain will be maximized if the network is conjugately matched (Section 2.5), and $G_P = G_A = G_T$.

Other terminologies used related to gain is Maximum Available Gain (MAG) and Maximum Stable Gain (MSG). MAG is a special case of G_T, used to estimate the trade-off made when increasing the stability of a PA. It is defined when $K > 1$ as

$$MAG = G_{T_{max}} = \frac{|S_{21}|}{|S_{12}|}(K - \sqrt{K^2 - 1}) \tag{2.38}$$

where K is Rollet's stability factor defined in (2.28). MSG is a further special case of $G_{T_{max}}$, defined when $K = 1$, i.e.

$$MSG = G_{msg} = \frac{|S_{21}|}{|S_{12}|} \tag{2.39}$$

and represents the maximum obtainable gain given stable operation of the device. It is as such an easy computable parameter and is convenient for comparing the gain of various devices [4].

Linearity

Common for all PAs is that the output voltage is not a linear amplification of the input signal, but rather a power series of this with individual amplification for each power of the input signal, i.e.

$$v_o = a_1 v_i^1 + a_2 v_i^2 + a_3 v_i^3 + \dots \tag{2.40}$$

as described in [3]. It is apparent that this puts limitations on v_i for the power terms to not become dominant and the output to become a less accurate copy of the input, or distorted. A simple result of this can be seen on a simple sinusoid in figure 2.8.

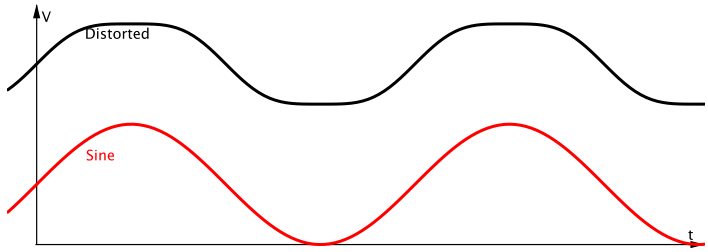

Figure 2.8: Example of sine wave with compressed equivalent.

This is called gain compression. It can be explained when a single frequency

$$v_i = V_0 \cos \omega t \tag{2.41}$$

is applied to the input, (2.40) gives the output voltage as

$$\begin{aligned} v_o =& a_0 + a_1 V_0 \cos \omega t + a_2 (V_0 \cos \omega t)^2 + a_3 (V_0 \cos \omega t)^3 + \dots \\ =& (a_0 + \frac{1}{2} a_2 V_0^2) + (a_1 V_0 + \frac{3}{4} a_3 V_0^3) \cos \omega_0 t + \frac{1}{2} a_2 V_0^2 \cos 2\omega_0 t \\ &+ \frac{1}{4} a_3 V_0^3 \cos 3\omega_0 t + \dots \end{aligned} \tag{2.42}$$

Thus the voltage gain at frequency ω_0 is given as [4]

$$G_v = a_1 + \frac{3}{4} a_3 V_0^2 + \dots \tag{2.43}$$

With a negative a_3 which is typically the case, the second term of (2.43) will typically cause the total gain to drop, as shown in figure 2.9, forcing a constant output level if increasing the input signal level.
There are several ways of addressing the linearity of a PA. When interested in the dynamic range with relation to power a common way is to refer to the 1dB compression point. This is the input power at which the output power is 1dB lower than would have it would have been given idealistic amplification, that is where

$$P_{1\text{ dB, out}} = P_{in} + G_P - 1\,dB \tag{2.44}$$

This is illustrated in figure 2.9. At input power levels higher than this the output power at the fundamental frequency does generally not increase, i.e. the gain and thus efficiency decreases. One can also regard the third order intercept point, the point where the input power is sufficient for the power of the third order harmonic to be as great as the power of the fundamental signal. At this point the gain is more compressed than at 1 dB compression. Both points are referred to as output and input power.

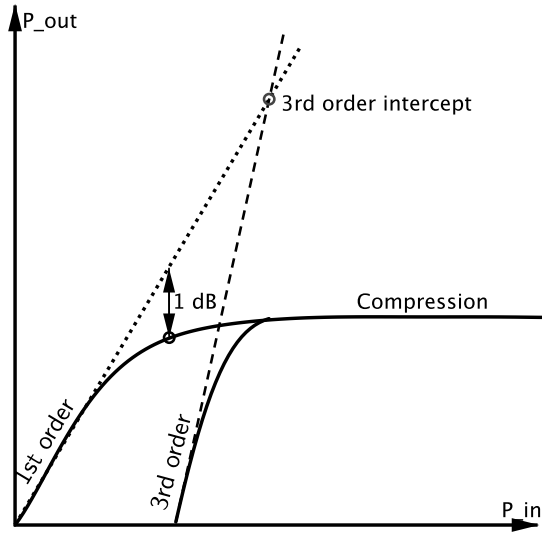

Figure 2.9: Output power showing 1dB compression point.

However when applied an input signal consisting of more than a single frequency, a two tone input, as shown in (2.45) gives a fair indication of the behavior with a continuous band, e.g.

$$v_i = V_0(\cos\omega_1 t + \cos\omega_2 t) \tag{2.45}$$

Now the output signal becomes considerably more coplex than the one in (2.42) [4]. In this case what is known as intermodulation occurs, a form of distortion where the harmonics of the different frequency components mix together, as shown in figure 2.10. As with the single frequency case harmonics of the tones appear, but also *intermodulation products*. That is tones at frequencies which are sums or differences of the fundamental frequencies and their harmonics. The main difference is that some of these products are inside the band of the device. The distortion caused by these products is called *intermodulation distortion* (IMD) and it is commonly measured in dBc, decibel relative to the carrier.

When comparing with the level of thermal noise of the PA, one can determine the dynamic ranges of the device. For PAs being used close to compression for maximum efficiency,

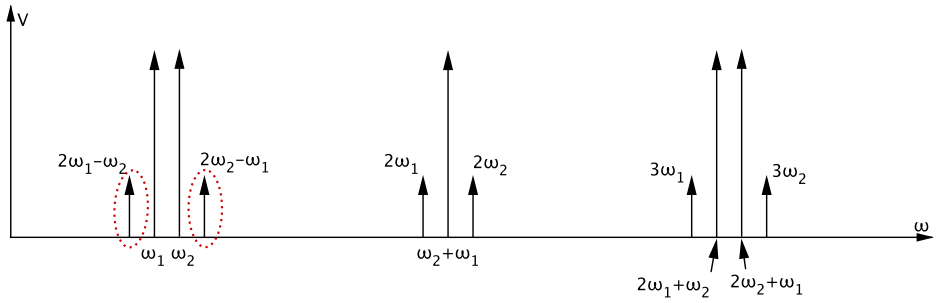

Figure 2.10: Output spectrum of two-tone input, showing harmonics and IMD-products. The in-band products are marked.

the common way to address the dynamic range is a linear dynamic range, DR_l. This is defined as the range of output power from where it is equal to the thermal noise to the 1 dB compression point. Alternatively gain can be plotted versus output power of the PA, showing gain compression.

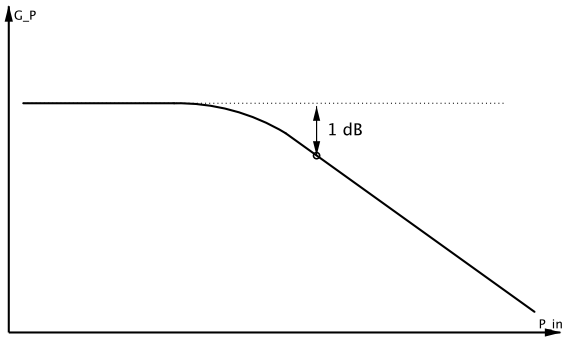

Figure 2.11: Gain as function of input power, showing the compression of the gain and $P_{1\,\mathrm{dB}}$.

Gain compression can also be referred to as AM-AM distortion, which is a characterization of the change in output amplitude versus input amplitude. A similar definition is the phase distortion, or AM-PM distortion, which is a characterization of the change in output phase vs. input amplitude.

2.4.2 Classes

As a result of the different trade-offs and requirements for PAs a common way to divide them has been through what is known as classes. Some of these are referred to as linear, however they are not linear in the sense of providing idealistic amplification. The output will still get compressed at some power levels, but the linear amplifiers preserve the original waveform of the signal [10]. These classes are referred to as class A, AB, B and C and

are distinguished by their bias point or bias current. Considering figure 2.7, the class of the PA is given by the bias voltage, V_g, and the quiescent current, I_{DQ}, through the channel of the transistor when no input RF signal is applied. This is most easily demonstrated through the IV-curves in figure 2.12. The different bias points give different quiescent currents, and when operation along a set load line, resulting in the transistor channel being cut off for parts of the input signal period. This means that when the voltage swing on the gate gets large enough, the transistor does not conduct any current. This is called conduction angle and the connection to amplifier class is shown in table 2.2, along with their theoretical maximum η_{PAE}.

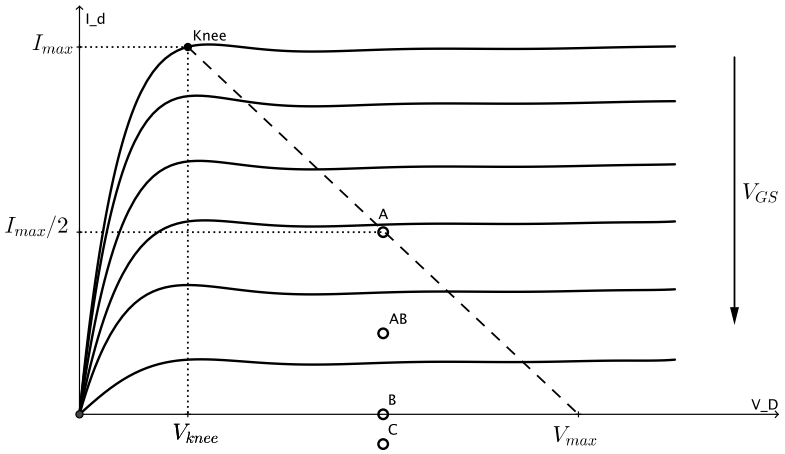

Figure 2.12: IV curves for FET transistor with operating points for amplifier classes A-C.

Table 2.2: PA classes.

Class	**Conduction angle**	**Max** η_{PAE}
A	2π	50%
AB	$\langle \pi, 2\pi \rangle$	50% - 78.8%
B	π	78.8%
C	$< \pi$	100 %

By refraining from conducting at lower amplitudes, there will only be a minimum of wasted power for these low voltages. Hence the theoretical achievable efficiency will be improved according to table 2.2, but the maximum output power will be reduced for class C due to the small conduction angle, and a theoretical $100\,\%$ efficiency can be obtained for 0° condiction angle. Class C also

In addition, there exist a large number of different architectures which is known as non-

linear or switch mode classes. As opposed to the linear classes they do not preserve the original waveform. The most common ones used for microwave applications are known as classes D, E and F [11], but class C is also sometimes regarded as a nonlinear amplifier [10]. These are mainly superior to classes A-C in terms of efficiency with practical η_{PAE} often close to 100 %, however they are inferior in linearity. As the output current and voltage waveforms can be quite different from the input waveforms, they are only suited for constant envelope signals and as a result they are not of interest here.

2.5 Impedance Matching

A PA can be viewed as a three-part system, as shown in figure 2.6, the main part being an active device along with appropriate bias and supply feeding networks, and stabilization components. In addition a design will generally include what is known as input and output matching networks as shown in figure 2.7. An important theorem is the maximum power transfer theorem, which states that maximum power transfer takes place when the impedance of a source is equal to the complex conjugate of the load, i.e.

$$Z_{src} = Z_{load}^{*} \tag{2.46}$$

However for transistors, having a limited voltage swing, that would generally require a too large load resistance. The large load would prevent the transistor from supplying a current large enough to ensure maximum swing and thus maximum power transfer. A lower resistance, R_{opt} is thus defined as

$$R_{opt} = \frac{V_{max}}{I_{max}} \tag{2.47}$$

Matching to this impedance is called load line matching, and is a real life compromise given the physical constraints on current and voltage [3].

For PAs these techniques are both used. On the input conjugate match is used to ensure as large portion as possible of the input signal is fed to the transistor, hence ensuring maximum gain. Therefore referred to as matching for gain. On the output however the transistor introduces the aforementioned constraints to voltage swing, making loadline matching the method of choice. This is not the optimum method for maximizing gain of the PA at back off, but ensures higher maximum power output, as is illustrated in fig. 2.13.

The techniques used for impedance matching in RF electronics consist of using the relation between a given system impedance, Z_0 and component impedance in a smith chart. Using the smith chart it is possible to exploit the wave transmission of RF circuits and tune impedances by using either reactive components or simple transmission lines. In modern CAD software this is highly automated and not higly necessary for understanding the work performed. In any case it is more than well described in literature [4] [6].

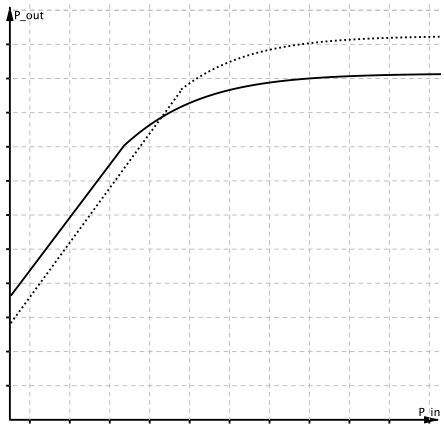

Figure 2.13: Output power versus input power for gain matched (solid curve) and power match (dotted curve).

2.6 GaN HEMT Technology

In an RF PA the performance and characteristics are largely defined by the chosen transistor technology. Both semiconductor material and transistor type hugely affect both the different characteristics of the PA, as well as the price. Common technologies include gallium arsenide (GaAs) heterojunction bipolar transistors (HBT) and Silicon Laterally Depleted Metal Oxide Semiconductor (Si-LDMOS), which are widely used in user equipment and base stations [12]. However in recent years CMOS based PAs have become a valid low-budget alternative. Also CMOS offers the possibility of integrating the RF front end with the rest of the system, alternatively using silicon germanium (SiGe) HBTs for increased performance.

For high power applications however, more efficient solutions are desired, getting more challenging at higher frequencies. As a result, research has been conducted in gallium nitride (GaN) high-electron-mobility transistor (HEMT), a high performing, yet expensive transistor technology that has seen use for some time, mainly in military and space related applications for some time, being available as commercial-off-the-shelf since 2005 [13]. General characteristics include low noise and high gain at high frequencies.

The concept of the HEMT is vertical alignment of two materials with different band gaps, a wide band gap such as aluminium gallium arsenide (AlGaN) and a narrow band gap such as GaN, as seen in the cross section in figure 2.14. The result is what is called a two-dimensional electron gas (2DEG) in the junction between the materials, a thin layer where the conduction band is below the fermi energy, making the channel highly conductive. This is also called a heterojunction, and the HEMT is therefore also referred to as an HFET. The HEMT technology is not exclusive for GaN/AlGaN, e.g. indium GaN (InGaN) can be used. Other base semiconducting materials are also used, such as GaAs,

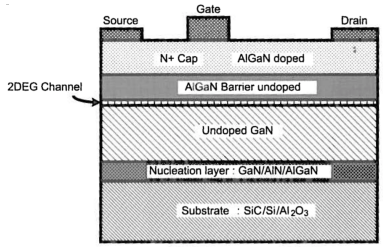

Figure 2.14: Cross section of GaN HEMT, figure from [1].

indium phosphide (InP) and indium gallium phosphide (InGaP) and it is constructed both as lumped transistors and MMIC devices.

Using GaN however not only gives a wide energy band gap, but also yield a lower relative dielectric constant, aiding larger RF currents and power to be generated, and resulting in low capacitive loading and parasitic delay [1]. Additionally the GaN HEMT has a high breakdown voltage,which allows large drain voltages, giving a high input impedance per watt of RF power as well as making matching easier and with less loss [13]. The 2DEG layer of the HEMT also gives a high power density per gate periphery, reducing output capacitance. All of this is making the GaN HEMT suitable for efficient high power, high frequency PAs.

2.7 Envelope Tracking

Envelope Tracking (ET) is a method of utilizing a PA in order to improve the efficiency at power back off. First proposed by Saleh and Cox [14], it is a similar technique to the Kahn technique (Envelope Elimination and Restoration) [3], which is shown in figure 2.15. Here the amplitude variation of a signal, or envelope, is extracted and the carrier limited to become a constant envelope signal, only varying in phase. The envelope, which is at a lower frequency is thus amplified and used as supply by a nonlinear or switch mode amplifier in order to amplitude modulate the carrier to form a replicated, high power signal. Reconstructing the signal, however, requires great attention to timing, and great delay for the envelope branch to accurately match the correct amplitude with the correct phase [3].

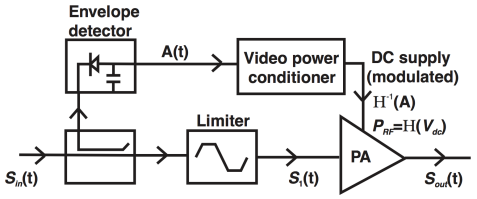

Figure 2.15: Kahn technique, excerpt from [3].

Due to the regeneration of the envelope through supply modulation, the Kahn technique is dependent on high accuracy in the envelope loop, and is subject to bandwidth and dynamic range limitations. As an alternative, ET does not need an as accurate replication of the envelope [1]. A schematic depicting an example ET system is presented in figure 2.16, where the DC-DC converter acts as a dynamic supply or envelope amplifier.

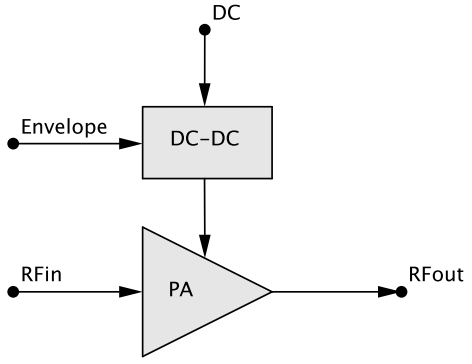

Figure 2.16: PA with envelope tracking power supply.

In an ET system the signal controlling the envelope amplifier, could be both the extracted envelope the RF signal or a designated envelope signal from a DSP, the latter the most

commonly used in modern implementations [3].

In ET however the input signal is not limited before reaching the PA itself, and therefore not a constant envelope signal. As a consequence a linear class amplifier is used, having its supply voltage controlled by the envelope amplifier[11]. By doing this it is possible for the PA to operate in saturation, or as a current source, for not only the peak amplitude but also at power back off [15]. In comparison the PA has to operate in linear region to constantly modulate the carrier in the Kahn technique. As the efficiency of a linear class PA is greatest close to compression, efficiency is improved for a backed off dynamic region. This is simply illustrated as having less supply voltage available for thermal dissipation, as shown in figure 2.17. This figure shows an output waveform for both static supply and ET operation, highlighting the amount dissipated as heat.

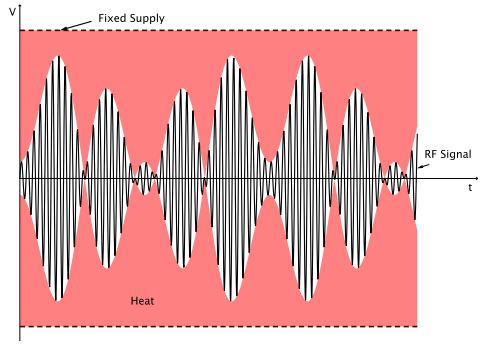

(a) Fixed supply PA.

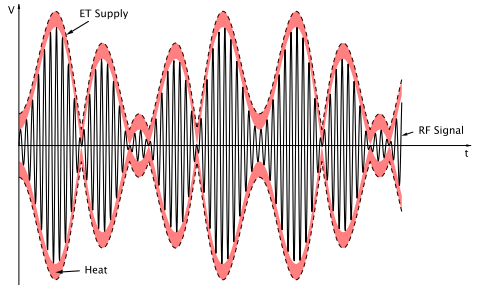

(b) PA with envelope tracking supply.

Figure 2.17: Comparison of thermally dissipated power for fixed supply PA and ET PA.

This figure shows how a fixed DC supply PA such as the one in figure 2.5 dissipates energy. The supply voltage is shared by the PA and the load in parallel, which with Kirchoff's current law yields

$$P_S = V_S I_S = V_S \left(I_d + I_L\right) = P_d + P_L \tag{2.48}$$

where P_S, V_S and I_S denotes supply power, voltage and current respectively, I_d and P_d is drain current and its dissipated power, and I_d and P_d is drain current and its dissipated power. This shows that

$$P_d = V_S I_d \tag{2.49}$$

shown in figure 2.17 is thermally dissipated in the PA, and not delivered to the load. Thus a dynamic supply like would adjust the delivered power, P_S, such that for an instantaneous output power, P_L, less power left over, P_d.

2.7.1 Supply Modulator for Envelope Tracking

The dynamic power supply in ET is also called envelope amplifier (EA), envelope tracker, supply modulator, and video amplifier. This is partly because there are, as with PAs, a wide range of different designs and technologies exist, each with their respective benefits and drawbacks. As with RF PAs and amplifiers in general, figures-of-merit and trade offs include bandwidth, efficiency, gain, dynamic ranges, slew-rates and linearity.

Typically modulators are divided into two main types - continuous and discrete. An example of a contious supply modulator is a linear regulator or amplifier that has a smooth voltage transfer function, which result in a smooth tracking response, as seen in figure 2.19. In comparison a discrete will have a finite set of discrete output levels, depending on the input envelope, such as a DC-DC converter or switched power supply.

An RF PA employing ET would in practice have an increased dynamic range with operation close to max efficiency. If a discrete switching supply is used, a stepwise net PAE function, as shown in figure 2.18 will be the result.

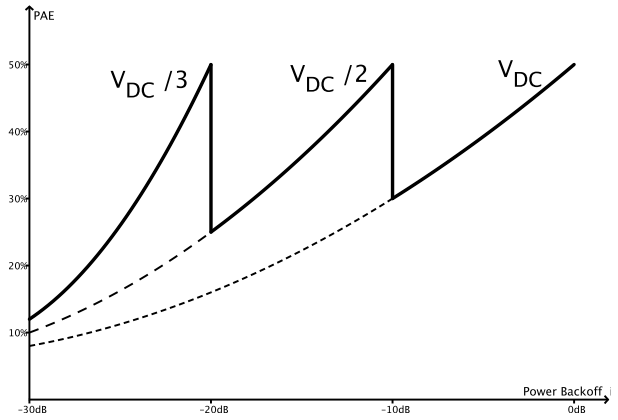

Figure 2.18: Efficiency of ET PA as a function of back off from maximum power.

Figure 2.18 shows the efficiency of a theoretical PA with three discrete DC voltages and the resulting efficiency of the PA when switching based on the desired P_o. The dotted and dashed lines indicate the efficiency of the PA should it be running on a corresponding fixed bias voltage, while the bold line shows the efficiency of the PA when it switches between the voltages. This method takes advantage of the higher efficiency at lower power levels at a lower bias voltage, making the PA more efficient over a wider range of output power levels.

A common alternative which is having a continuous, linearly amplified envelope signal as supply. This can be illustrated as switching between a high number of individual curves, minimizing the steps, and thus achieving a continuous, improved efficiency response. An example of this can be seen in figure 2.19. Comparing the two types of supply modulators, discrete supplies are often very efficient compared to continuous supply modulators due to minimizing resistive losses. Continuous voltage regulators however tend to be superior in high-speed, low-noise conversion, but are generally less efficient due to resistive regulation [1]. It is however possible to use what is called a hybrid supply, a combination of linear and discrete supplies, combining the advantages of both.

The PA efficiency of an ET PA is however not the overall efficiency of the transmitter for an ET system. The PA is no longer only consists of the RF amplifying transistor, but also incorporates the additional DC-DC converter or envelope amplifier. This is also a component which has a given power drain and a component which is not perfectly efficient. Thus the power saved by improving the efficiency of the PA has to outweigh the added power consumption introduced by the EA for the solution to be worth the hassle.

2.7.2 High-PAPR Signal Properties and Statistics

A lot of common modulation schemes not only vary slightly in amplitude, but also have a quite large peak-to-average power ratio (PAPR). Multi carrier systems, e.g. OFDM exhibits a very large PAPR, as it increases with the amount of carriers [16]. Figure 2.19 shows the output power PDF histogram for a hypothetical modulation scheme, and PAE levels for a PA at fixed and reduced supply levels. The histogram is showing a PAPR of 6 dB.

For a signal to be amplified equally for all amplitudes, peak amplitudes should be no higher than the 1 dB compression point, thus making the average amplitudes operating with an efficiency equal to the corresponding back off level. When operating at a fixed supply the efficiency can be seen from the rightmost PAE curve to be significantly reduced, as the PA will not be saturated. By applying a different supply voltage, the efficiency can be raised at the average power level, however the required peak output will not be obtainable at a lower supply voltage. Thus by dynamically varying the PA supply the PA can be forced to operate in saturation for a larger dynamic range, yielding a PAE trajectory as shown in red in figure 2.19. This figure shows the η_{PAE} for max static supply voltage in green, along with the η_{PAE} at reduced supply levels in blue. When comparing the η_{PAE} for static supply and η_{PAE} when tracking along the red trajectory, significant improvement can be

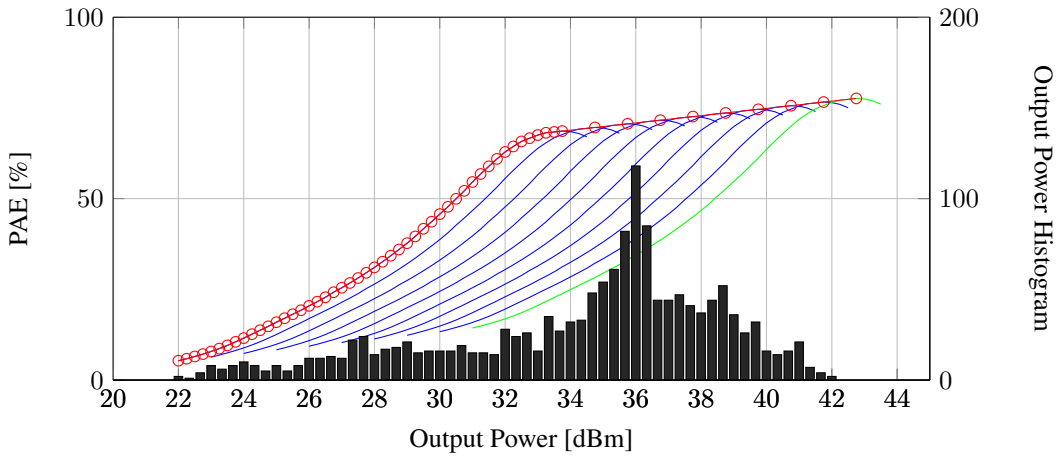

Figure 2.19: PAE for PA for various supply voltage levels and ET trajectory and output power PDF histogram.

confirmed, most notably for the most frequent occurring levels of P_{out} between around 34 and 39 dBm. This is an extreme, mocked up example made for illustrational purposes, realistic solutions give less net improvement and not quite as far into back off.

The signal corresponding to the probability density function in figure 2.19 is a hypothetical QAM signal, which commonly have PAPR in the range from 3 to 6 dB [1], depending on order and coding. A wide variety of modern communication standards are however based on OFDM, having an even greater PAPR, sometimes even as large as 13 dB [1] [17]. In addition OFDM based signals have Rayleigh PDFs, yielding a greater probability for the signal level to be close to the average, far away from the peak values, as shown in figure 2.20. The red curve here corresponds to a large PAPR signal, whilst the blue signal has a somewhat smaller PAPR.

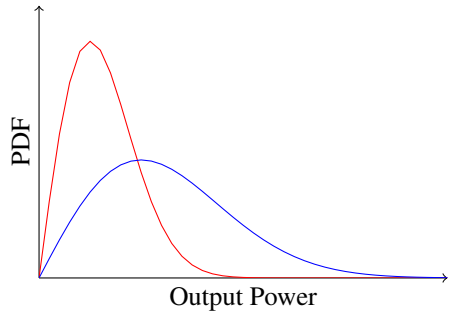

Figure 2.20: Examples of Rayleigh probability density functions (PDF).

2.7.3 Drawbacks and Challenges of Envelope Tracking

Added Power Dissipation

The overall efficiency of the PA will however be somewhat less improved, as it now also incorporates the Envelope amplifier (EA) to dissipate more power. Combining a high current supply and high bandwidth makes envelope trackers a challenge to design, resulting in designs with varying complexity and performance. However designs for modern cellular base stations fielding efficiencies approaching 90 % have been demonstrated [18].

The overall drain efficiency of an ET PA can be approximated as the product of the efficiencies of the static RF PA and the envelope amplifier

$$\eta_{ETPA} = \eta_{RFPA}\eta_{EA} \tag{2.50}$$

where η_{ETPA} is the instantaneous drain efficiency while tracked and η_{RFPA} the instantaneous drain efficiency at fixed supply of an arbitrary value. Thus to have an overall increase in efficiency compared to with static supply, i.e.

$$\eta_{ETPA} > \eta_{static} \tag{2.51}$$

the criterion for envelope amplifier efficiency, η_{EA} would be

$$\eta_{EA} > \frac{\eta_{static}}{\eta_{RFPA}} \tag{2.52}$$

where η_{static} is the efficiency at maximum static supply voltage, and η_{RFPA} the efficiency at lower, fixed supply voltages. It is thus essential for ET PAs to have an EA with η_{EA} as large as possible to not waste the efficiency improvement in η_{RFPA}. However an effective PA will reduce the necessary input power delivered by the EA, and thus help minimize the EA dissipated power.

Envelope Bandwidth and Shaping

A problem somewhat related to the problem with EA efficiency is the bandwidth of the EA. It is not only required to supply fairly large power, that is IV, but over a relatively large bandwidth. Considering a complex example signal $V(t)$,

$$V(t) = I(t) + jQ(t) \tag{2.53}$$

an in-phase, $I(t)$, and quadrature-phase, $Q(t)$, signal is combined to create a baseband signal with envelope signal $E(t)$ and phase signal $\phi(t)$, given as

$$E(t) = \sqrt{I(t)^2 + Q(t)^2} \tag{2.54}$$

and

$$\varphi(t) = arg\left(V(t)\right) \arctan\left(\frac{Q(t)}{I(t)}\right) \tag{2.55}$$

When mixed into RF, the real part will be transmitted, given as

$$S(t) = \Re\left(V(t) \cdot e^{j\omega_c t}\right) = \Re\left(E(t)e^{j\phi(t)}e^{j\omega_c t}\right) \tag{2.56}$$

where ω_c is the RF carrier frequency, yielding a passband phase component of

$$\Phi(t) = e^{j\varphi(t)}e^{j\omega_c t} \tag{2.57}$$

The RF envelope is thus equal to the baseband envelope given in (2.54), but the bandwidth of the envelope can be shown to be far wider than the bandwidth of the baseband signal [1]. For that reason the bandwidth of the envelope is one of the most important issues of high efficiency of an ET system is having an EA with sufficiently large bandwidth to modulate the supply correctly. Even though the requirement is not as great as for EER systems, the EA therefore becomes a bottleneck of wide bandwidth designs as it requires bandwidth at least three times greater than the RF bandwidth [3], which is often considered a rule of thumb [1]. There are however also cases where the bandwidth of the envelope can be expanded by as much as a factor of 10 [1], due to the nonlinear transformation of modern complex signals to the envelope signal. As a result, methods for increasing EA have been developed. Multiple alternatives exploit the possibility of adding a switched mode power supply, creating a Hybrid Supply, to boost the EA efficiency. This however increases complexity and requires high switching frequencies to suppress output ripple sufficiently, which again degrades efficiency [1].

Another alternative is more straight forward, dealing with the bandwidth itself by either increasing the modulator bandwidth or reducing the envelope signal bandwidth. This is done by shaping the envelope signal into a version with reduced bandwidth, removing the one-to-one relationship with the RF signal envelope and thus reducing the efficiency of the RF PA. This is a trade-off and has to be tuned or optimized for the efficiency improvement in the supply modulator to make up for the reduced efficiency improvement in the RF PA, to find the overall efficiency maximum. Reducing the bandwidth will also degrade the linearity somewhat. Simply low-pass filtering the envelope is not considered straightforward because it will alter the gain and linearity of the supply, and therefore more advanced

methods are required [1].

Shaping of the envelope is also used to properly obtain the desired trajectories regarding the performance metrics, such as maximum efficiency or flat gain trajectories. In practice, a fully linear supply modulation is not desirable as performance breaks down for supply voltages significantly lower than the voltage designed for as V_D approaches V_{knee}. Therefore a lower threshold for tracking is defined, often greater than the knee voltage so that the Supply voltage does not follow the envelope all the way into the shallowest troughs. This obviously impedes the performance somewhat, and the shaping has to be configured to achieve either optimum efficiency or linearity, by applying an EA transfer function as shown in figure 2.21. $V_{\text{sm out}}$ is the output of the supply modulator applied to the drain, and $V_{\text{sm in}}$ is the voltage of the input signal, found through the power as

$$V_{\text{sm in}} = \sqrt{50P_{in}} \tag{2.58}$$

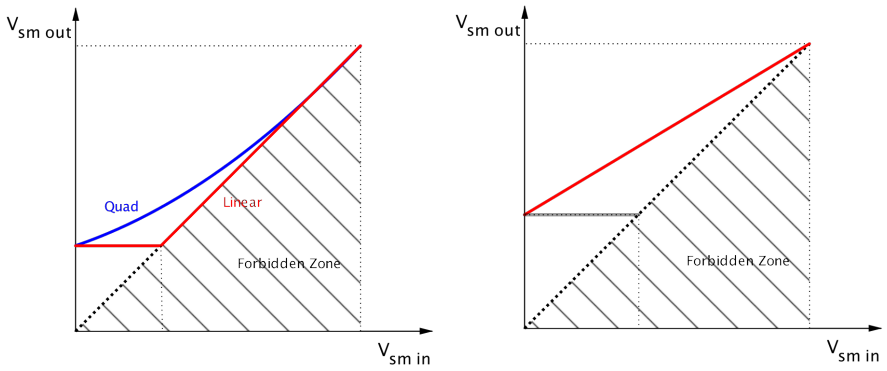

Figure 2.21: Supply modulator transfer function for (a) efficiency and (b) linearity.

Simply linear tracking will keep the RF PA in compression, for envelope voltages greater than a certain value, below which a constant voltage is applied, shown in figure 2.21a. This value is typically greater than the knee voltage of the PA, to avoid entering linear region where the output capacitance increases, causing the gain to collapse and introducing phase distortion. This sharp corner however expands the bandwidth, and instead a smoothed shaping can be applied, trading off some efficiency at lover levels. As an example, shown in figure 2.21a, the smoother transfer function is on the form of

$$V_{sm\,out} = aV_{sm\,in}^2 + V_{const} \tag{2.59}$$

tracking from the constant V_{const} at $V_{sm\,in} = 0$.

Shown in figure 2.21b is a supply transfer function trading off even more efficiency of the RF PA for better linearity, however having increased efficiency compared to static supply.

Removing the sharp turn in the tracking curve removes a significant amount of the high frequency power, and thus improves the efficiency of the supply, and reducing the need for extensive digital predistortion.

Both figures however have a forbidden region, where the supply voltage leads to operation at insufficient output power.

Linearity

Envelope tracking is mainly a technique developed for efficiency improvement, basically by increasing the dynamic range at which the PA operates in saturation. To achieve optimum efficiency deep saturation is often required, which is the operation mode where the PA is the least linear. This not only results in a distorted gain response and increased intermodulation, but also leads to strong non-linearities due to memory effects and imperfect drain supply.

In addition in order to achieve the correct tracking characteristics, the envelope signal has to be aligned with the correct RF phase. These requirements are however not as strict as for EER, but can still be a source for non-linearity in an ET PA unless an alignment functinonality is implemented.

The nonlinearity of the ET PA is a concern, and has to be corrected. A common solution, having powerful signal processors available, is digital predistortion, a solution however which can increase overall power consumption if extensive enough. It is however possible to use ET itself as a mild linearization technique. Instead of using the efficiency characteristics as a basis for tracking the PA, choosing maximum efficiency trajectories, it is possible to use the gain or power characteristics as a basis for tracking. By choosing a trajectory which yields a nicer overall gain characteristic, some efficiency can be traded off for extra linearity.

Chapter 3

Design and Simulation of GaN PA

3.1 Device Technology and Basis for Design

The PA this work concentrates on is a continuation or improvements of the PA covered in [19]. Similar to [19], the aim was to design a PA that could be suitable in an ET architecture, however a few improvements were deemed necessary. In order to reach the specifications in table 1.1 class-AB operation was still intended, using the same CREE CGH40010 GaN HEMT and microstrip lines with FR4 substrate, which has the properties in table 3.1. As CAD software Agilent's Advanced Design System was used along with a large signal model for the CGH40010 in order to perform the design of the PA.

Table 3.1: FR4 substrate properties.

Parameter	**Value**
Height, h	$1.6\,\text{mm}$
Dielectric loss tangent, $\tan\delta$	0.02
Dielectric permittivity, ε_r	4.4
Magnetic permeability, μ_r	1
Conductivity, σ_d	$5.96 \cdot 10^7$ S/m
Conductor thickness, T	$36 \cdot 10^{-6}$ m

Among the changes decided to be made, the most comprehensive was to discard the matching networks as conjugate match was performed, providing insufficient efficiency. As such new impedances would have to be mapped and matched to, using source and load pull benches developed by associate professor Morten Olavsbråten. This allowed to set the matched input and output reflection coefficients at the fundamental frequency, second and third harmonic with interpolated values in between whilst continuously considering the performance. By tuning these values while simulating, performance of the PA could be reviewed, allowing to find optimum reflection coefficients for a combination of high effi-

ciency, output power and gain.

Having to create new matching networks, a slight change in bias was also opted for, wanting to improve efficiency even more. From the previous bias current, $i_D = 220\ mA$, a lower bias current approaching $i_D = 150\ mA$ would possibly provide some more efficiency while not trading off too much gain. After running a IV-simulation of the transistor model in ADS, a bias current $i_D = 160\ mA$ was decided as it was in the desired range and showed nice performance when used with the load and source pull benches.

Furthermore, the DC feed networks, or RF-chokes from figure 2.7, were decided to be modified, by making the $\lambda/4$-transmission line narrower in order to slightly increase the input impedance from the PA, as in [19] it was more than wide enough.

3.2 Stabilisation and DC-feed Networks

As the matching networks were to be redesigned, small alterations were made to the stabilisation part on the gate of the transistor, consisting of a lumped RC filter for stabilization and transmission lines for connecting the filter to the gate, bias-T and output. The microstrip line dimensions were slightly reduced, as there was plenty of room for the lumped RC-filter providing the stabilization and transmission lines could be.

In addion DC-feed networks were redesigned, the aim being to increase the input impedance by using a high-impedance transmission line as opposed to a $50\,\Omega$ line used in [19]. Thus the general design, shown in figure 3.1, consisting of two $\lambda/4$-transmission lines would still be used. At fundamental frequency the open-circuit at the end of the $\lambda/4$-fan is transformed to short in the intersection between the fan and the $\lambda/4$-transmission line, which again transforms the short into open where the network is connected to the PA. Thus there will be little or no RF leakage through the feeding networks.

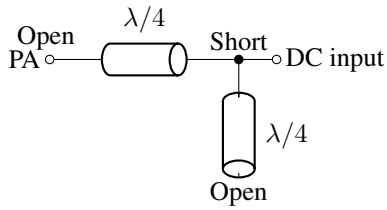

Figure 3.1: General bias-T design.

The gate and drain DC feed networks were designed separately as the drain network also incorporated a second fan stub, tuned to be $\lambda/4$ at $2f_0$. As the $\lambda/4$-line at f_0 is approximately the same length as a $\lambda/2$-line at $2f_0$, the DC-feed network would have very low input impedance seen from the PA, allowing to short second harmonic components from

the output of the PA. The design was done in turns of one component at a time, starting with the fan stubs and T-section on the gate side, and X-section on the drain side. The length and angle were tweaked and optimized for minimum input impedance at f_0, having a constant width of the X-section of $1\,mm$. The LineCalc tool in ADS was then used to find the characteristic impedance of a $1\,mm$ wide transmission line with the FR4 substrate parameters, and thereafter finding the physical length of a $\lambda/4$-line with the resulting impedance. This line was then added to the design, which was slightly optimized to achieve the largest possible input impedance at f_0. For the DC-feed network on the drain side, attention was also paid to $2f_0$, where low impedance was desired. An additional line was then attached to the T and X-sections where decoupling capacitors were connected, and at the end, DC input. For the gate DC feed the length of the $\lambda/4$-line was reduced by 1 mm as a 1 mm long, $10\,\Omega$ resistor was to be added at the PA entrance of the DC-feed network for stability.

At this point the component values of the RC-filter on the gate of the transistor was kept at $R = 22\,\Omega$ and $C = 3.3\,pF$ as it had yielded sufficient stability thus far. The values would however be changed to $R = 33\,\Omega$ and $C = 3.6\,pF$ during mapping of the optimal source impedance, as it would give a slightly different input impedance that proved easier to create a matching network for. The respective cut-off frequency for the filter would also be somewhat smaller, from (2.31)

$$f_c = \frac{1}{2\pi \cdot 33 \cdot 3.6 \cdot 10^{-12}} \approx 1.34 \text{ GHz} \tag{3.1}$$

as opposed to 2.2 GHz in [19], which quite possibly was too close to the operational frequency.

The unmatched part of the PA is shown in figure 3.2, with the component values and transmission line dimensions listed in table 3.2.

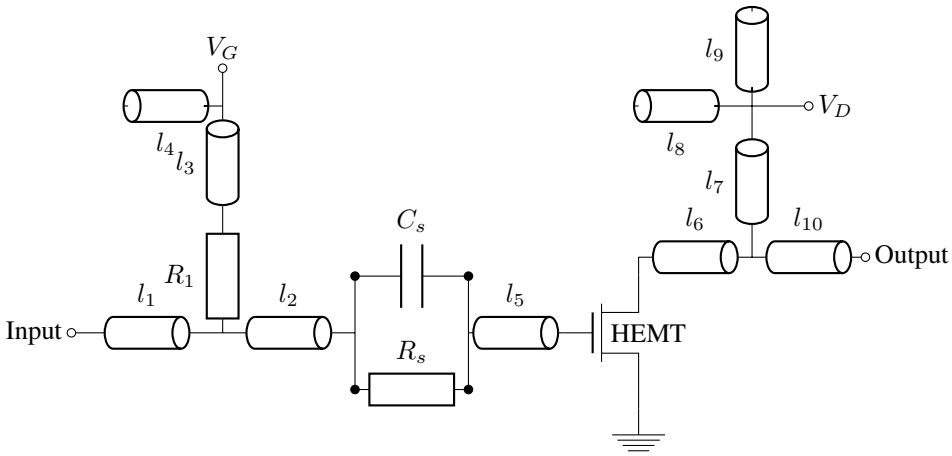

Figure 3.2: Unmatched PA.

Table 3.2: List of component values and transmission line dimensions for unmatched PA design in figure 3.2.

Component	Values	Comment
R_1	$10\,\Omega$	
R_s	$33\,\Omega$	Stabilization
C_1	3.6 pF	Stabilization
l_1	$l = 1.0$ mm, $w = 2.25$ mm	Taper on input side not shown
l_2	$l = 1.0$ mm, $w = 2.25$ mm	
l_3	$l = 16.97$ mm, $w = 1.0$ mm	$\lambda/4$ at f_0, shortened 1 mm due to R_1
l_4	$l = 11.27$ mm, $\angle = 93°$	$\lambda/4$ fan stub at f_0
l_5	$l = 3.0$ mm, $w = 2.25$ mm	
l_6	$l = 2.8$ mm, $w = 3.04$ mm	
l_7	$l = 17.97$ mm, $w = 2.25$ mm	$\lambda/4$ at f_0
l_8	$l = 6.26$ mm, $\angle = 46.35°$ mm	$\lambda/4$ fan stub at $2f_0$
l_9	$l = 10.80$ mm, $\angle = 44.26°$ mm	$\lambda/4$ fan stub at f_0
l_{10}	7.3 mm, $w = 3.04$ mm	

3.3 Matching Networks

3.3.1 Source and Load Pull

The first step of the impedance matching process was to find the desired impedances which when matched to yield the optimal performance. The design shown in figure 3.2 was connected with source and load pull instances in figure 3.3 on the input and output respectively. Using these would make it possible to simulate and find the optimal Γ_S and Γ_L for to which the design in figure 3.2 would be matched to. This design was then used in an ADS standard harmonic balance (HB) test bench, HB1TonePAE_Pswp, where the respective design is simulated using a single tone input with a specified frequency, sweeping the power. By tuning the input parameters of the source and load pull benches, it was possible to review the resulting performance, most notably P_{out}, G_T and η_{PAE}.

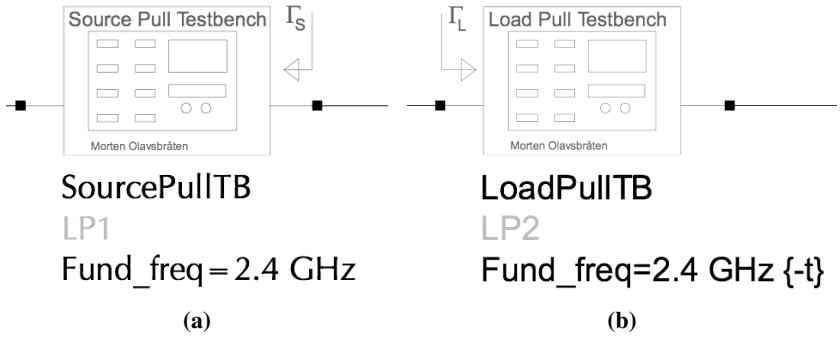

Figure 3.3: ADS source pull (a) and load pull (b) instances.

Initially the source impedance was tuned from the point where the DC-feed is connected, as shown in figure B.3. This was done while leaving the load at $\Gamma_L = 0.4\angle -180^\circ$ as a start value as it approximately corresponds to the reflection from a load line resistance $R_L = 20\,\Omega$. $|\Gamma_{S,\,f_0}|$ was then swept from -180° to 180° in steps of 20°, at amplitudes 0.2, 0.4, 0.6 and 0.8, noting the gain at every combination. The combination yielding the largest G_T, was then used as basis for further tuning by tuning $|\Gamma_{S,\,f_0}|$ and $\angle\Gamma_{S,\,f_0}$ about one another until no increase was possible. Tuning of Γ_S was therefore done in order to maximize G_T, as it had very little impact on P_{out} and η_{PAE}.

Similar methodology was used for tuning Γ_L on the output. In this case the goal was to increase, and maximize P_{out} and η_{PAE} without trading off too much gain. According to the HB simulations, max P_{out} was found to not correspond to the same Γ_L which yielded max η_{PAE} and therefore a compromise was made. A Γ_L such that $P_{out} = 40.7\,dBm$ was chosen to leave some headroom for the specifications, in case the prototype did not match simulations perfectly. This reflection coefficient corresponded to $\eta_{PAE} = 65\,\%$ and $G_T = 15\,dB$ after small adjustments had been made to Γ_S and Γ_L to squeeze out a little more, as the input and output impedances would change slightly when tuning Γ_L and Γ_S respectively. The load pulling was performed with an added $10\,mm$ $50\,\Omega$-line, l_6 and l_{10} as seen in figure 3.2, attempting to reduce the complexity of the output matching network by determining the transistor side transmission line and DC-feed entry from the start.

The resulting source and load reflection coefficients that the PA was matched to were

$$\Gamma_S = 0.6\angle -110^\circ \tag{3.2}$$

and

$$\Gamma_L = 0.5\angle -100^\circ \tag{3.3}$$

3.3.2 Design of Microstrip Matching Networks

The topologies of the matching networks were determined using the Smith Chart tool in ADS. In order to do this, the reflection coefficients in (3.2) and (3.3) were converted to their respective impedances, rearranging (2.7) to give their respective impedances

$$Z_S = \frac{1+\Gamma_S}{1-\Gamma_S} = 18.05 - j31.845\,\Omega \tag{3.4}$$

and

$$Z_L = \frac{1+\Gamma_L}{1-\Gamma_L} = 26.34 - j34.585\,\Omega \tag{3.5}$$

For the input, Z_S^* was matched to $50\,\Omega$ with the design in figure 3.4, and $50\,\Omega$ was matched to Z_L^* with the design in figure 3.5 in the smith chart tool. The input of the PA is here connected to the left terminal of the input matching network, and the right terminal is connected to the gate network of the design. For the output matching network, the drain is connected on the left side and the output on the right so that the transistor with the accompanying design can be put in the middle to obtain a matched PA.

The topologies found using the smith chart tool are considering ideal lines and does not include effects from the microstrip T-sections used to branch out the stubs. Therefore the matching networks, including T-sections had to be modified. This was done by optimization against desired S-parameters and input impedances, calculated using the Z-in S-parameter module. For both matching networks the S-parameter optimization goals were $S_{11} = S_{22} = -50$ dB and $S_{21} = 0$ dB at 2.4 GHz. Obviously, the goals were not met, but the general idea of aligning the peak of S_{21} and the dip in S_{11} at 2.4 GHz. The impedance goals, which in theory should not be needed, were set to equal the impedances in (3.2) and (3.3) for the transistor side on the input and output matching networks respectively, and $50\,\Omega$ on the input/output ports. After achieving satisfactory performance with no improvement possible, microstrip tapers were added on the side of each of the transistors, and a last optimization was performed.

The resulting matching networks are shown in 3.4 and 3.5, with T-sections and tapers excluded for simplicity. ADS excerpts are shown in appendix B.

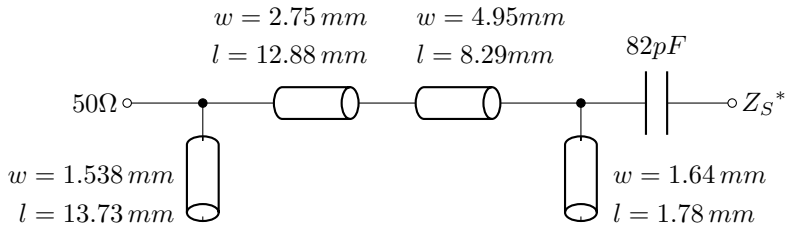

Figure 3.4: Resulting input matching network.

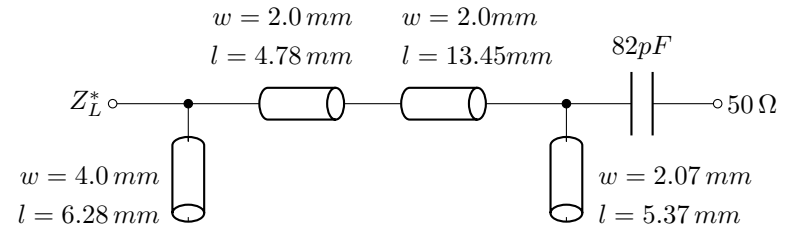

Figure 3.5: Resulting output matching network.

3.4 Simulations

3.4.1 DC-feed Networks

Simulation of the PA was done in several steps. The bias feeds and matching networks were simulated as they were being designed to verify correct behavior. The simulated s-parameters of the gate and drain bias feeds are shown in figures 3.6 and 3.7 respectively with their corresponding input impedances in figures 3.8 and 3.9. All the simulation results are done with the final DC feed design using FR4 microstrip models with the substrate properties in table 3.1.

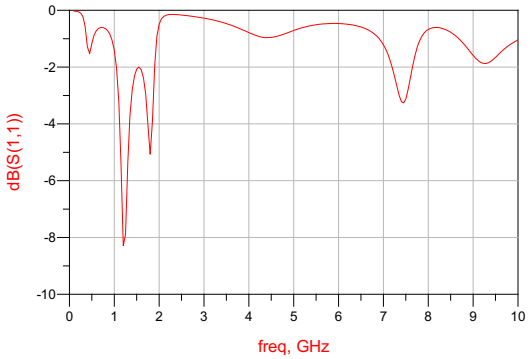

Figure 3.6: Simulated s-parameters of gate bias network vs. frequency.

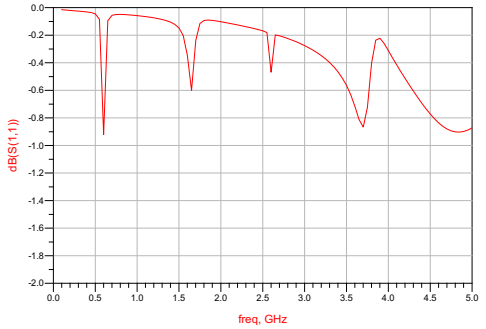

Figure 3.7: Simulated s-parameters of drain bias network vs. frequency.

The simulated input impedances in figures 3.8 and 3.9 show the impedance seen by the PA, with a DC source, ideally ground, connected on the far side.

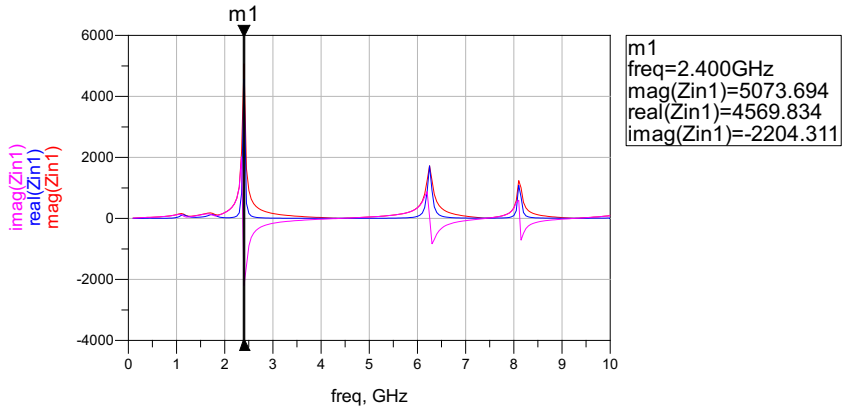

Figure 3.8: Simulated input impedance of gate bias network vs. frequency.

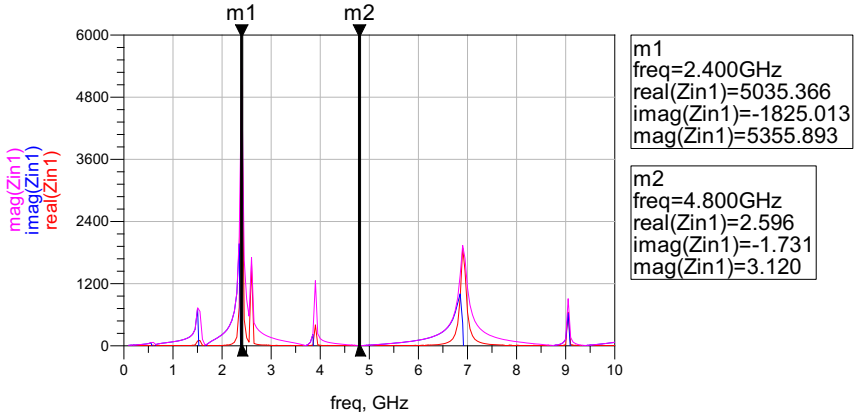

Figure 3.9: Simulated input impedance of drain bias network vs. frequency.

3.4.2 Matching Networks

As with the DC-feed networks, the input and output matching networks were simulated during the work in order to verify the design and obtain as good results as possible. Figures 3.10 and 3.11 show the s-parameters and input impedances of the input matching network isolated, with port 1 being the $50\,\Omega$ source, and port 2 being the unmatched PA gate side. Similarly, figures 3.12 and 3.13 show the s-parameters and input impedances of the output matching network, with an opposite port configuration compared to the input matching network - port 1 being the unmatched PA drain side, and port 2 being the $50\,\Omega$ output. The simulation results are for the final matching network designs using FR4 microstrip models with the substrate properties in table 3.1.

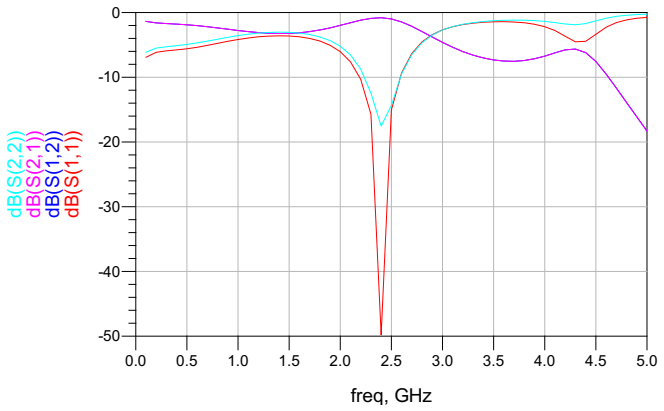

Figure 3.10: Simulated s-parameters of input matching network vs. frequency.

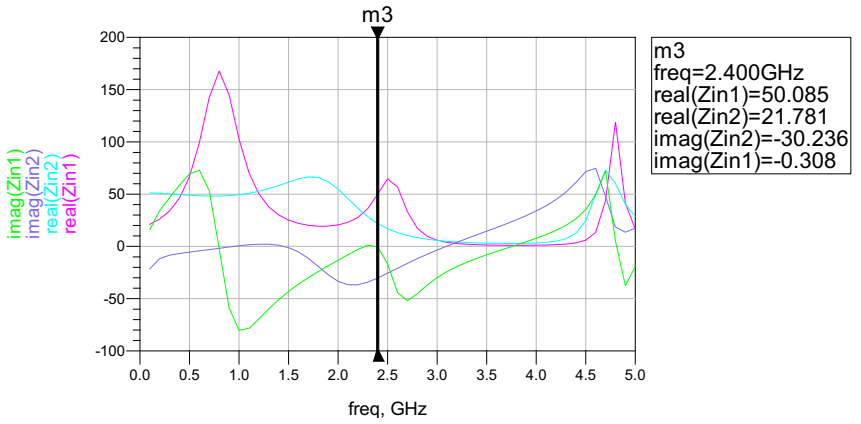

Figure 3.11: Simulated input impedances of input matching network vs. frequency.

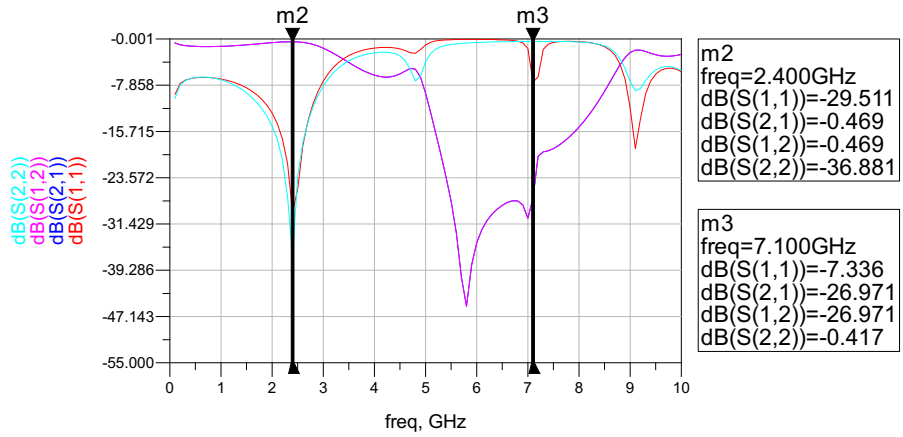

Figure 3.12: Simulated s-parameters of output matching network vs. frequency.

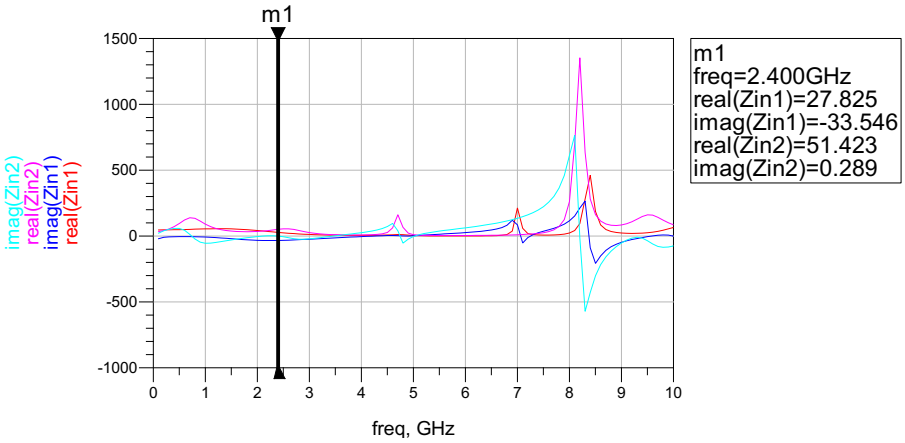

Figure 3.13: Simulated input impedance of output matching network vs. frequency.

3.4.3 Complete Design

Once the matching networks showed the correct impedances and S-parameters, the full PA design was completed by adding the matching networks to the PA design, running a s-parameter simulation to verify unconditional stability. When the μ-factors seen in figure 3.14 was achieved, complete simulations were performed. Relatively high μ can be seen, having a low extreme $\mu = 1.043$ at 3.0 GHz, but at most frequencies staying above 1.150.

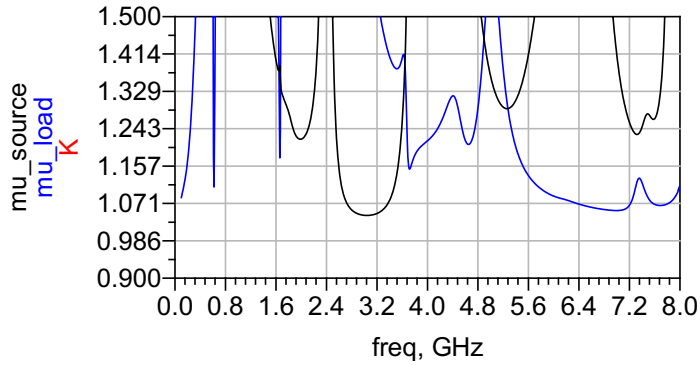

Figure 3.14: Simulated μ (source) and μ' (load) vs. frequency.

The simulated s-parameters are shown figure 3.15, with port 1 being the input and port 2 being the output. At 2.4 GHz, a $|S_{11}| = -19$ dB and $|S_{21}| = 14.3$ dB can be seen.

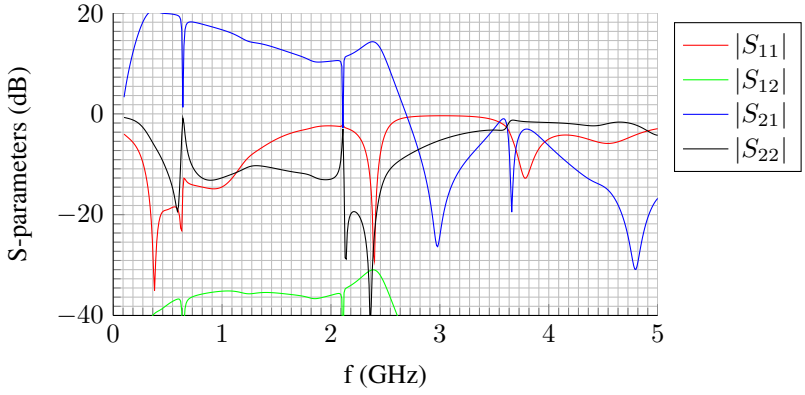

Figure 3.15: Simulated s-parameters of full PA design vs. frequency.

Finally the end design was simulated using the same harmonic balance simulation testbench that was used in the load and source pulling, with the microstrip matching networks replacing the load and source pull benches. The resulting power gain, output power and η_{PAE} is shown in figures 3.16, 3.17 and 3.18 respectively. For the complete design, a flat gain of $G_T = 14.8$ dB and $G_T = 12.8$ dB at 38 dBm output power, where the PA is starting to enter compression. In addition, peak values of $P_o = 40.9$ dBm and $\eta_{PAE} = 61.5\,\%$ were achieved in simulations.

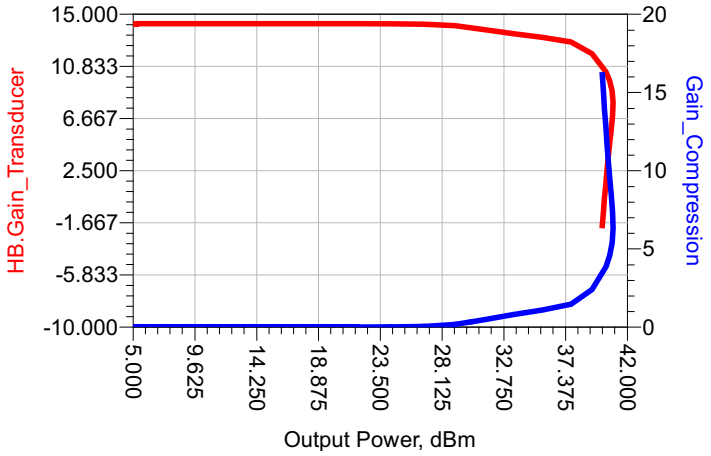

Figure 3.16: Simulated G_T and gain compression vs. output power.

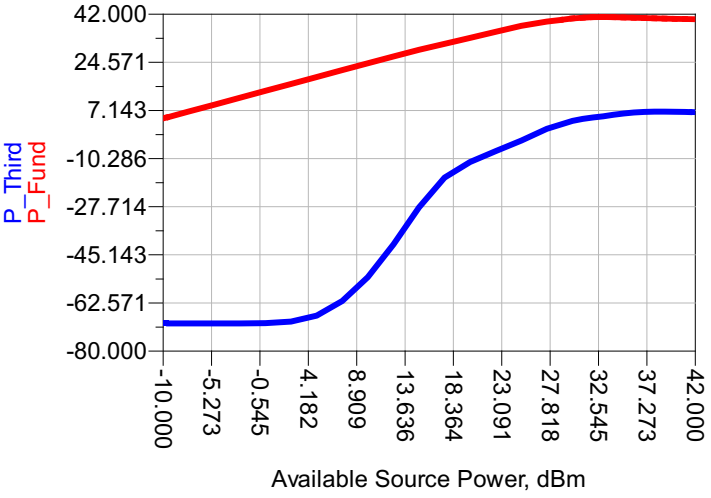

Figure 3.17: Simulated fundamental and third harmonic P_o vs. input power.

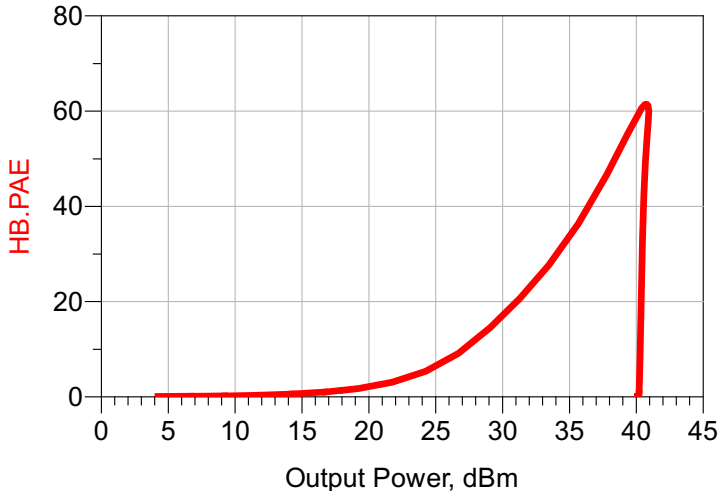

Figure 3.18: Simulated η_{PAE} vs. output power.

3.5 Fabrication of Prototype

In order to produce a prototype of the PA, gerber files for milling the microstrip had to be generated. The design was collected in one single file, eliminating all sub-designs such as the matching and DC-feed networks. Thereafter the lumped components were replaced with microstrip step models, in case they had not already been included. All lumped components that were to be used were 0603 size, except from some of the decoupling capacitors, which were 1208, therefore gap lengths of 1 mm were used. Thus the complete microstrip was converted from schematic to layout design, which is the basis for the milled design.

The design was intended to fit on a lab standard 85x85 mm^2 aluminium cooling plate. As such boundaries were drawn in the bound:drawing layer, to define the outer edges of the PCB and correspond with the cooling plate. In order to get thermal and electric conduction, the transistor also needs contact with the cooling plate, and therefore the boundary layer was used to define the hole in the microstrip PCB where the transistor would be placed.

The main RF path was then aligned with the SMA contacts at the end of the cooling plate, and $50\,\Omega$ lines were added for the PA to reach the SMA contacts. Also the DC feeds were aligned one on each side of the RF path to avoid getting the fan stubs too close to each other, and the corners and sections far away from the circuit design were filled using the conductor layer, to use as ground planes and hopefully make milling of the PCB take a little less time. Ultimately holes were defined to overlap with the ones in the cooling plate to make attachment with screws possible.

The layout design was exported as gerber/drill files, which by appointment were handed to the Elprolab at NTNU, performing the milling. Once milled, lumped components, simple DC-cables, the transistor and SMA-contacts were soldered on, and the PCB was attached to the cooling plate. As RF capacitors, Johanson S-series EIA 0603 ceramic capacitors [20] in addition to 1% 0603 SMC resistors from Distrelec. Decoupling was done using the capacitors in table 3.3 on both the gate and drain sides of the PA, in the same order as listed in the table with the 10 pF Johanson being the closest to the fan stubs and the 10μF Murata the closest to the DC cable. The 10 pF was made sure to be as close to the intersection between the DC-feed $\lambda/4$-line and the fan stubs, but for the drain side this was not possible due to the double fan design. It therefore had to be installed at a distance from the intersection.

Table 3.3: Capacitors used for decoupling PA.

Capacitance	**Type**
10 pF	Johanson 0603
47 pF	Johanson 0603
82 pF	Johanson 0603
1 nF	Distrelec 0603
100 nF	Murata 0603
10 μF	Murata 1208

Chapter 4

Measurements

In order to test the performance of the PA, measurements were performed at the NTNU microwave laboratory. S-parameters were measured by performing using a vector network analyzer (VNA) and the power related performance by doing a P_{in}-P_{out} sweep. Before this could be done, a visual confirmation of stable operation was performed. This was done by examining the output power spectrum with a Signal Analyzer, using the same output coupler termination as shown in figure 4.1, but without a RF drive signal, with both unterminated and $50\ \Omega$ terminated input connector. The PA was confirmed to have no spurious components, and was also left on for about 15 minutes to check if oscillations would occur with increasing temperature. No oscillations were detected, thus unconditional stability could be assumed and measurements commence.

4.1 Output Power Sweep

The power performance of the PA examined by sweeping input power and measuring the output power, using the setup in figure 4.1. A Rohde & Schwarz SMU200A vector signal generator was used to generate a signal, whose power was swept and, the output power of the PA was measured by a Rohde & Schwarz FSQ40 Signal Analyzer.

The signal generator was not able to supply a signal with sufficient power to drive the PA fully into compression, as that would require a PA input power exceeding 30 dBm. Therefore a driver, or buffer PA was required, and a previous wideband linear prototype PA based on the same Cree CGH40010 HEMT was used, and insufficient input power would not be a problem. To avoid damaging the driver in case of any reflections from the DUT PA, a circulator was included. This is a triport device that for a certain frequency band transmits from one port to only one of the other two. A circulator is shown in figure 4.2, where incident waves on port 1 go to port 2, while incident waves on port 2 go to port 3. The circulator used had a forward loss of approximately -0.5 dB, which was included in the characterization of the driver.

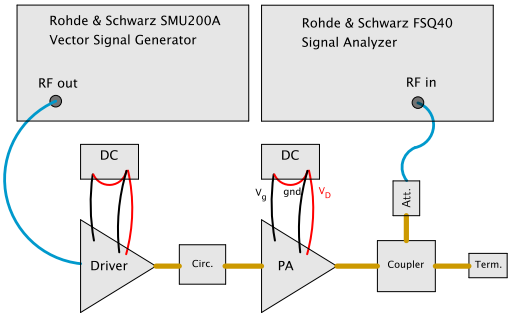

Figure 4.1: Power sweep measurement setup.

In addition some passive loss was included on the output of the DUT PA, as the signal

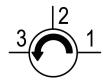

Figure 4.2: Circulator port configuration.

analyzer has a maximum input power of 30 dBm, which is quite a bit less than the output power the PA was designed for. This was done using a directional coupler, which splits the signal between two ports. The signal analyzer was connected to a port having a 10 dB loss compared to the input, and was further attenuated using a 10 dB, 2 W attenuator, which should give more than 10 dB headroom for the limit on the signal analyzer. The third port on the coupler was terminated with a 25 W rated termination load, dissipating the rest of the signal.

Single-tone measurements were then performed, sweeping the input power from -10 to 22 dBm VSG output power, at 2.30 GHz, 2.35 GHz, 2.4 GHz, 2.45 GHz and 2.50 GHz and measuring the output power and DC drawn by the PA. Similarly a two-tone measurement was done, with input signal consisting of two frequencies with 5 MHz spacing equally spaced around 2.40 GHz. Matlab was used for automatization of the measurements, communicating with the instruments over GPIB. Scripts were generated for looping VSG output levels and signal frequencies, while reading measured power and drain current for each level.

Thereafter, in order to estimate the performance in an envelope tracking setup, single-tone power sweeps at 2.4 GHz were performed, while sweeping the supply voltage in steps of 2 V. The same setup as for the regular single-tone and two-tone measurements were used, shown in figure 4.1, but the Matlab scripts were slightly modified. Functionality for communicating with the TTi CPX200DP power supply that was used already added was included in the previous single-tone measurements, but not used for setting the supply voltage. This was added such that the supply voltage could be swept for every even value of V_D between 4 and 28 V. A similar single-tone power sweep was then performed for

every supply voltage level, however only at 2.4 GHz.

Following the measurements of the PA, the output coupler loss and the driver had to be characterized, and Matlab was used for sweeping these for the same VSG output power as for the DUT PA. First the loss of the cable between the VSG and the driver was measured as,

$$L_{pass,in}\ [\text{dB}] = P_{FSQ} - P_{SMU} \tag{4.1}$$

where P_{FSQ} is the power measured by the signal analyzer, and P_{SMU} is the power of the signal generator both in dBm. The coupler loss on the output of the PA could thus be found as

$$L_{pass,out}\ [\text{dB}] = P_{FSQ} - P_{SMU} - L_{pass,in} \tag{4.2}$$

with the setup in figure 4.3 and the driver output power as

$$P_{driver}\ [\text{dBm}] = P_{FSQ} - L_{pass,out} \tag{4.3}$$

which included the loss through the circulator. P_{driver} could thus be used as the input power for the DUT PA, used for calculation of gain and PAE. Ideally input power would be measured during the DUT PA measurements themselves, but the only RF power meter at the lab was already being used in other ongoing measurements. A quick measurement was however possible, measuring the difference in actual power of the signal, and the values indicated by the signal generator and signal analyzer.

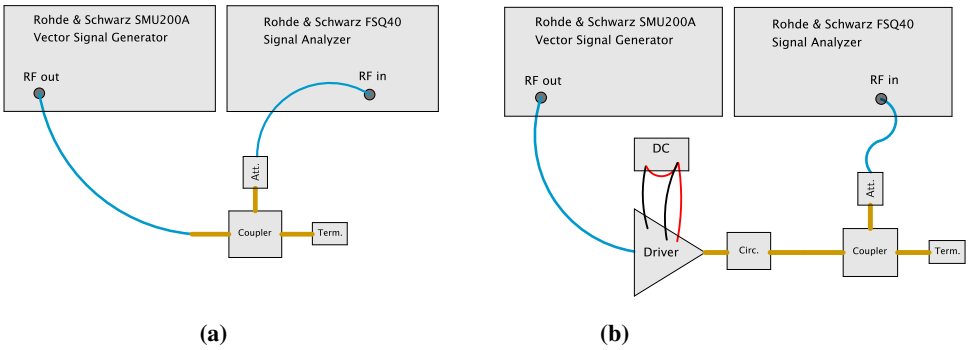

Figure 4.3: Setup for characterisation of output termination (a) and driver (b).

Having characterized the losses of the passive components and the gain of the driver PA the measurement data of the DUT PA had to be corrected to achieve the correct output power and be able to calculate the gain and PAE of the PA. This was all done in Matlab, as this was an easy and efficient option and the data had already been measured using Matlab. The calculated output power would be given as

$$P_{out}\ [\text{dBm}] = P_{FSQ} - L_{out} \tag{4.4}$$

where P_{FSQ} is the power measured by the signal analyzer and L_{out} is the output passive loss from (4.2). Having measured this, calculation of available gain and PAE of the PA was possible. The available gain of the PA calculated as

$$G_A \text{ [dB]} = P_{out} - P_{driver} \tag{4.5}$$

where P_{driver} is the output of the driver found in (4.3) and P_{out} the measured output power. The PAE of the PA would be given as

$$\eta_{PAE} \text{ [\%]} = \frac{10^{\frac{P_{out}-30}{10}} - 10^{\frac{P_{driver}-30}{10}}}{V_D I_{drain}} \tag{4.6}$$

using the drain current I_{drain} in ampere and supply voltage V_D in volts. Both P_{out} and P_{driver} were given in dBm, and had to be converted to W, the same as $I_{drain}V_D$, in order for η_{PAE} to be calculated.

4.2 S-parameters

In addition to the power sweeps, an S-parameter characterization was performed using a vector network analyzer (VNA), as shown in figure 4.4. No driver PA was used as this would make measurement of the input S-parameters, S_{11} and S_{21} impossible. Also, being a small signal measurement, the extra gain was not needed. The same attenuation as in the large signal power sweeps was used even though the VNA power level of -20 dBm was used, as the VNA has a maximum power rating of 30 dBm and damaging the VNA would be regrettable.

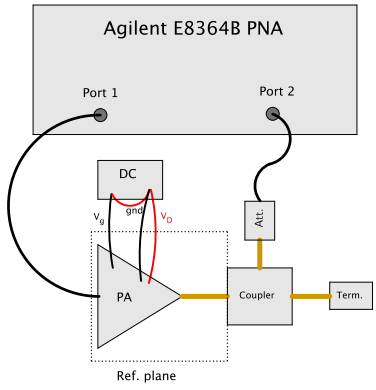

Figure 4.4: S-parameter measurement setup.

SOLT calibration of the VNA was performed with the coupler-attenuator attached to port 2, accounting for the loss introduced. The measured S-parameters would therefore be correct at the entrance of the coupler, not the VNA cable, marked as 'reference plane' in figure

4.4. With the PA connected and warmed up, S-parameters were measured and dumping of data was done using the software WinCal XE, and dumped to SnP-files for analysis in Matlab.

Complete list of all the equipment used during the measurements is given in table 4.1.

Table 4.1: Equipment used in measurements.

Equipment	**Name**
VNA Calibration Kit	HP 85052D2
VNA Cables	HP 08515-60003
Network Analyzer	Agilent E8364B
Signal Analyzer	Rohde & Schwarz FSQ40
Vector Signal Generator	Rohde & Schwarz SMU200A
RF Power Meter	Anritsu ML2438
Power Supply DUT	TTi CPX200DP
Power Supply buffer	TTi CPX200DP
Circulator	MCLI CS-144-32 2-6 GHz
-10 dB Coupler	ATM P/N C124H-10, SMA, 2-18 GHz
-10 dB Attenuator	Huber+Suhner 5910_ SMA-50-010, SMA, DC-18 GHz, 10 W
RF Termination	ATM PNR T2516, DC-12 GHz, 25 W
RF Cables	Huber+Suhner Sucoflex ex 100

Chapter 5

Results and Envelope Tracking

Having performed the measurements as described in chapter 4, comparison between the performance of the PA and the specifications was possible. Table 5.1 shows the specified parameters, and their simulated and measured values. Center frequency is the frequency at which the PA is optimized for operation, where the specifications for input reflection, output power and available gain applies. The 1 dB bandwidth is defined as the frequency range around the center frequency with less than 1 dB gain than at the center frequency.

Table 5.1: Comparison between specified parameters and their simulated and measured values.

Parameter	**Specification**	**Simulated**	**Measured**
Center frequency, f_0	2.4 GHz	2.390 GHz	2.395 GHz
1 dB bandwidth, $B_{1\text{ dB}}$	$<$ 100 MHz	145 MHz	150 MHz
Input reflection, $\lvert S_{11}\rvert$	< -10 dB	-29.2 dB	-14.0 dB
Output power at compression, P_{o_1}	$>$ 40 dBm	40.9 dBm	41.7 dBm
Available gain, G_A	$>$ 12 dB	12.7 dB	12.2 dB

The simulated and measured values for P_{o_1} is the maximum achievable single-tone output power, at 3 dB compression, while the values for G_A is the single-tone gain at the point where compression is starting to appear, that is at $P_{o\_1} = 38.0$ dBm. The values for $\lvert S_{11}\rvert$ are the values at 2.4 GHz.
Parameters that were not specified to be in any range, but are necessary in order to describe the performance of the amplifier correctly, are included in section 5.1.

5.1 Static Supply

The small and large signal characteristics of the PA operating from a static 28 V rail is shown in table 5.2. Specifications are included in table 5.1. The center frequency is the

Table 5.2: Complete list of measured parameters under static operation.

Parameter	Simulated	Measured
Center frequency, f_0	2.390 GHz	2.395 GHz
1 dB bandwidth, $B_{1\text{ dB}}$	145 MHz	150 MHz
Peak single-tone output power, P_{o_1}	40.9 dBm	41.7 dBm
Peak two-tone output power, P_{o_2}	40.0 dBm	39.2 dBm
Peak single-tone drain efficiency, η_1	71.6%	78.0%
Peak single-tone PAE, η_{PAE_1}	61.5%	68.2%
Peak two-tone PAE, η_{PAE_2}	47.0%	56.3%
Single-tone 1 dB compression point, $P_{1\text{ dB},1}$	40.0 dBm	41.0 dBm
Two-tone 1 dB compression point, $P_{1\text{ dB},2}$	37.8 dBm	38.5 dBm
Third-order intermodulation, IMD_3	-11.0 dBc	-18.9 dBc
Single-tone Available gain, $G_{A,1-tone}$	12.8 dB	12.2 dB
Two-tone Available gain, $G_{A,2-tone}$	11.5 dB	10.2 dB
Input reflection, $\|S_{11}\|$	-29.2 dB	-14.0 dB
Small signal gain, $\|S_{21}\|$	14.3 dB	14.1 dB

frequency at which the PA is designed for operation, and all parameters in table 5.2 are supplied for this frequency, with exception of the two-tone parameters, where a signal consisting of two-tones at 2.395 GHz and 2.405 GHz was applied. $B_{1\text{ dB}}$ is still the frequency range with less than 1 dB gain compared to the center frequency.

The peak output power levels, P_{o_1} and P_{o_2} are both the peak output power, measured at $P_{i\_1} = 33.1$ dBm and $P_{i\_2} = 29.0$ dBm respectively. For the two-tone signal this value corresponds to the tone power, which with two-tones of equal power yields a peak envelope power 3 dB higher. Figure 5.1 shows the single-tone output power for corresponding input power values at 2.30, 2.35, 2.4, 2.45 and 2.50 GHz respectively. This figure shows that the peak output power at f_0 is $P_{o\_1} = 41.68$ dBm, for $P_{i\_1} = 33.07$ dBm. The peak values at the other respective frequencies are also shown to be at approximately this input power, but with lower output power due to the reduced gain. The 1 dB compression point, $P_{1\text{ dB},1}$, can be found, as illustrated in figure 2.9, to be $P_{1\text{ dB},1} = 41.0$ dBm output power, for $P_{i\_1} = 30.50$ dBm.
The single-tone available gain of the amplifier is plotted in figure 5.2 at the frequencies of 2.30, 2.35, 2.4, 2.45 and 2.50 GHz.
At all the frequencies the same general characteristic can be considered, however at lower levels for the frequencies furthest away from f_0, as can also be seen as lowered output power in figure 5.1. At f_0 however the, $G_A = 12$ dB for $P_{o\_1} = 38.5$ dBm, and the 1 dB compression can be confirmed to be at $P_{o\_1} = 41.0$ dBm, where $G_A = 10.5$ dB. The peak output power, $P_{o\_1} = 41.68$ dBm is reached in deep compression, with $G_A = 8.5$ dB, dropping quickly.

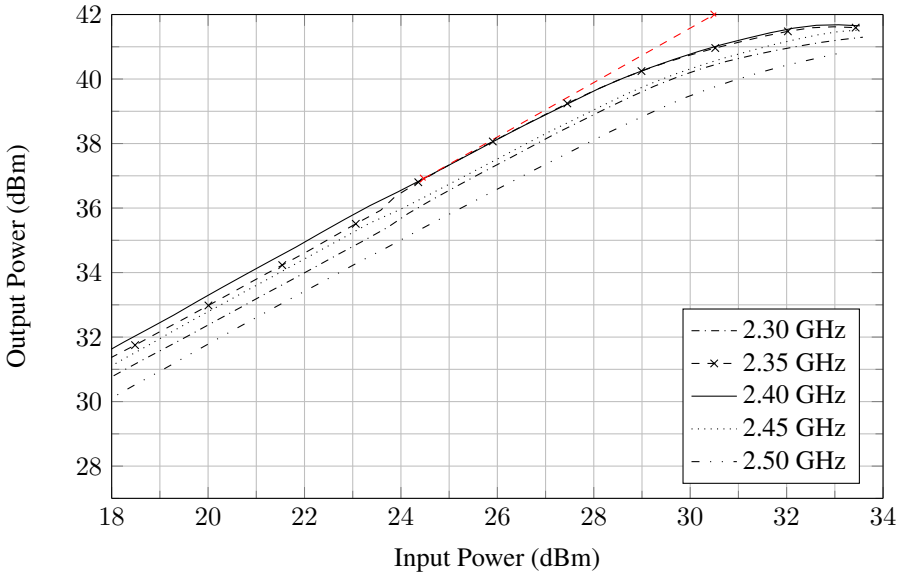

Figure 5.1: Single-tone output power characteristics.

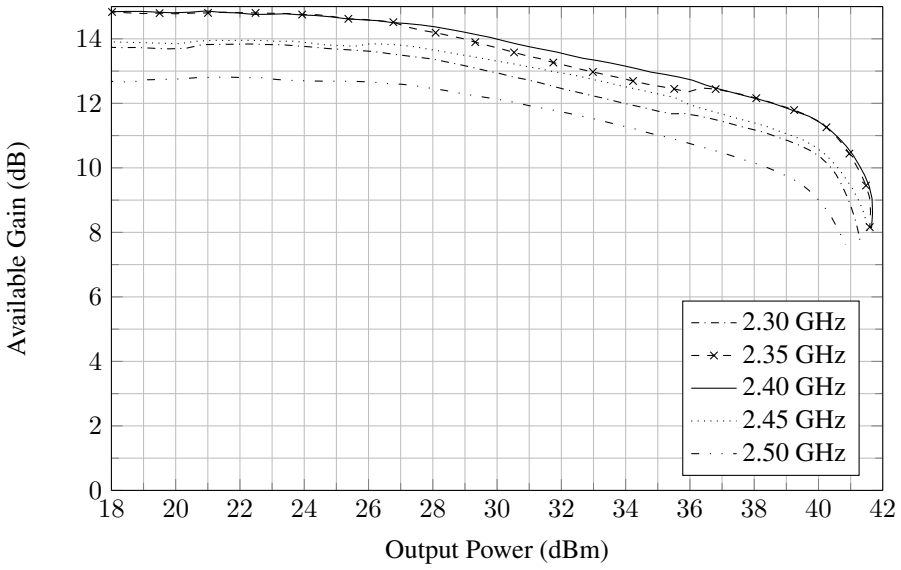

Figure 5.2: Single tone available gain as function of output power.

The η_{PAE} of single tone signals at 2.30, 2.35, 2.4, 2.45 and 2.50 GHz is shown in figure 5.3. The individual curves are not easy to distinguish from one another as there is not as

large difference in η_{PAE} for the respective frequencies at power levels other than the ones close to peak. For f_0 however a $\eta_{PAE} = 68.4$ % can be seen for $P_{o\_1} = 41.66$, essentially at the peak output power.

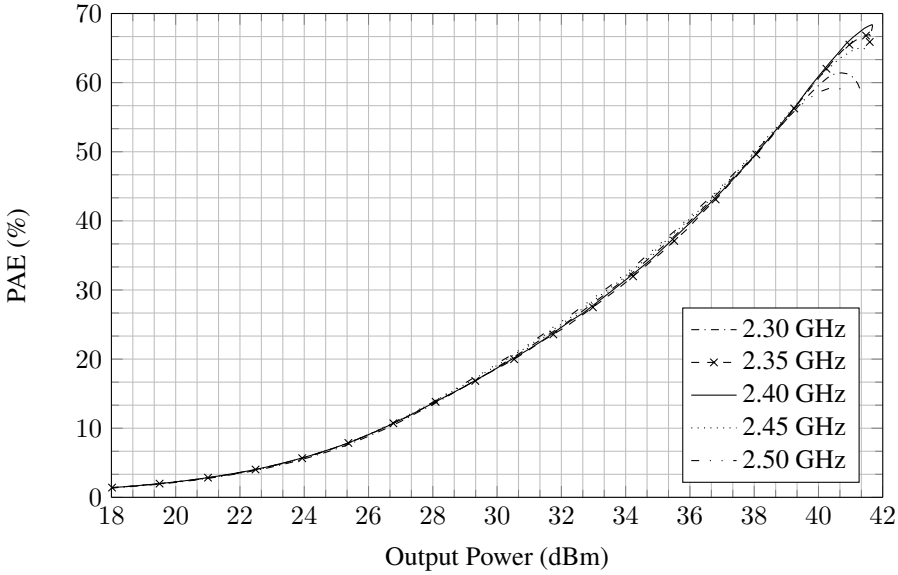

Figure 5.3: single-tone a η_{PAE} as function of output power.

Figure 5.4 shows the results from the two-tone power sweep, which was only done around 2.4 GHz. Peak two-tone output power can be found to be $P_{o\_2} = 39.2$ dBm, for a $P_{i\_2} = 29.0$ dBm, however at this point the PA is not fully compressed. The fundamental output power is included for comparison.

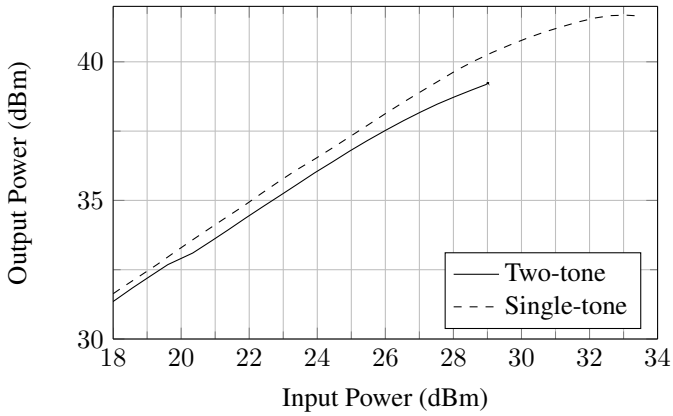

Figure 5.4: Measured two-tone output power vs. input power.

Figure 5.5 shows the gain computed from the output power in figure 5.4. A slight reduction gain relative to the single-tone gain is apparent, crossing the $G_A = 12$ dB line at $P_{o\_2} = 36.1$ dBm, and having a $G_A = 10.2$ dB at the peak output power, $P_{o\_2} = 39.2$ dBm.

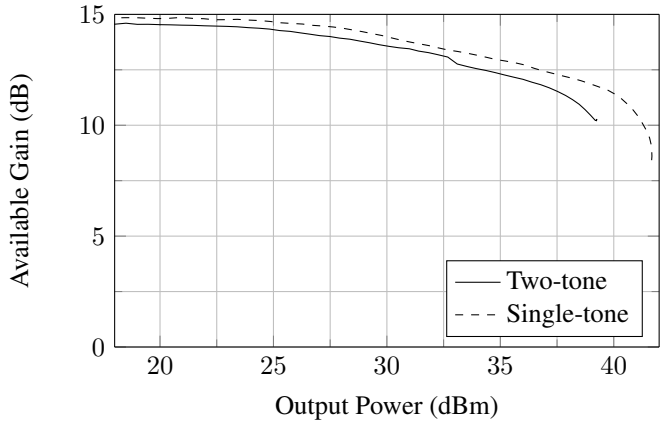

Figure 5.5: Measured two-tone available gain vs. P_{o_2}

The two-tone η_{PAE_2} of the PA is presented in figure 5.6 along with the single-tone η_{PAE_1}. As the output power does not go as high, the peak power-added efficiency is only $\eta_{PAE\_2} = 56.3$ % at $P_{o\_2} = 39.2$ dBm. For lower power values however, the single and two-tone curves follow one another closely, with the two-tone power added efficiency even slightly higher in the range between $P_{o\_2} = 32$ dBm and $P_{o\_2} = 38$ dBm.

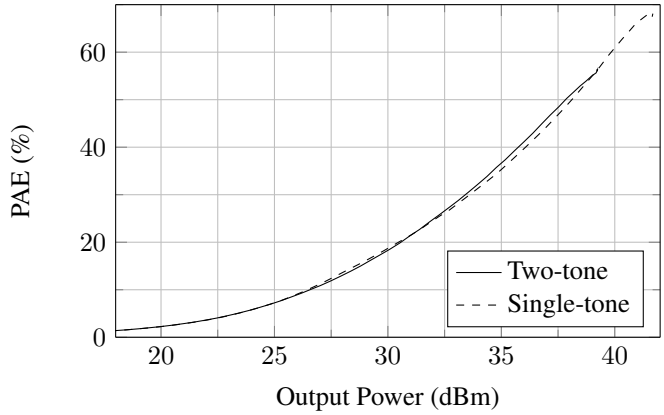

Figure 5.6: Measured two-tone η_{PAE} vs. P_{o_2}

The 3rd order intermodulation distortion measured in the two-tone test is shown in figure 5.7 in dB relative to the carrier, dBc. Below $P_{o\_2} = 35$ dBm the intermodulation is below -30 dBc, and rapidly growing to a peak value of $IMD_3 = -18.9$ at the peak output power, $P_{o\_2} = 39.2$ dBm.

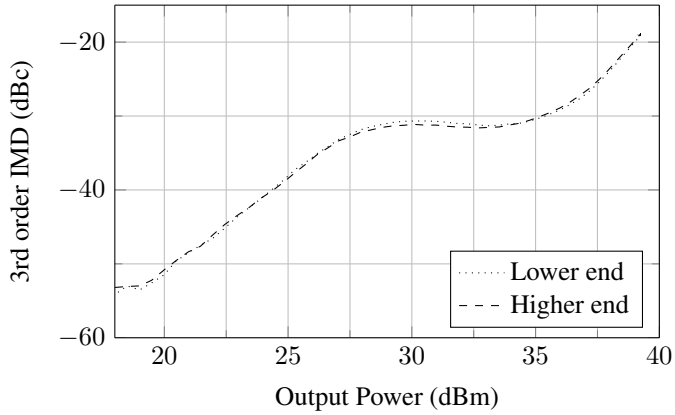

Figure 5.7: Measured 3rd order IMD vs. P_{o_2}

The measured s-parameters are shown in the following figures. S_{11} and S_{22} are displayed in 5.8 while S_{21} and S_{12} are displayed in rectangular plots in figures 5.9 and 5.9, respectively. S-parameters were measured two times, as a faulty measurement of S_{22} was discovered and recalibration had to be done. Difference in absolute value of the s-parameters are shown in figures B.8 and B.9, showing corresponding responses for the other s-parameters.

Considering the input reflection, S_{11}, and output reflection, S_{22}, in figure 5.8, plotting is done for $f \in (1.90 \text{ GHz}, 2.90 \text{ GHz})$ to be able to see the values in a 1 GHz band around f_0. A mismatch can be seen, as neither S_{11} nor S_{22} cross through the center of the smith

diagram, but approximately $50\ \Omega$ with some capacitive reactance, at f_0 . The mismatch leads to input and output return loses $|S_{11}| = -13.4$ dB and $|S_{22}| = -13.8$ dB at f_0 as seen in figure B.9.

As for the forward gain, $|S_{21}|$, the measurements show $|S_{21}| = 14.1$ dB, at 2.40 GHz. However reviewing the data closer it is apparent that the matched frequency is 2.395 GHz, where $|S_{21}| = 14.15$ dB. In addition the 1 dB bandwidth around f_0 to be $B_{1\,\mathrm{dB}} = (2.31\ \mathrm{GHz}\ , 2.46\ \mathrm{GHz}\ )$, or 150 MHz. $|S_{12}|$ is displayed in figure 5.10, showing fair isolation across the whole range, with a maximum of $|S_{12}| = -31.5$ dB at 2.4 GHz.

Although the PA was considered unconditionally stable from evaluating the output spectrum, μ was calculated from the s-parameters using (2.30), and is shown in figure B.7.

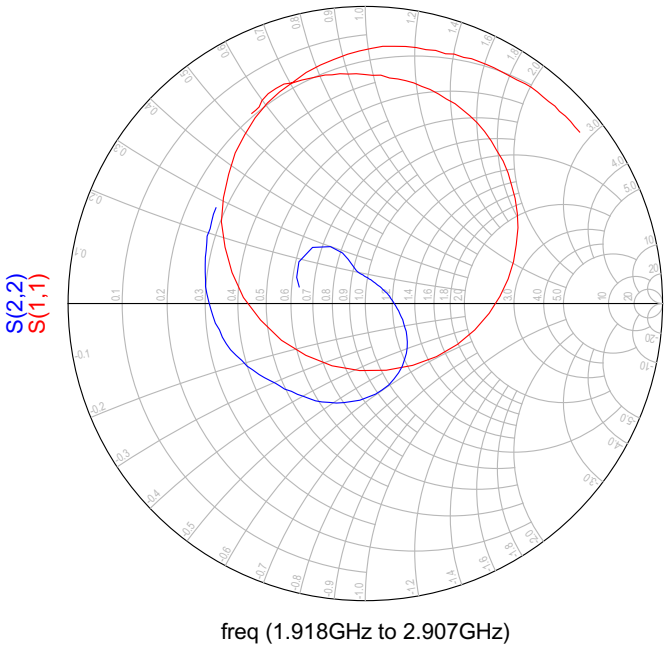

Figure 5.8: Measured S_{11} and S_{22} in smith chart.

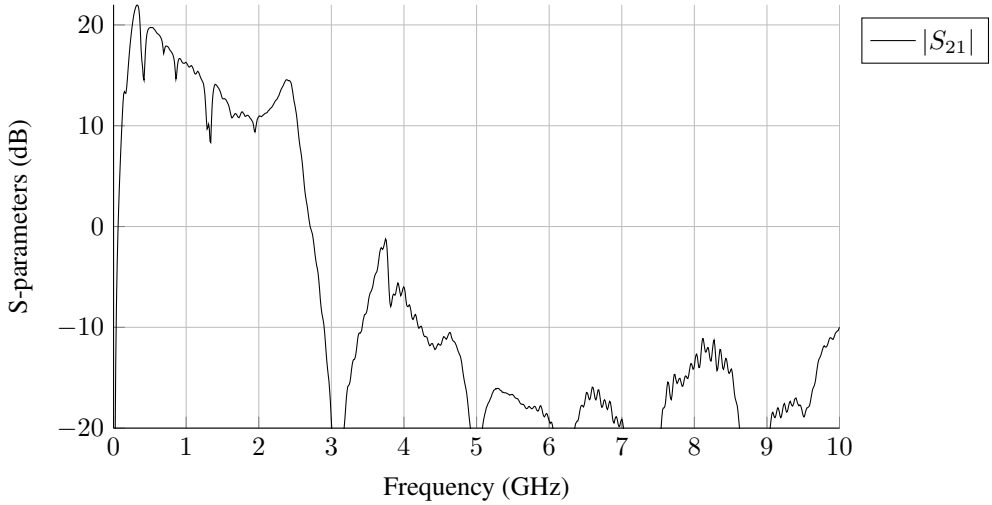

Figure 5.9: Measured $|S_{21}|$ for complete design.

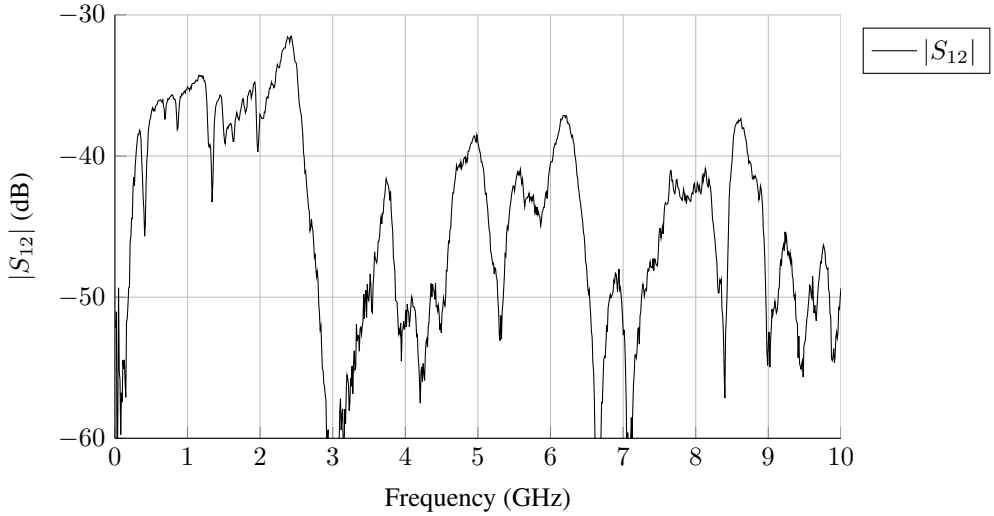

Figure 5.10: Measured $|S_{12}|$ for complete design.

5.2 Envelope Tracking Trajectories

The large signal characteristics of the PA were also investigated at reduced supply voltages in order to estimate the performance in an envelope tracking setup. The result being a similar collection of curves as seen in figure 2.19. As the resulting trajectories can give varying performance and complexity, a series of cases of desired characteristics are to be investigated. These are tracking for maximum efficiency, tracking for flat gain and linear controlling of the supply, and will be investigated in the following sections.

5.2.1 Maximum Efficiency

The first case to be analyzed is tracking the amplifier to stay in compression also at reduced input levels by reducing the supply voltage. Figure 5.11 presents the single-tone η_{PAE} between 28 and 14 V in steps of 2 V descending from right to left. In addition the resulting trajectory from successfully tracking for maximum efficiency is seen on the peaks of the curves, which results in an improved $\eta_{PAE} = 52\,\%$ at $P_{o\_1} = 35$ dBm, as opposed to $\eta_{PAE} = 35\,\%$ during static 28 V operation. For power levels below $P_{o\_1} = 35.3$ dBm, the supply voltage is kept at $\frac{V_D}{2} = 14\,V$, as not much more improvement is achieved compared to the reduction in gain.

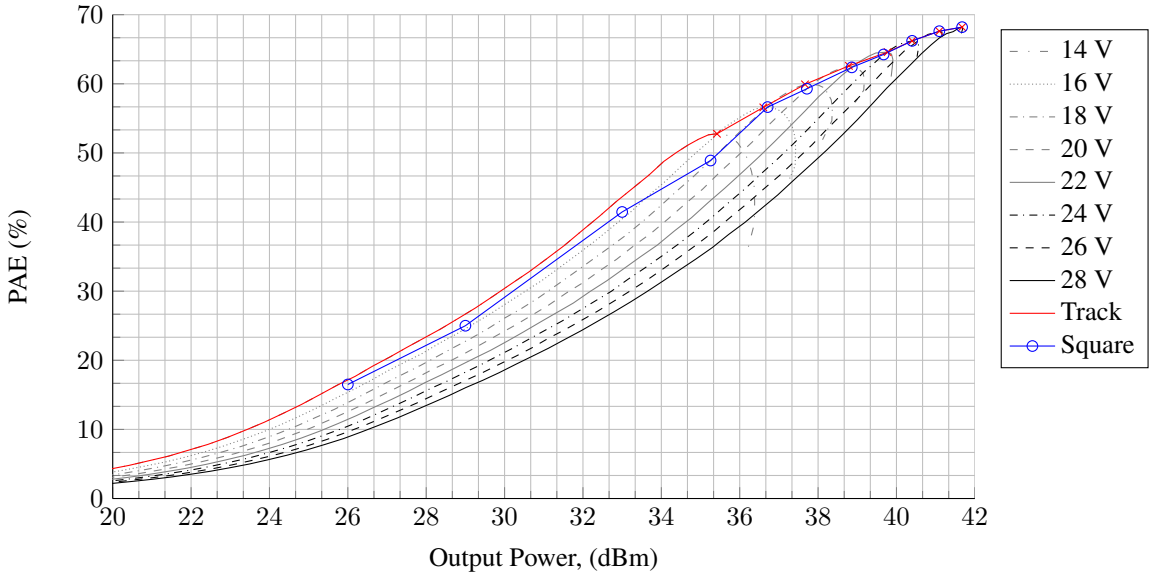

Figure 5.11: η_{PAE}-curves and maximum efficiency trajectory vs. P_{o_1}.

By following this trajectory a gain characteristic as seen in figure 5.12 is achieved. As a result of tracking in quite deep compression, the resulting gain is not very high, ranging from 9 dB at peak output power to 6.6 dB for $P_{o\_1} = 35.4$ in a highly nonlinear fashion,

before following the 14 V curve.

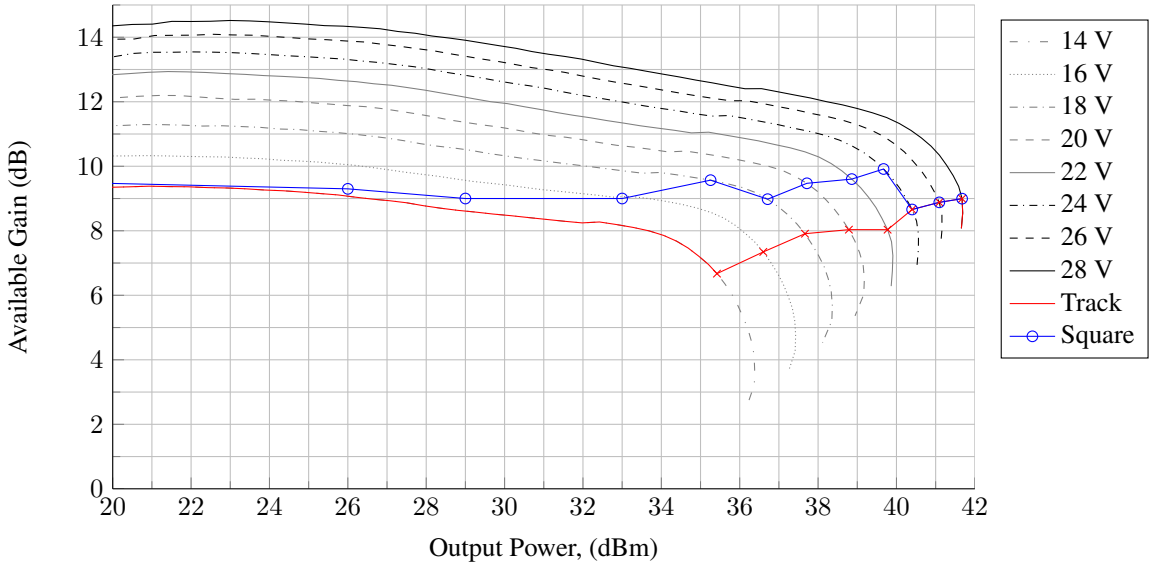

Figure 5.12: G_A-curves and maximum efficiency trajectory vs. P_{o_1}.

Similarly the resulting output power trajectory is shown in figure 5.13. The shape of this is close to the shape of the gain curve, highly nonlinear, and drops rapidly into compression at the 28 V curve.

The resulting supply voltage functions can be computed using (2.58), and drain voltage is shown vs. output and input voltage in figure 5.14.
The drain supply voltage is a fairly linear response relative to the output RF voltage. This is due to the high efficiency of operation, where as much of the supplied voltage is transmitted on the output, and therefore it lies close to the forbidden zone where $V_{out} > V_S$. When plotted versus the input RF voltage however a highly nonlinear supply response can be seen, due to the nonlinear gain. This is worth noting as this is the voltage gain a supply modulator need in order to track for maximum efficiency.

Included in figure 5.14 is also a curve called square, which is a quadratic interpolation between $V_{out} = 0$ V and $V_{out} = 28$ V, as a possible alternative supply response. The resulting η_{PAE}, output power and gain curves are shown in blue in figures 5.11, 5.13 and figure 5.12 respectively. This is an attempt at trading off some η_{PAE} performance in favor of a nicer supply characteristic.

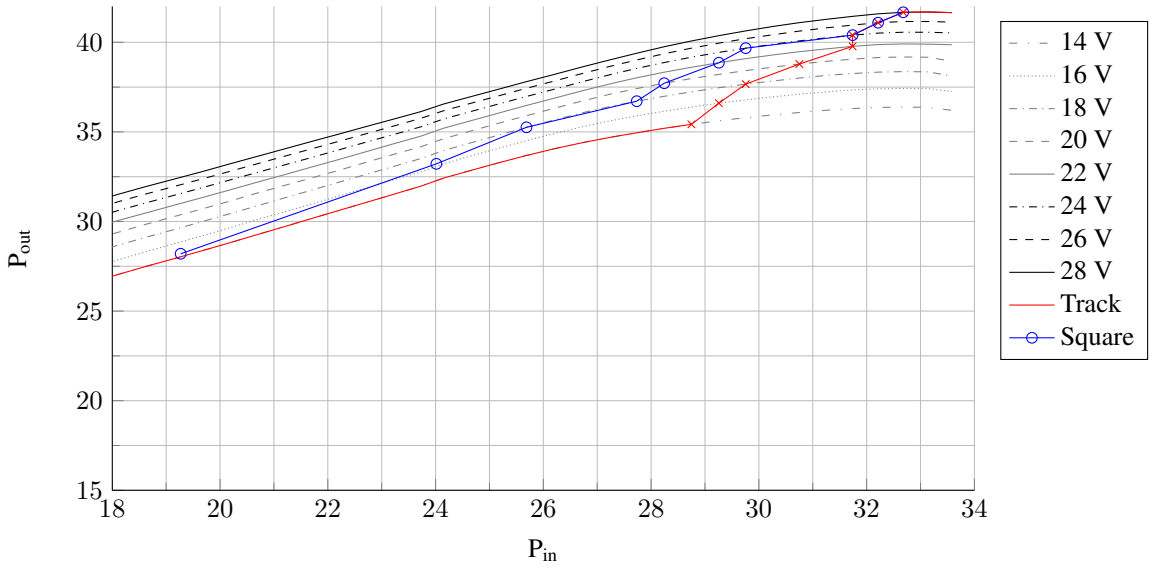

Figure 5.13: P_{o_1}-curves and maximum efficiency trajectory vs. P_{i_1}.

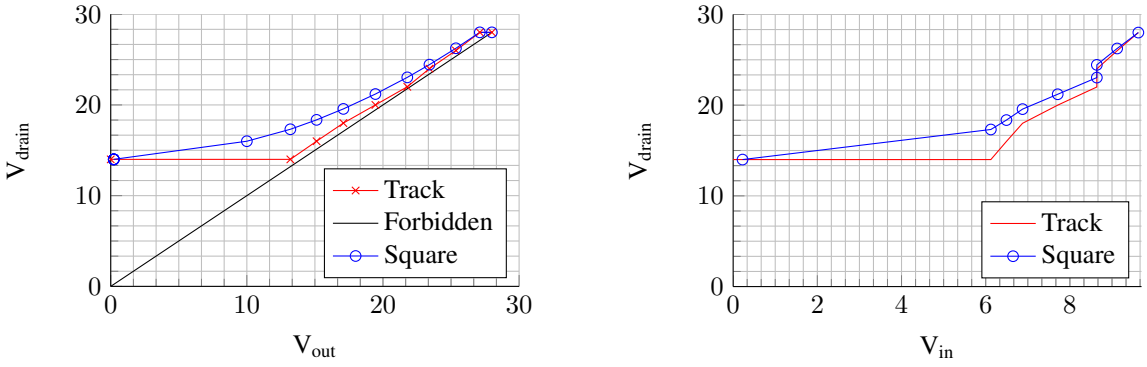

Figure 5.14: Drain voltage vs. PA output (a) and input (b) voltage for maximum efficiency tracking.

5.2.2 Flat Gain

A different way of tracking the PA can be choosing a trajectory that ensures a flat gain characteristic. The results while doing this will be presented for a flat available gain of 12 dB, 10 dB and 9 dB.

12 dB

By tracking for 12 dB flat gain, the goal a gain characteristic as seen in figure 5.15. Here the measured gain curves of the PA is shown between 28 and 14 V in steps of 2 V descending from right to left, with the ideal track crossing each curve where it yields 12 dB gain. For an instantaneous output power greater than $P_{o\_1} = 38.2$ dBm the supply voltage is held at 28 V constant as any lower values give less gain, if the given output power is obtainable at all.

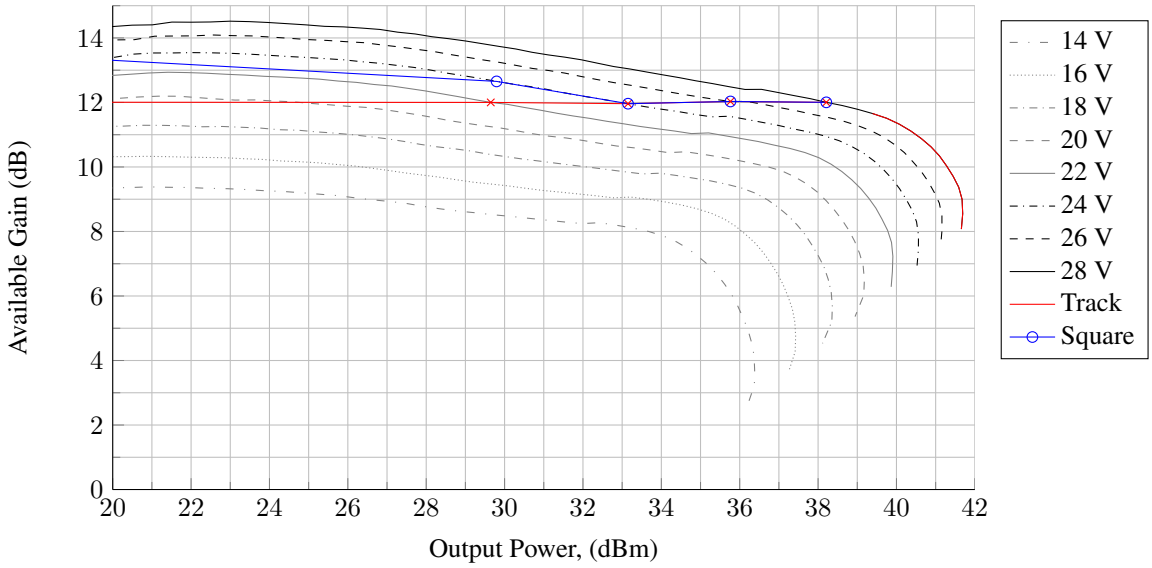

Figure 5.15: G_A-curves and 12 dB flat gain tracking trajectory vs. P_{o_1}.

When looking at the output power, the resulting characteristic can be viewed in figure 5.16, which naturally is very similar to the gain characteristic.
The resulting η_{PAE} is shown in figure 5.17, showing $\eta_{PAE} = 38\%$ for $P_{o\_1} = 35$ dBm, which is not an as large improvement over the 28 V curve at $\eta_{PAE} = 35\%$, as when tracking for maximum efficiency.

The drain supply voltage vs. output and input signal voltage in figure 5.18. These responses show quite similar behavior, quite linear tracking from about $V_{drain} = 20$ V to

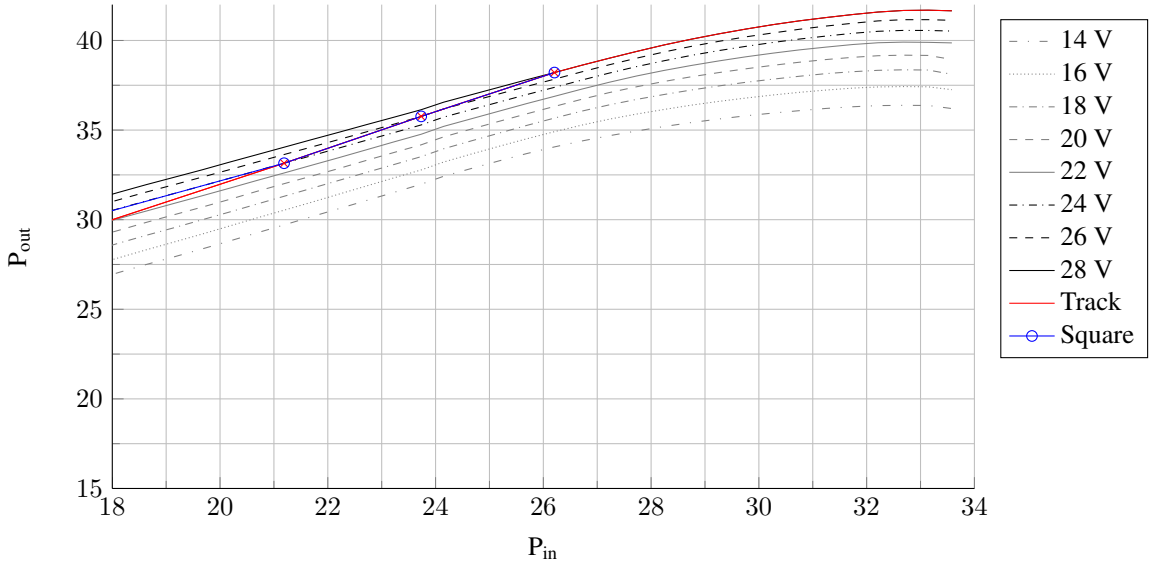

Figure 5.16: P_{o_1}-curves and 12 dB flat gain tracking trajectory vs. P_{i_1}.

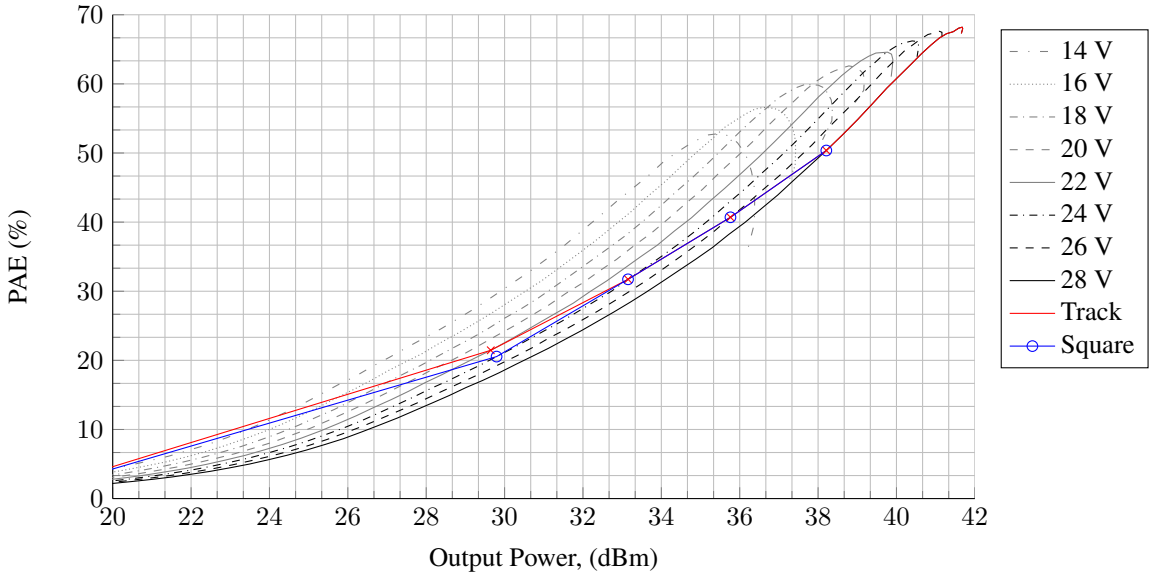

Figure 5.17: η_{PAE}-curves and 12 dB flat gain tracking trajectory vs. P_{o_1}.

$V_{drain} = 28$ V while $V_{out} = 2$ V, $V_{in} = 0.25$ V and $V_{out} = 20$ V, $V_{in} = 4.5$ V, respectively. For the peak levels operation is done with constant 28 V supply.

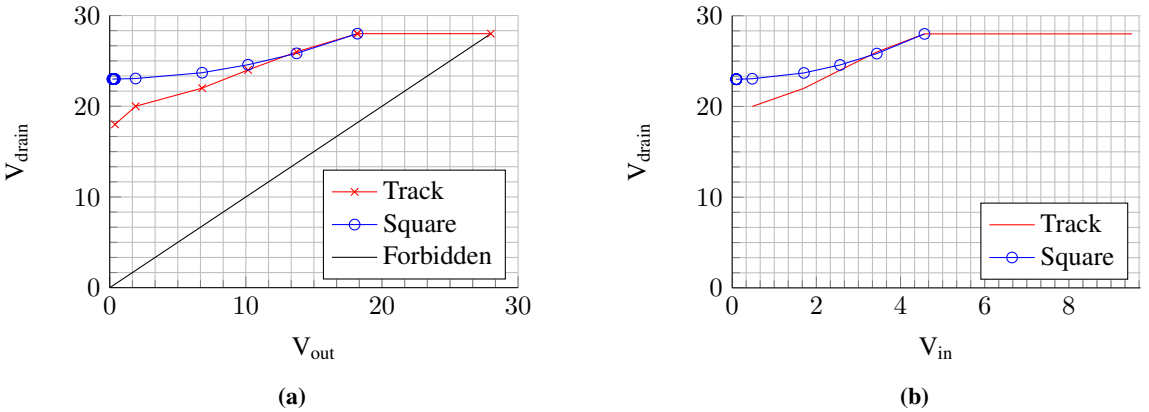

Figure 5.18: Drain voltage vs. PA output (a) and input (b) voltage for 12 dB flat gain tracking.

As an alternative to the ideal track, shown in red, a square supply function is analyzed, showing the resulting η_{PAE}, power gain and output power in figures 5.17, 5.15 and 5.16 respectively. By doing this the PA operates at a higher supply than would give the desired flat gain operation, especially at lower signal levels, thus increasing the gain closer to 13 dB at $P_{o\_1} = 29$ dBm and lower. A slight reduction in η_{PAE} at lower signal levels is also a consequence of this.

10 dB

As the PA is operating at 28 V for a rather large dynamic range when tracking for 12 dB flat gain, the efficiency could possibly be improved by operating closer to compression. By lowering the constraint to 10 dB flat gain, as seen in figure 5.19, the tracking trajectory would pass through the individual gain curves closer to compression than for 12 dB flat gain.

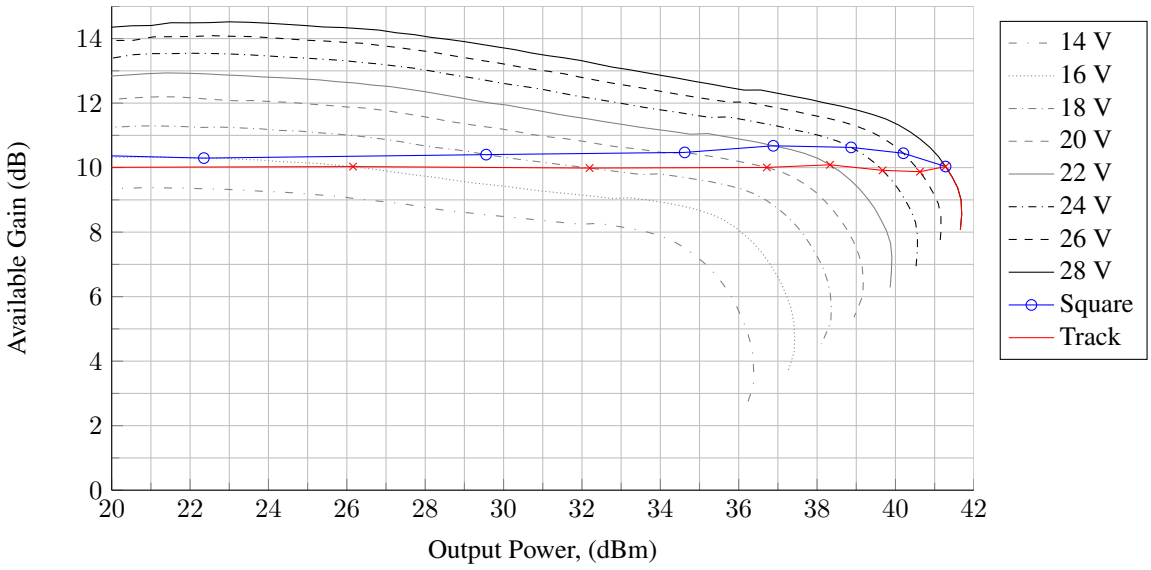

Figure 5.19: G_A-curves and 10 dB flat gain tracking trajectory vs. P_{o_1}.

In this case, the range where following the 28 V cirve is reduced, starting the tracking at $P_{o\_1} = 41.3$ dBm, as can be seen in figure 5.19 and 5.20. The power response in figure 5.20 shows the effect of the reduced gain constraint, staying in compression from $P_{i\_1} = 26$ dBm and all the way to peak power.

The efficiency resulting from this extended dynamic range at which the PA stays in compression is shown in figure 5.21. At $P_{o\_1} = 35$ dBm, $\eta_{PAE} = 47\%$, a 9% improvement gained from the 2 dB gain trade off.

Obtaining a 10 dB flat gain tracking characteristic is done using the supply response in figure 5.22. The supply response is a fair bit lower, and closer to the forbidden zone compared to the 12 dB as operation in deeper compression is wanted. However as a result the response is somewhat curved, and resembles the square, alternative, response fairly closely.

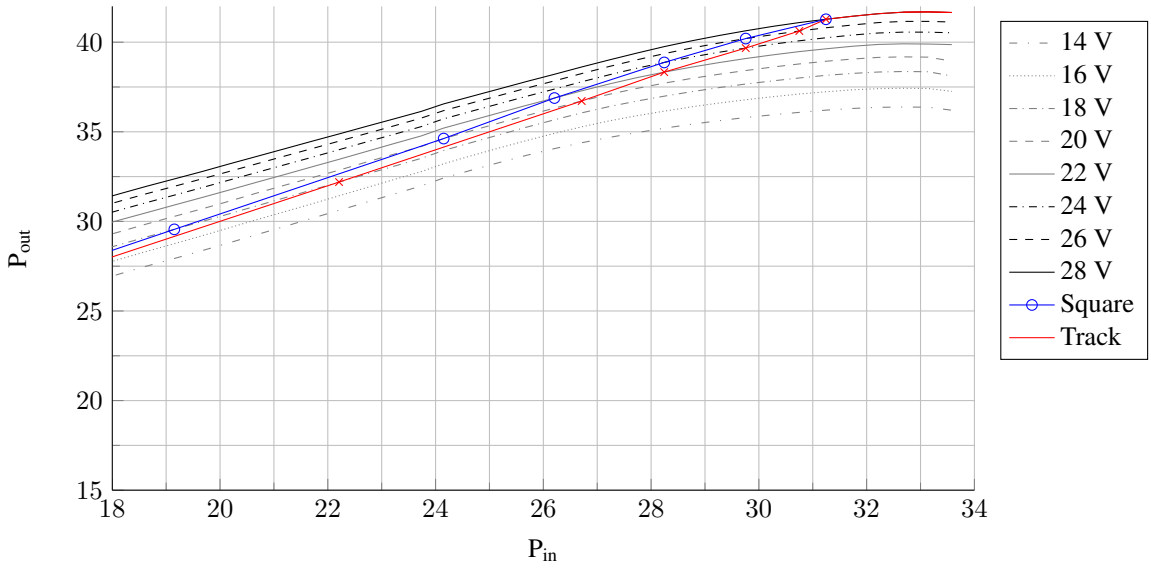

Figure 5.20: P_{o_1}-curves and 10 dB flat gain tracking trajectory vs. P_{i_1}.

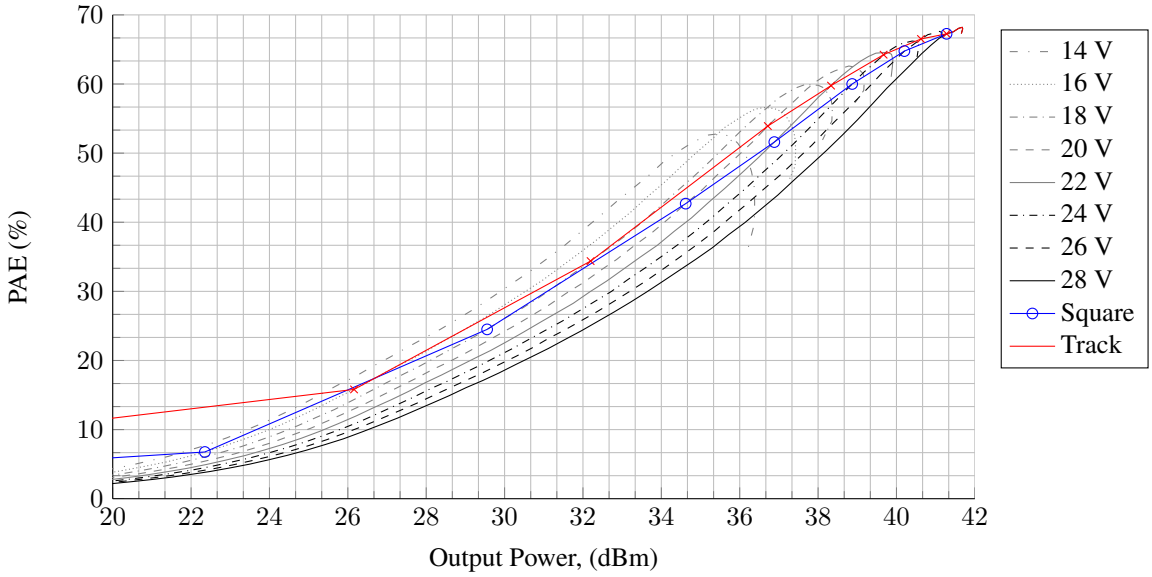

Figure 5.21: η_{PAE}-curves and 10 dB flat gain tracking trajectory vs. P_{o_1}.

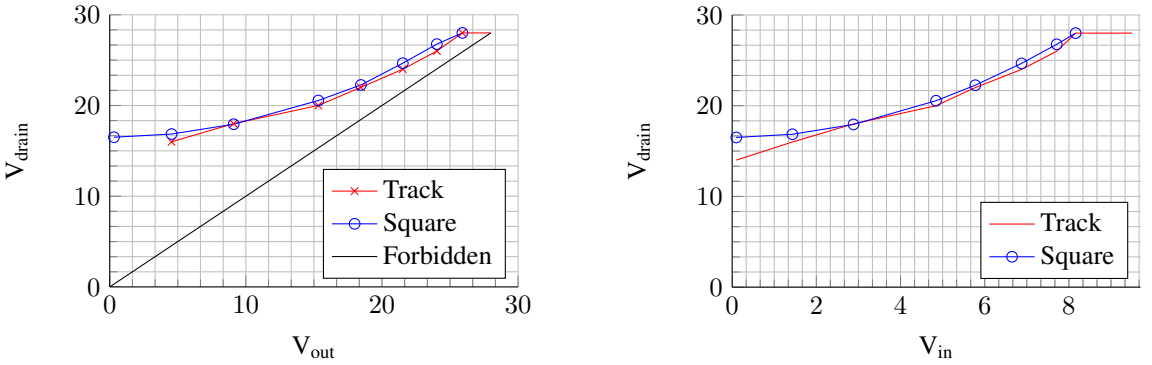

Figure 5.22: Drain voltage vs. PA output (a) and input (b) voltage for 10 dB flat gain tracking.

9 dB

Wanting to characterize the PA for several cases, the possibility of a scenario hopefully joining together the best features of both the maximum efficiency and flat gain would be investigated as 9 dB flat gain. This gain trajectory is shown in figure 5.23, where tracking is done almost all the way to peak power, reaching the 28 V curve at $P_{o\_1} = 41.5$ dBm.

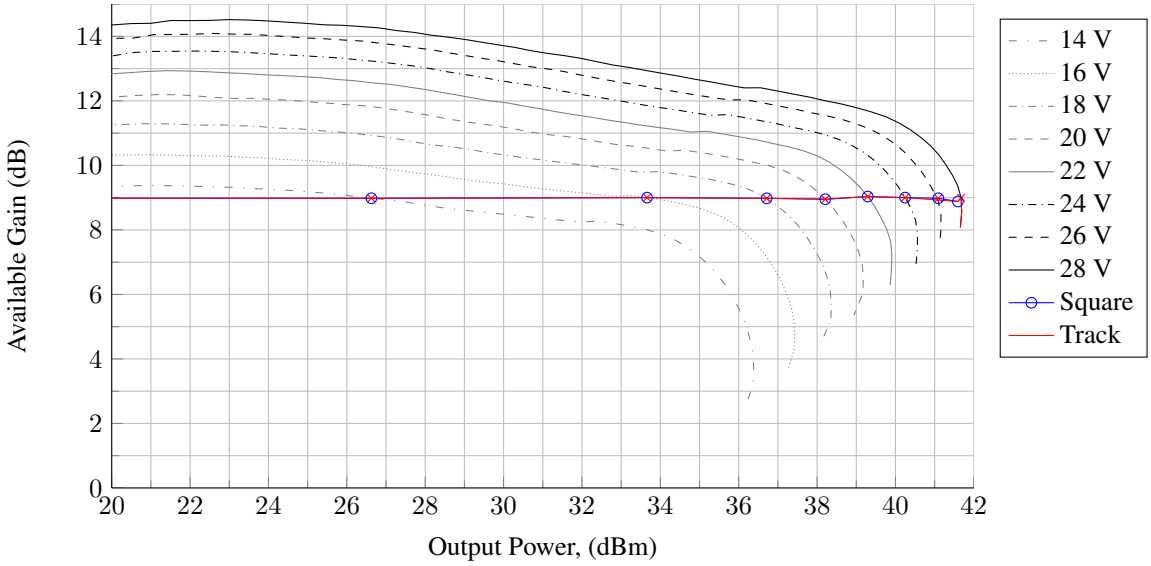

Figure 5.23: G_A-curves and 9 dB flat gain tracking trajectory vs. P_{o_1}.

The 9 dB flat gain trajectory fields an even larger dynamic range in which the PA is compressed, starting even slightly at $P_{i\_1} = 23$ dBm, as seen in figure 5.24. With 9 dBm gain, this equates to $P_{o\_1} = 32$ dBm, yielding a 8 dBm dynamic range where tracking leads to the PA operating in compression.

The η_{PAE} for the case with 9 dB flat gain is shown in figure 5.25. The resulting trajectory can be seen to intersect the individual η_{PAE}-curves very close to the peaks, however this is only the case for the 28 V and 26 V curves, at $P_{o\_1} = 41.1$ dBm and $P_{o\_1} = 41.6$ dBm, respectively. At larger back off than this, the curves are intersected further away from their peak values, at lower η_{PAE}. The linear interpolation between the individual points however show that the trajectory will be close to maximum anyway. An example of this can be seen at $P_{o\_1} = 36.7$ dBm, where the η_{PAE} with $V_D = 18$ V approximately equals the η_{PAE} with $V_D = 16$ V. At $P_{o\_1} = 35.0$ dBm, the $\eta_{PAE} = 48\,\%$, yielding a $13\,\%$ increase compared to fixed 28 V operation.

The drain supply response needed for this behavior is shown in figure 5.26. As with the 10 dB flat gain case, a curved response is needed, with the 10 dB one perhaps a slight better fit to the square alternative. The close resemblance of the square alternative track-

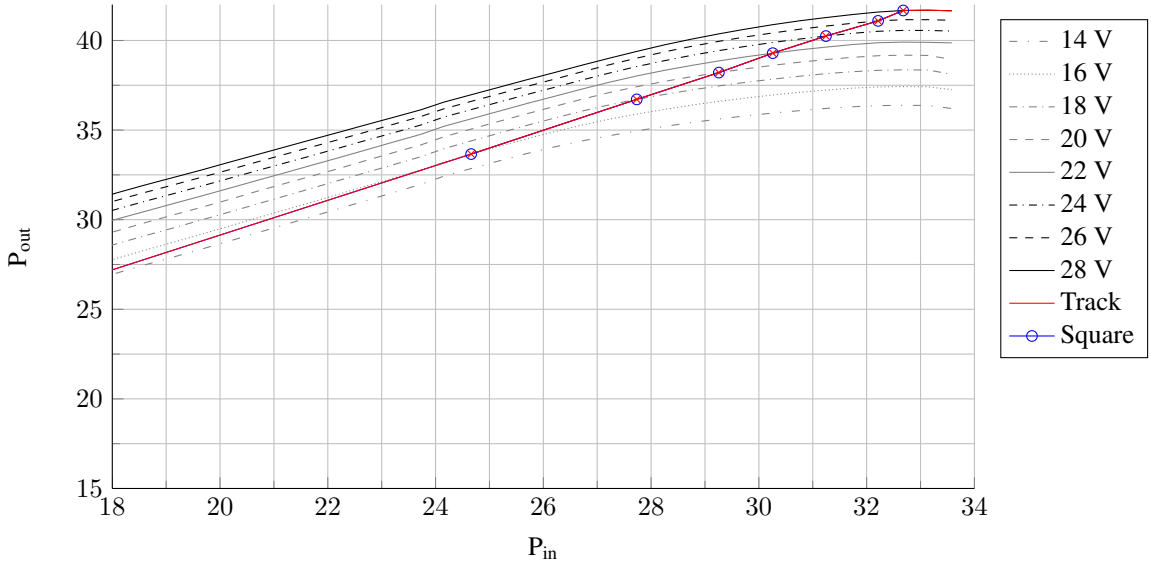

Figure 5.24: P_{o_1}-curves and 9 dB flat gain tracking trajectory vs. P_{i_1}.

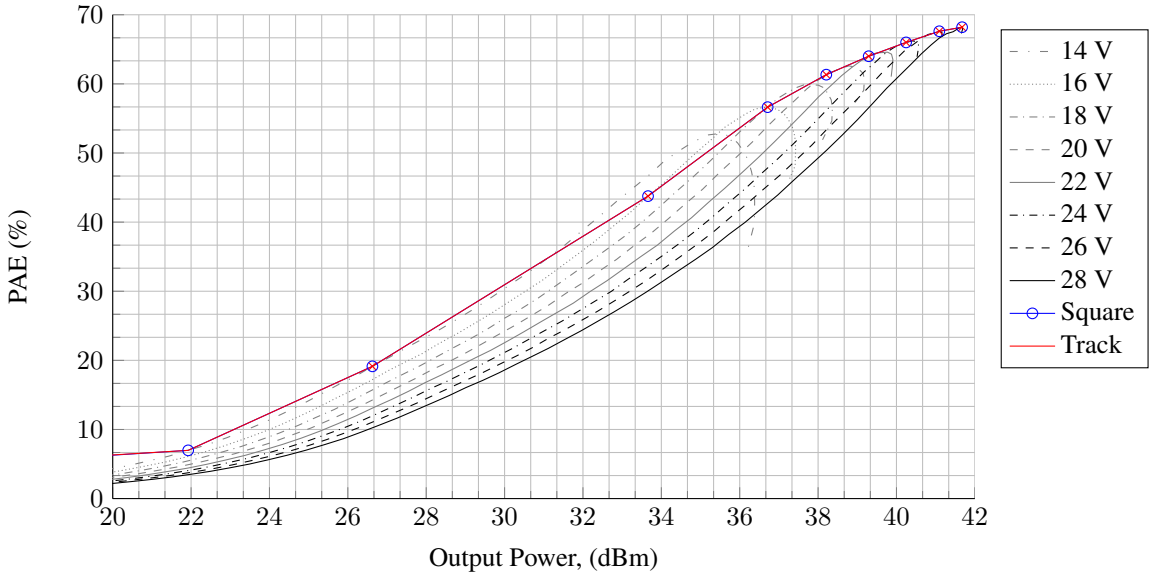

Figure 5.25: η_{PAE}-curves and 9 dB flat gain tracking trajectory vs. P_{o_1}.

ing function however leads its gain, output power, η_{PAE}, plotted in blue in figures 5.23, 5.24 and 5.25 respectively, being equal to the ideal track, seen in red. This is due to the resolution of the data being too low, only having measurements for every 20 V, and the

deviation between the square and ideal tracking function is less than 1 V. The resulting performance for the square track would therefore be slightly worse than the ideal.

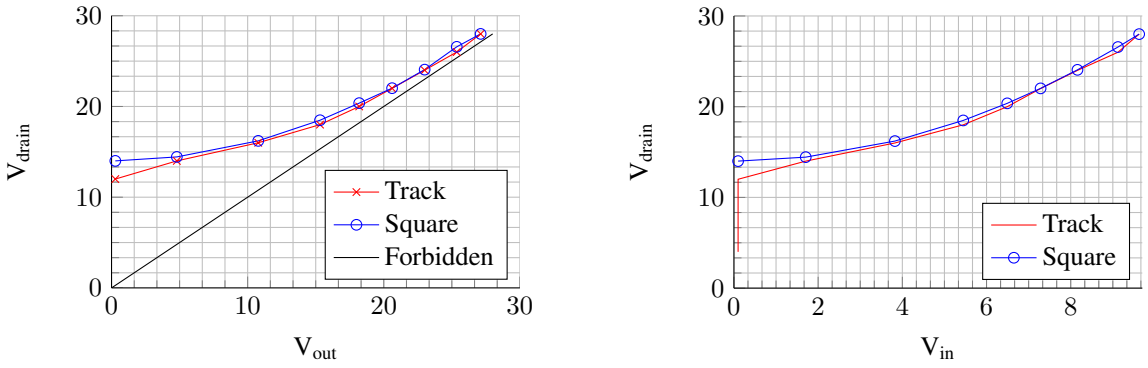

Figure 5.26: Drain voltage vs. PA output (a) and input (b) voltage for 9 dB flat gain tracking.

5.2.3 Linear V_D vs. V_{in}

In addition to tracking for maximum efficiency and flat gain, a case where the supply voltage is a linear function of the input signal voltage, as shown in figure 5.27(b), in order to estimate the performance of the PA in such a case. This was done by starting the tracking at two different power gains, 12 dB and 10 dB respectively. The supply was then reduced linearily with the output signal voltage, and mapped to create trajectories for the respective basis.

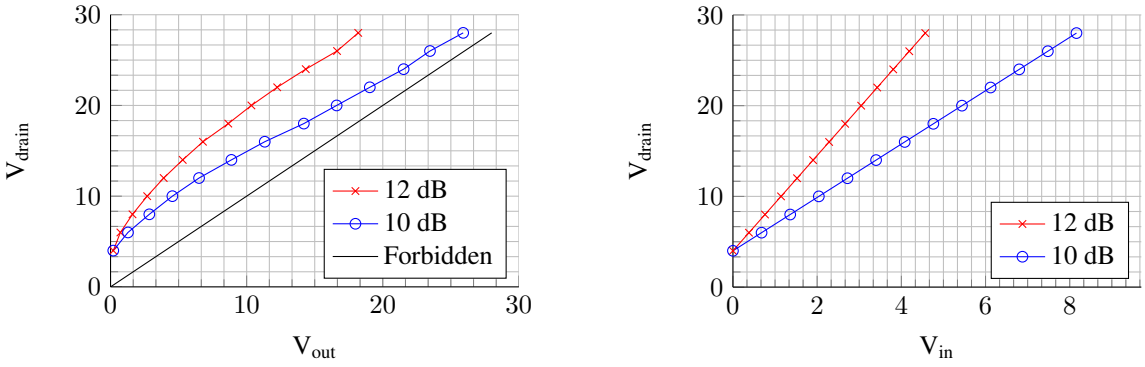

Figure 5.27: Drain voltage vs. PA output (a) and input (b) voltage for linear V_D tracking.

A 4 V lower bound was chosen to ensure a nonzero supply at all times, resulting in the depicted response. The supply plotted vs. the output power, in figure 5.27(b), is the resulting supply response, and was not used as a basis for defining the trajectory.

The power gain resulting from the linear tracking is shown in figure 5.28, and can be seen to have a nonlinear response. This is due to the response being linear all the way to $V_{in} = 0$ V, not clipped at e.g. $V_{out} = 14$ V as in figure 5.14. The gain curves for even lower supply levels are therefore also included. The gain drops rather fast and at $P_{o\_1} = 35.0$ dBm the gain is 10.75 dB and 8.5 dB for the 12 dB and 10 dB curves respectively.

The output power can be seen in figure 5.29. As an effect of the reduced gain, a reduced power response is evident, needing $P_{i\_1} = 23.8$ dBm and $P_{i\_1} = 25.8$ dBm to get to $P_{o\_1} = 35.0$ dBm, along the 12 dB and 10 dB trajectories respectively.

The resulting η_{PAE} is shown in figure 5.30, quite different efficiencies for the 12 dB and 10 dB solutions. 10 dB gain is sufficiently deep compression that tracking is performed almost all the way to peak output power, and as the trajectory taken keeps the PA compressed at lower supply levels, the η_{PAE}-trajectory is close to maximum possible. The 12 dB gain alternative keeps constant 28 V supply for $P_{o\_1} = 38.0$ dBm and greater, and

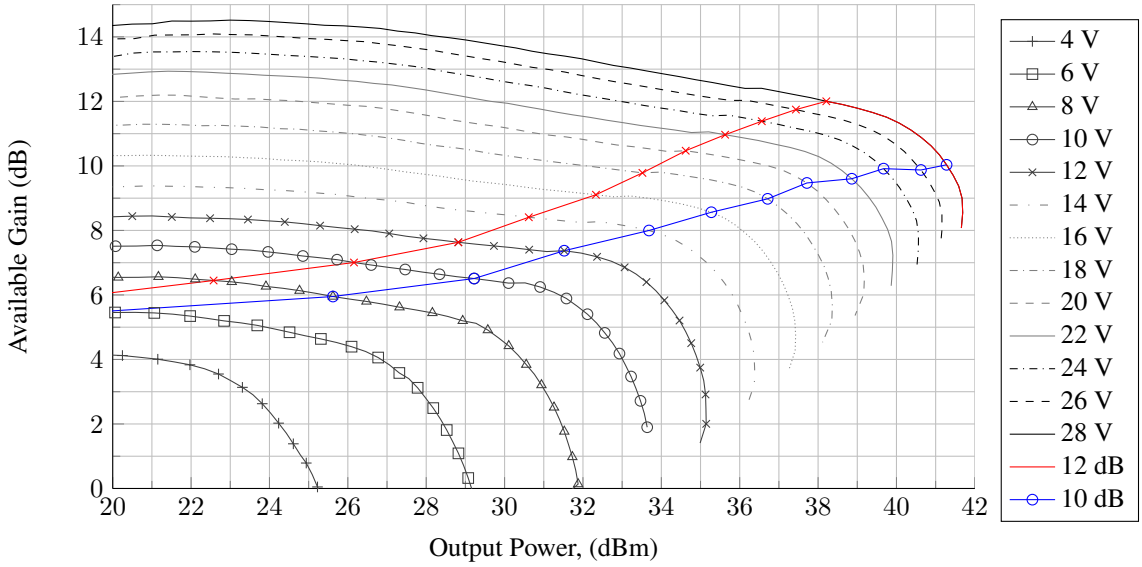

Figure 5.28: G_A-curves and linear V_D tracking trajectory vs. P_{o_1}.

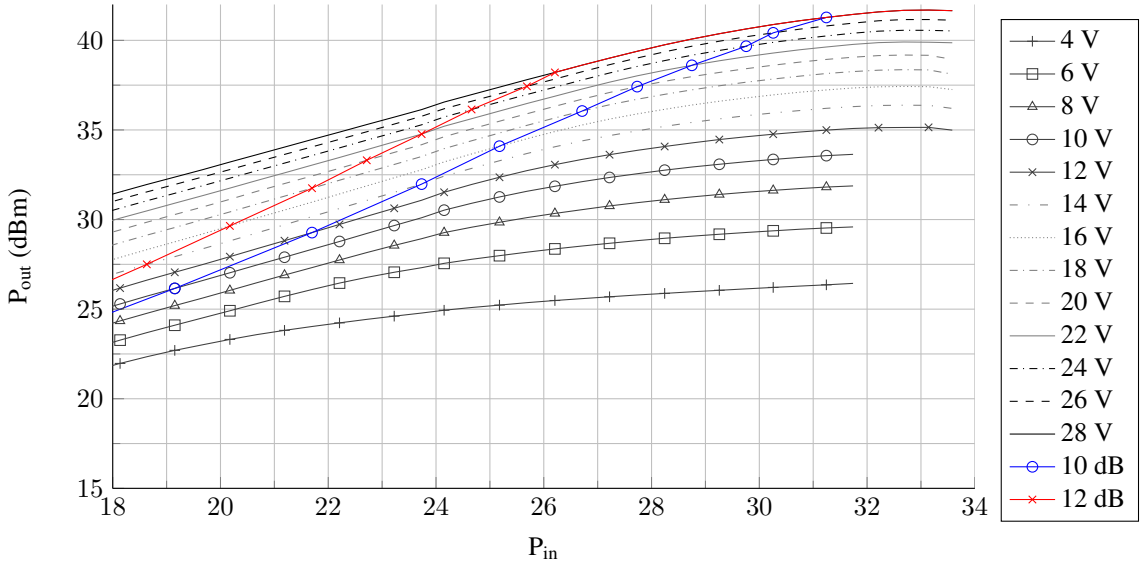

Figure 5.29: P_{o_1}-curves and linear V_D tracking trajectory vs. P_{i_1}.

tracks through each individual curve at fairly large back off, however closing in on the 10 dB gain trajectory at $P_{o\_1} = 30.0$ dBm and lower. At $P_{o\_1} = 35.0$ dBm there is improvement over static 28 V operation however, at $\eta_{PAE} = 51$ % and $\eta_{PAE} = 43$ % for the 10 dB and 12 dB trajectories respectively.

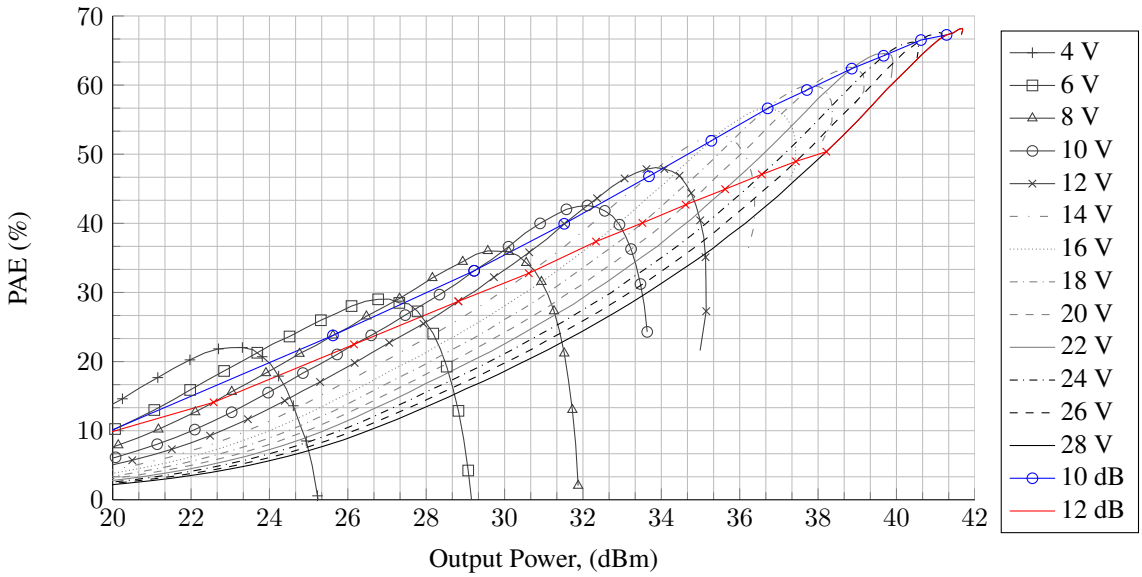

Figure 5.30: η_{PAE}-curves and linear V_D tracking trajectory vs. P_{o_1}.

Chapter 6

Discussion

6.1 Static Supply Performance

Reviewing the measurement results in table 5.1, performance can be considered to fulfill the specifications. However the grade at which specifications are met, is dependent on the meaning of the specifications. That is, at what output power should $G_A > 12$ dB, should $|S_{11}| < -10$ dB across the whole $B_{1\,\mathrm{dB}}$-band, and is $P_{o\_1} > 40$ dBm the peak output power, or where an output power that should be reached without entering compression. In any case, the performance is not too far away from specified values.

If considering the measured center frequency and 1 dB bandwidth however, $f_0 = 2.395$ GHz is a deviation of 5 MHz. As this also turns out to be the simulated center frequency it is likely to not be a fabrication error or measurement error, but due to a poor design effort. No matter the reason it can be considered a small problem, if a problem at all, as the resulting 1 dB bandwidth overlaps with the frequency range that would have been the 1 dB bandwidth with $f_0 = 2.4$ GHz, $B \in (2.35, 2.45)$ GHz, as shown in figure 6.1.

The input reflection, $|S_{11}| = -14.0$ dB is the local minimum at 2.41 GHz, which is ac-

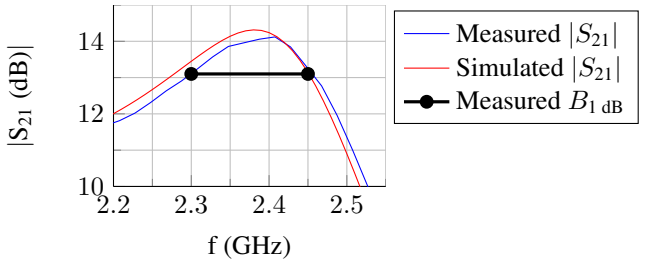

Figure 6.1: Comparison between simulated and measured $|S_{21}|$, and 1 dB bandwidths.

cording to specifications, considering that it is not meant as $|S_{11}| < -10$ dB $\forall\, f \in B_{1\,\mathrm{dB}}$. The measurements show that this is only the case for $f \in (2.37\,\mathrm{GHz}, 2.447\,\mathrm{GHz})$. In any case $|S_{11}| = -14.0$ dB is not very impressive, as it results an input return loss, wasting power and improving the risk of the reflection damaging whatever preceeds the PA in the transmission chain. The latter can however be solved by a circulator, coupler or similar. Comparing to the simulated values, as seen in figure B.10 a better match would have been expected.

What is a problem actually is the large $|S_{21}|$ at frequencies lower than $B_{1\,\mathrm{dB}}$. There are small dips of $|S_{21}| = 9.4$ dB at 1.95 GHz and $|S_{21}| = 8.5$ dB at 1.3 GHz, but apart from those $|S_{21}| > 10$ dB for frequencies above 100 MHz even as high as 21 dB. This is of course not good as it raises the chance of out-of-band transmission and instability, and should have been suppressed. This should have been paid more attention to when designing the IMN and OMN, as $|S_{21}|$ in the frequency range is rather large, causing the overall $|S_{21}|$ to approach the MAG. The overall consequence is requiring to high-pass filter the signal prior to, but possibly also following, the PA, which is unnecessary as this should have been done using the matching networks. And in the case of needing a wideband PA, there are most likely better options, having a smoother gain characteristic.

According to figure B.8, the measured s-parameters show a fairly questionable S_{22}, which even exceeds 0 at some frequencies. As this is strange, a control measurement was performed, having recalibrated the VNA, suspecting the distortion being result of bad calibration. As can be seen in figure B.9, a smoother response is achieved after recalibration, with similar values for the other s-parameters.

Fairly convincing however is the output power, which when the PA operates in deep compression reaches 41.7 dBm. As a result, the specified output power, 40.0 dBm, can be reached without compressing too much, increasing the gain at $P_{o\_1} = 40.0$ dBm compared to $P_{o\_1} = 41.7$ dBm. Compared to if the peak power was reduced, and the gain curve shifted downwards in power so that the peak aligns at aronud 40.0 dBm, less input power is needed, which means a less powerful driver can be used, and less power is wasted. A result is also reduced distortion, as this is worst in deep compression, but this is also where the PA is the most efficient.

When operating without a output power constraint a peak $\eta_{PAE} = 68\,\%$ can be reached at peak $P_{o\_1} = 41.7$ dBm. However due to the higher output power the efficiency is reduced if operating with 40.0 dBm maximum output power, yielding a peak $\eta_{PAE} = 60\,\%$, an $8\,\%$ reduction and $12\,\%$ deterioration. No specified value for η_{PAE} was supplied, but $\eta_{PAE} = 68\,\%$ is a $28\,\%$ improvement over [19], increasing the peak η_{PAE} by $15\,\%$.

Also whether the power gain is according to specifications, depends on how they are interpreted. A power gain exceeding 12 dB is experienced below about $P_{o\_1} = 38$ dBm, which can be considered as the linear region gain. However due to the reduced conduction angle of class AB amplifiers, the gain is not constant beyond about $P_{o\_1} = 26$ dBm, but linearily reduced from 14.7 dB to 12 dB before compression kicks in. This is an intended reduction

compared to [19], as it was desired to trade some of the excessive gain for efficiency.

Considering the measurement results that were not given any specified values, listed in table 5.2, the resulting linearity can be evaluated through the 1 dB compression point, $P_{1\,\mathrm{dB},\,1}$. Thus the deviation from the linear gain trend, exceeds 1 dB beyond $P_{1\,\mathrm{dB},\,1} = 41.0$ dBm, which allows for linear operation beyond a hypothetical power constraint at the specified $P_{1\,\mathrm{dB},\,1} = 40.0$ dBm. Related is also the third order intermodulation distortion, IMD_3, which at -18.9 dBc is a 1.1 dB increase compared to [19]. This was however measured in the two-tone test, where the input power was not sufficient to drive the PA fully into compression, and would therefore likely be slightly higher. Comparing to the simulated value, an estimated guess would be around -15 dBc. This is also used to estimate the saturated ACPR, which at -15 dBc peak is not very good, even being optimized for efficiency. At backoff, below $P_o = 35$ dBm, however the IMD3 is below -30 dBc, which is just short of the performance presented in [21] and [22].

It is unfortunate the input power during the two-tone tests was capped, resulting in failure to characterize the PA performance in compression with a two-tone drive signal. The reason for this being the signal generator [23] having a maximum ouput peak envelope power of 19 dBm, 7 dBm lower than the maximum single-tone power of 26 dBm. This could have been solved using a second driver PA, adding some gain to the signal chain and amping the signal at the input of the DUT to a level that drives it into sufficient compression. However due to multiple time demanding ongoing projects, there was a limited amount of equipment and time available for multiple measurements.

The measured peak two-tone parameters were however $P_{o\_2} = 39.2$ dBm, $G_{A,2-tone} = 10.2$ dB and $\eta_{PAE\_2} = 56,3\,\%$. Considering figures 5.4, 5.5 and 5.6 and simple extrapolating the curves, approaching $P_{o\_2} = 40$ dBm, $G_{A,2-tone} = 8$ dB and $\eta_{PAE\_2} = 60\,\%$ could be approximated peak values.

It can also be questioned to what degree the design of the PA was good or not. The performance is satisfactory for some applications, but the PA is rather large. The outer boundaries were made to fit an 85×85 mm^2 cooling plate, and this was taking advantage of when designing the IMN and OMN, and the length of the design is barely fitting inside the cooling plate. However the width of the design is far less than the width of the cooling plate, thus should the PA be commercialized it would likely be of interest to create a more compact design. This could have been done if not trying to aviod using lumped components in the matching networks. Additionally the DC bias and supply cables could have been replaced with 4 mm connectors, or in case of ET, BNC connectors. In either case, the design serves its purpose as a prototype for investigating possibilities of ET well.

An overall, last-minute optimization of the PA was not performed as design was carried out on a low-power ultrabook computer, having limited CPU power. This optimization was attempted, but aborted as optimization iterations took extremely long to complete and the Elpro lab requested the finished design to be delivered shortly. Had this been completed, even trying to limit the number of optimization variables and goals, or even using

a more powerful PC, the performance could have been improved slightly. Especially the input return loss, although according to specifications, could have gained from this.

6.2 Envelope Tracking

As a means to characterize the ET performance of the PA, power sweeps at reduced supply voltage levels were performed. As this is essentially a single-tone test, which means the supply voltage and RF signal amplitude can be considered constant in between being changed. Additionally a fixed supply uses solid decoupling on both drain and gate side, and when doing ET the drain side decoupling must be removed to avoid shorting the time-varying supply, which could introduce memory effects causing distortion. Also the time varying supply will further Nonlinear simulations using the CGH40010 showing this is done in [24]. Still, an envelope tracker is a low impedance termination, which will reduce the problem, but the performed measurements can still only be considered a fair estimate of the resulting ET performance.

Reviewing the results in section 5.2, a set of possible cases for tracking have been presented, yielding different characteristics. Considering a 5-6 dB PAPR transmitted signal, which results in 35 dBm average output power, improvements to power-added efficiency range from 3 % to almost 20 %, and gain levels and responses vary greatly due to variable levels of compression.

The η_{PAE}, available gain and supply voltage for the considered cases is compared in figures 6.2, 6.3 and 6.4, respectively.

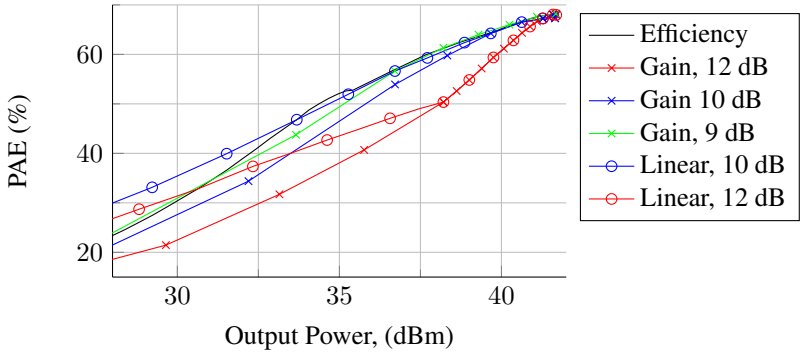

Figure 6.2: Comparison of η_{PAE} vs. $P_{o\text{-}1}$ for different tracking cases.

At 35 dBm output power the fixed 28 V $\eta_{PAE} = 35\,\%$, and the far smallest improvements resulting from ET is the 12 dB flat gain, only giving an improvement for about three percent, that is $\eta_{PAE} \approx 38\,\%$. The small improvement is a result of the tracked supply being to high to keep the PA saturated, only being saturated at output power greater than about $P_o = 38$ dBm, where the supply is fixed at 28 V.

This is also the point at which the linear 12 dB tracking starts, but with a steeper supply response, as seen in figure 6.4, resulting in staying closer to compression, and a larger improvement to efficiency, yielding $\eta_{PAE} = 44\,\%$, a $6\,\%$ improvement over the 12 dB flat gain case. Except from the 10 dB flat gain case at about $47\,\%$, the remaining cases all result in roughly the same η_{PAE} at 35 dBm output power and beyond, and having between $\eta_{PAE} = 51\,\%$ and $\eta_{PAE} = 52\,\%$.

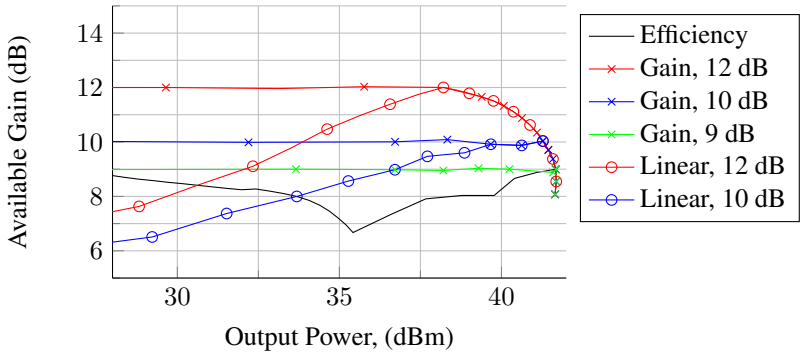

Figure 6.3: Comparison of G_A vs. P_{o_1} for different tracking cases.

The improved η_{PAE} is a result of dynamic varying of the supply voltage, keeping the PA saturated, or at least closer to saturation at back off. This however affects the gain of the PA, as can be seen in figure 6.3, where the most efficient cases yield the lowest and, with exception of the 9 db flat gain case, least linear gain. The gained energy efficiency may therefore be lost as a larger input power is needed, which leads to a greater power dissipation for the system preceding the PA in the signal chain, and it may require more power demanding linearization, such as digital predistortion.

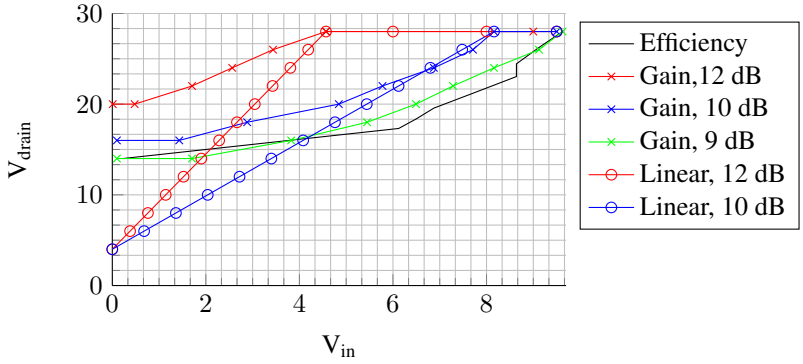

Figure 6.4: Comparison of V_S vs. V_{in} for different tracking cases.

Another thing that may have a great impact on the overall system efficiency for the given cases is the envelope amplifier. This because the envelope bandwidth is several times the RF bandwidth, and either a complex, high-performance EA is needed, or using a low-performance EA, reducing the efficiency. Similarly if the envelope is not amplified correctly the efficiency improvement of the RF PA is decreased.

Especially the maximum efficiency case is going to be hard to realize the supply response for, and the resulting gain response is fairly non-linear. The supply voltage tracking function is however rather similar to the 9 dB flat gain case, but not compressing quite as much, raising the gain to about 9 dB. Conveniently enough it is also fairly similar to a square design, thus reducing the bandwidth needed by the EA, possibly increasing its efficiency. This is also the case for the 10 dB flat gain case, but compressing a little less. The efficiency is not too much worse, and it could as such be considered a fair alternative for trading some efficiency for extra gain.

The 10 dB linear supply voltage case also gives a reasonable increase in efficiency of the RF PA, but also require high envelope bandwidths, especially if a lower level is set, as seen in figure 2.21. This is most likely required as well, as the gain is severely reduced at voltages below 14 V, where it is reduced below 8 dB. The 12 dB flat gain and 12 dB linear supply cases however may very well not improve η_{PAE} enough to improve the overall system efficiency, as the power dissipated by the EA may exceed the reduction in the RF PA.

The performance for the cases when applying a square supply function was also investigated. The overall improvement to efficiency was somewhat reduced due to the tracker keeping the PA further away from compression, but especially for the 10 dB and 9 dB flat gain cases, the ideal supply function is already almost similar to the square function. Using a square supply function can thus be regarded as an alternative to the linear, as PA efficiency is not terrible in comparison, and as the tracker requirements are far lower for a square function. In addition, as can be seen, the gain responses are far less linear for the maximum efficiency and linear supply cases, reducing the need for extensive predistortion in the flat gain cases. It could therefore be beneficial to investigate this deeper, bringing actual tracker characteristics into the calculation to estimate the overall system efficiencies for the different cases.

Chapter 7

Conclusion

In this thesis, the design of a 10 W class AB S-band power amplifier has been presented, displaying the potential of the GaN HEMT. Performance at static supply has been investigated at center and possible bandlimit frequencies have been investigated, shown to be within specified limits. The load and source impedances of the PA has been optimized for efficiency by using load and source pull techniques, also achieving higher gain and wider bandwidth than specified. The PA featured a single-tone 41.7 dBm peak output power with 68.2% peak η_{PAE} and 12.2 dB uncompressed gain.

Despite meeting the specifications and fielding good overall performance, the s-parameter measurements show a somewhat bad match, resulting in some input loss. Designing of the matching networks also failed to suppress low frequencies, resulting in high gain from the center frequency down to 100 MHz, which in some transmitters can be problematic. The possible solution of more extensive filtering in the rest of the system should not be necessary as this gain of the PA in question should have been suppressed.

In addition the PA was characterized at reduced supply voltages in order to estimate the performance when employing envelope tracking. Three sets of cases were investigated, tracking for maximum efficiency, flat gain and linear supply response respectively. The maximum efficiency case resulted in the largest possible improvement to the efficiency of the PA, but at the largest cost. The resulting gain was severely reduced and nonlinear. In comparison, the flat gain cases had slightly less improvement to efficiency, but a nicer gain response. Applying a linear supply function yielded a fair improvement to the efficiency, but lowering gain at increasing back off. Based on the measurements conducted, improvements to η_{PAE} can be as high as 17 % at 5-6 dB back off when adding envelope tracking.

The measurements however show a clear trade off between gain and efficiency resulting in fairly poor gain for the cases with the largest improvement to efficiency. This can be deceiving as reduced gain will increase the required input power, contributing to power dissipation outside the PA and thus overall efficiency improvement may be reduced.

The performance in the envelope tracking cases were also estimated when applying square supply functions. Deviating from their respective ideal tracking functions showed some reduction to the initial improvement, however the flat gain shows similar ideal supply functions, minimizing the reduction. Utilizing a square function supply modulator can thus improve overall system efficiency, as less bandwidth is required by the supply modulator, improving its respective efficiency. In any case a less complex supply can be used, reducing complexity and costs.

Further continuation on this project would include studying of the complete system for the investigated cases, including the efficiencies in order to determine which combination of case and envelope amplifier that result in the highest overall system efficiency.

In the case of further improving the PA, a rematch will be appropriate in order to reduce the input return loss and deal with the low frequency gain. The source and load impedances resulting from the source pull are thought to yield a good combination of efficiency and gain, however there could very well be better solutions. Should it be possible to increase the gain at compression, the gain could be though to still be high even when tracking close to compression and it Would be interesting to know the efficiency reduction.

Bibliography

[1] Zhanchang Wang. *Envelope Tracking Power Amplifiers for Wireless Communications*. Artech House Inc., 1st edition, 2014.

[2] David M. Pozar. *Microwave Engineering*. Artech House Inc., 4th edition, 2011.

[3] Peter Cripps. *RF Power Amplifiers For Wireless Communications*. Artech House Inc., 2nd edition, 2006.

[4] David M. Pozar. *Microwave and RF Design of Wireless Systems*. Artech House Inc., 1st edition, 2002.

[5] David K. Cheng. *Field and Wave Electromagnetics*. Addison Wesley Publishing Company, Inc., 2nd edition, 1989.

[6] Michael Steer. *Microwave and RF Design - A Systems Approach*. Scitech Publishing Inc., 1st edition, 2010.

[7] G. Gonzales. *Microwave Transistor Amplifiers, Analysis and Design*. Prentice-Hall Inc., 2nd edition, 1997.

[8] J. M. Rollett. Stability and power gain invariants of linear two-ports. *IRE Trans. Circuit Theory*, 9(1):29–32, 1962.

[9] M. L. Edwards and J. H. Sinsky. A new criteria for linear 2-port stability using a single geometrically derived parameter. *IEEE Trans. Microwave Theory and Techniques*, 40:2803–2811, 1992.

[10] Peter B. Kenington. *High-Linearity RF Amplifier Design*. Artech House Inc., 1st edition, 2000.

[11] Frederick Raab, Peter Asbeck, Steve Cripps, Peter B. Kenington, Zoya B. Popovich, Nick Pothecary, John F. Sevich, and Nathan Sokal. RF and Microwave Power Amplifier and Transmitter Technologies. *IEEE Transactions on Microwave Theory and Techniques*, 2002.

[12] C. Weitzel. Will gaas survive for wireless pas?? In *2005 International Conference on Compound Semiconductor Manufacturing Technology*.

[13] Pengellym Raymond S., Simon M. Wood, James W. Milligan, Scott T. Sheppard, and William L. Pribble. Review of gan on sic high electron-mobility power transistors and mmics. *IEEE Transactions on Microwave Theory and Techniques*, 60(6), June 2012.

[14] Adel A. M. Saleh and Donald C. Cox. Improving the Power-Added Efficiency of FET Amplifiers Operating with Varying-Envelope Signals. *IEEE Transactions on Microwave Theory and Techniques*, 1983.

[15] E. McCune. Envelope Tracking or Polar - Which Is It? *IEEE Microwave Magazine*, June 2012.

[16] Rohde & Schwarz. The Crest Factor in DVB-T (OFDM) Transmitter Systems and its Influence on the Dimensioning of Power Components, 2007. Application Note.

[17] Sulaiman A. Aburakhia, Ehab F. Badran, and Darwish A. Mohamed. Distribution of the PAPR for Real-Valued OFDM Signals. *International Conference on Information Technology (ICIT)*, 2009.

[18] Timo Aitto-oja. High efficiency envelope tracking supply voltage modulator for high power base station amplifier applications. *Microwave Symposium Digest (MTT), 2010 IEEE MTT-S International*, 2010.

[19] Bognøy, A. Design of a PA for use in an Envelope Tracking architecture. Technical report, NTNU, 2014.

[20] Johanson Technologies. *Multi-Layer High-Q Capacitors - Datasheet*, 2012.

[21] Junghwan Moon, Junghwan Son, Juyeon Lee, Jungjoon Kim, Seunghoon Jee, Seungchan Kim, and Bumman Kim. A multimode/multiband envelope tracking transmitter with broadband saturated power amplifier. *IEEE MTT-S International Microwave Symposium*, 2011.

[22] P. Suebsombut, O. Koch, and S. Chalermwisutkul. Development of a GaN HEMT Class-AB Power Amplifier for an Envelope Tracking System at 2.45 GHz. *Electrical Engineering/Electronics Computer Telecommunications and Information Technology (ECTI-CON), 2010 International Conference on*, 2010.

[23] Rohde & Schwarz. *Vector Signal Generator SMU200A*, September 2006.

[24] Junghwan Moon, Juyeon Lee, Junghwan Son, Jungjoon Kim, Seunghoon Jee, Seungchan Kim, and Bumman Kim. Effects of even-order terms on behavior model of envelope tracking transmitters. *Microwave Integrated Circuits Conference (EuMIC), European*, 2011.

Appendix A

Extrapolation of Two-tone Measurements

Due to the signal generator output power being insufficient to drive the PA into compression during the two-tone measurement, simple extrapolation of the measurements were made. Figures A.1, A.2 and A.3 show the measured two-tone output power, power gain and η_{PAE} and their corresponding extrapolations, respectively. The extrapolated thrid order intermodulation is shown in figure A.4.

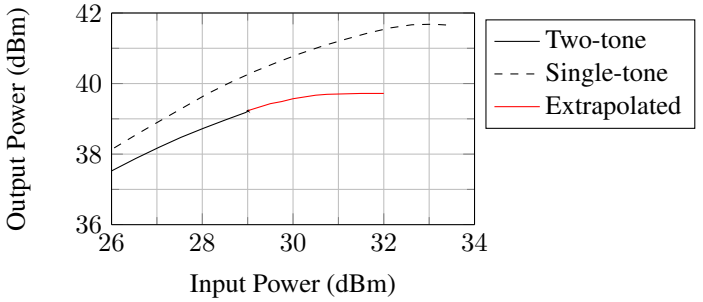

Figure A.1: Measured two-tone output power vs. input power.

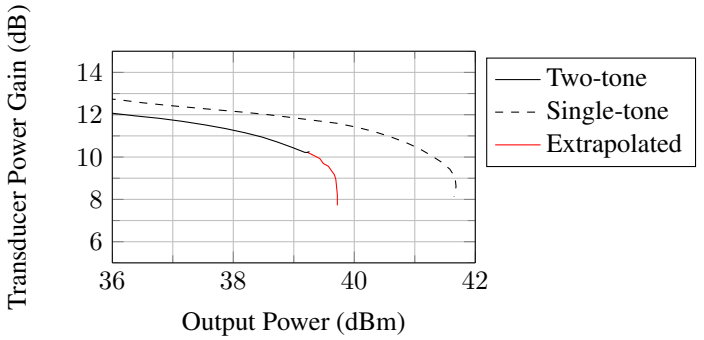

Figure A.2: Measured two-tone available gain vs. P_{o_2}

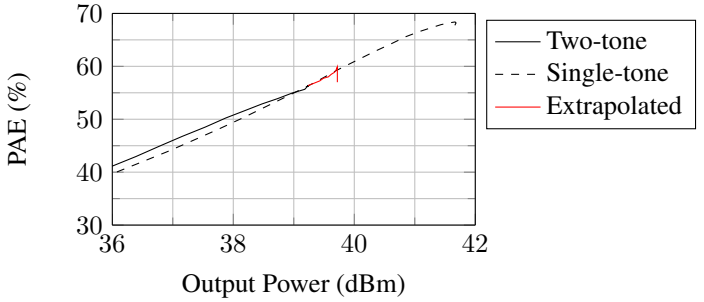

Figure A.3: Measured two-tone η_{PAE} vs. P_{o_2}

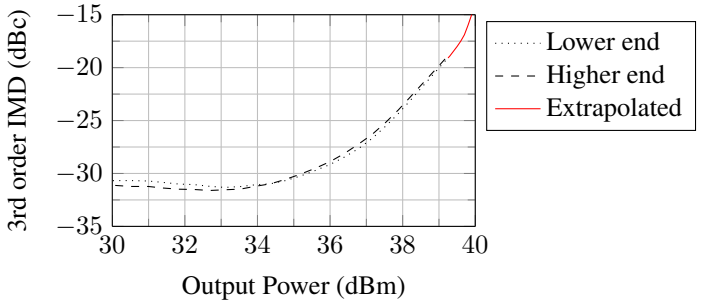

Figure A.4: Measured 3rd order IMD vs. P_{o_2}

Appendix B

Figures

ADS Design and Simulation

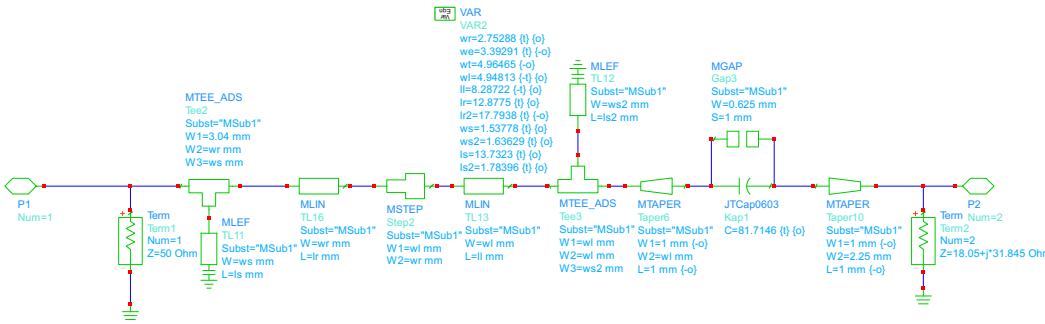

Figure B.1: Input matching network design in ADS

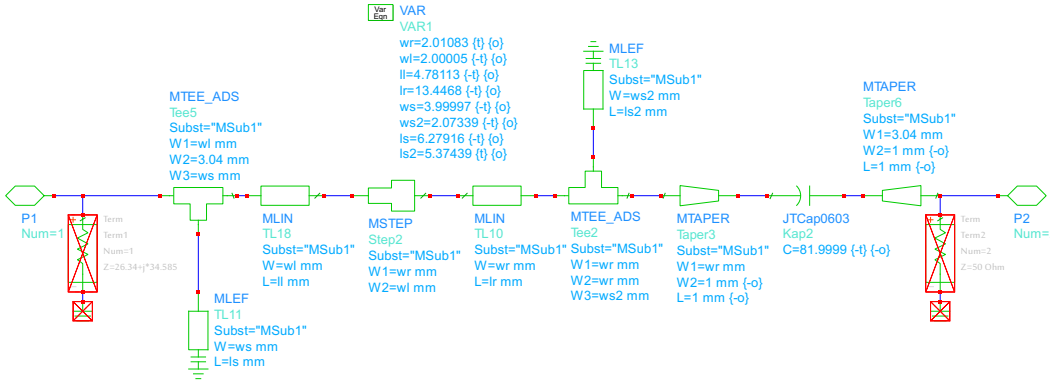

Figure B.2: Output matching network design in ADS

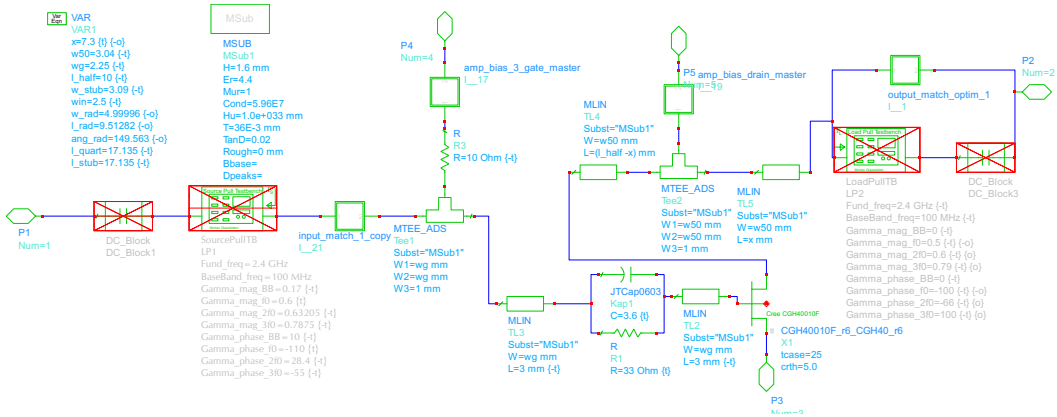

Figure B.3: Complete PA design in ADS

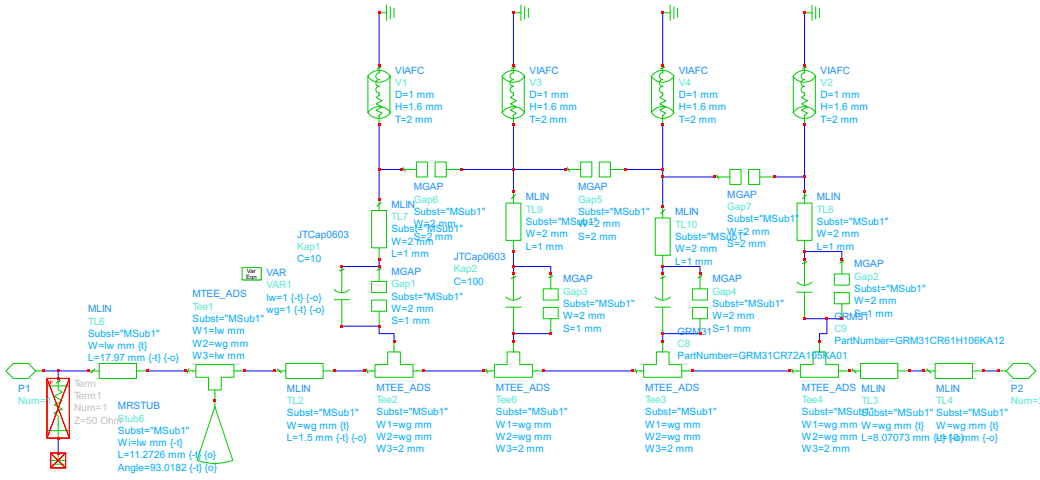

Figure B.4: Gate bias-T design in ADS

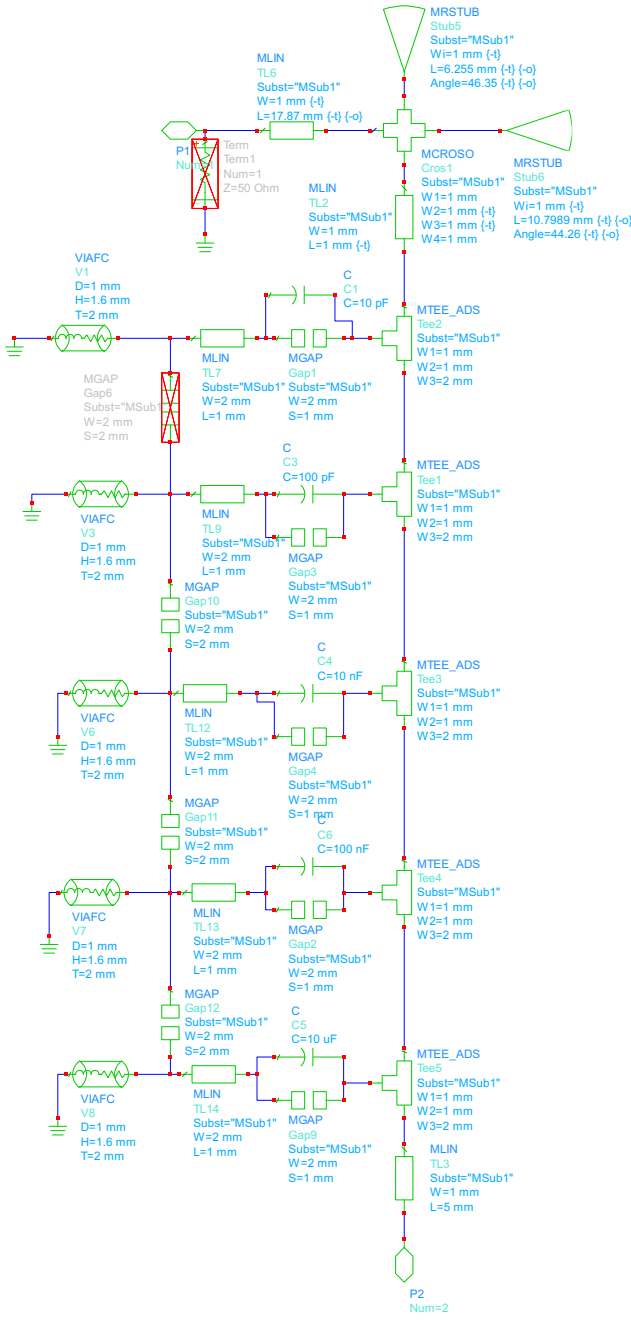

Figure B.5: Drain bias-T design in ADS

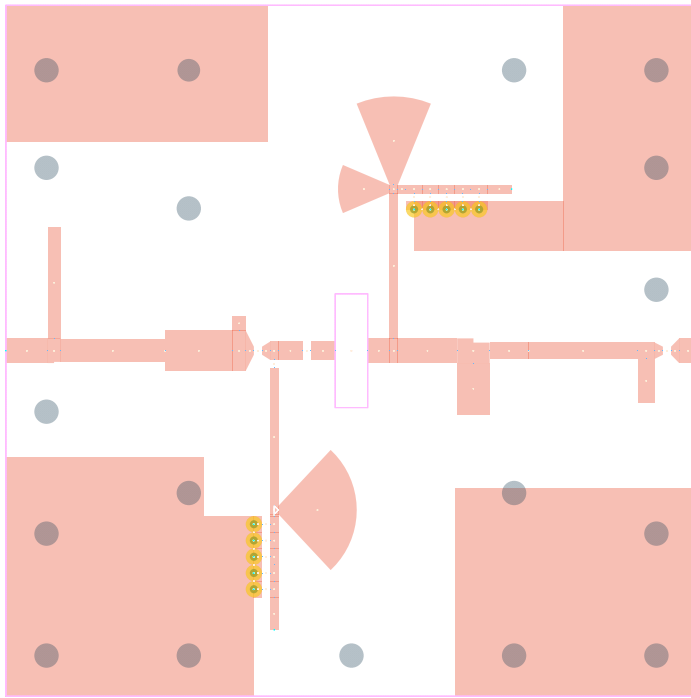

Figure B.6: Generated microstrip design for prototype PA.

Plots

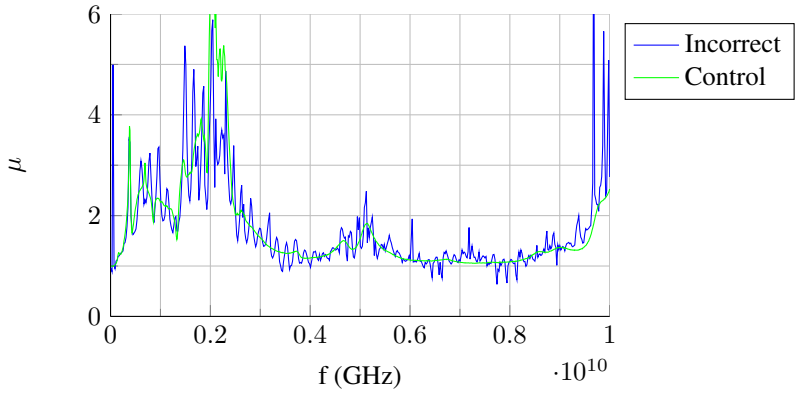

Figure B.7: μ-factor computed from measured s-parameters.

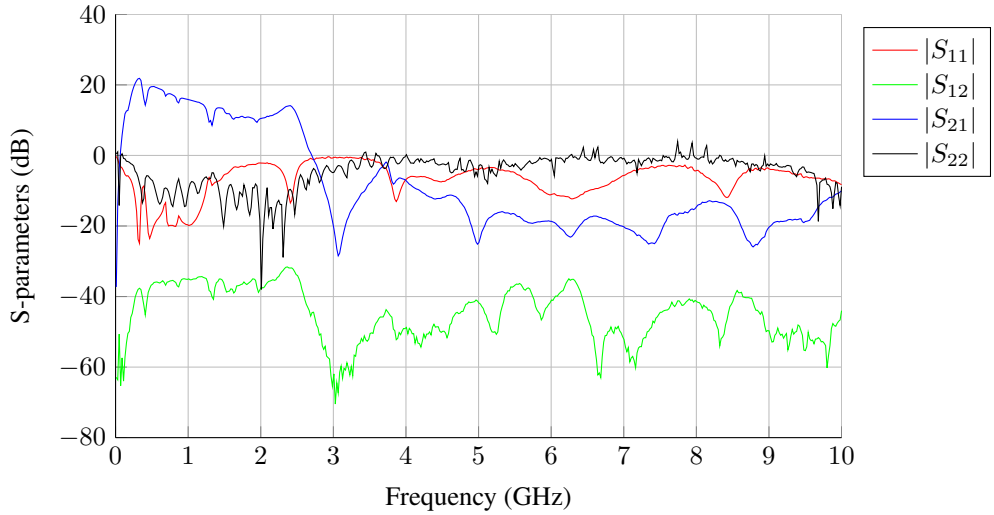

Figure B.8: Measured s-parameters for complete design.

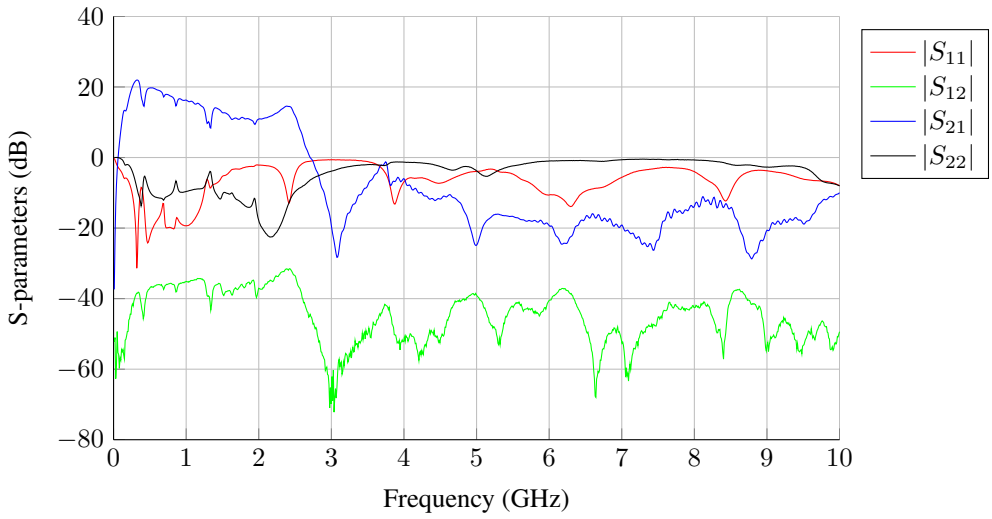

Figure B.9: Control measured s-parameters for complete design.

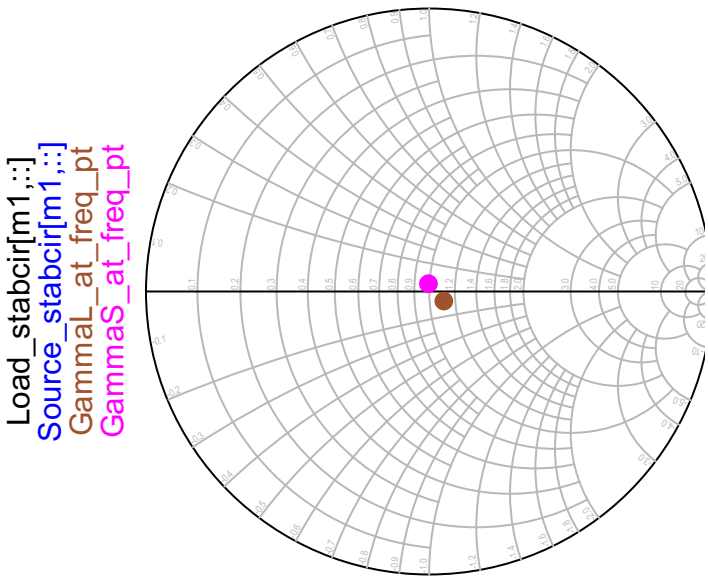

Figure B.10: Simulated stability circles and reflection coefficients of full system.

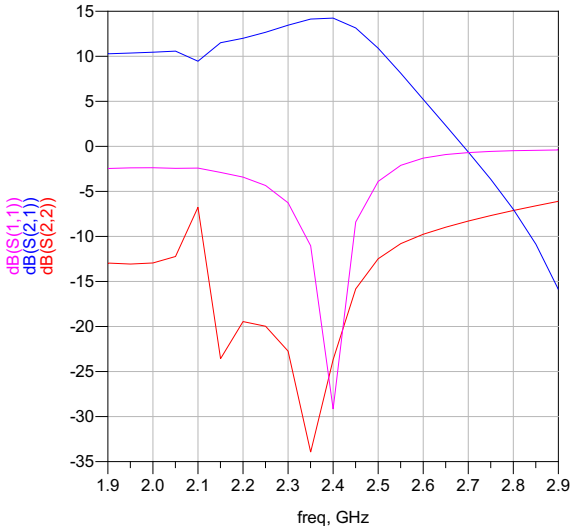

Figure B.11: Simulated s-parameters full system.